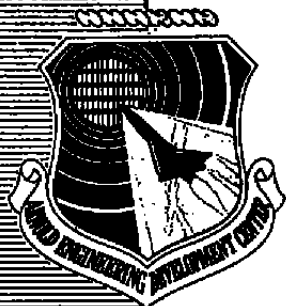


C2



# Comparison of Wind Tunnel and Flight Test Measurements of Static Aerodynamic Loading of a Captive Store

R. E. Dix and G. R. Mattasits  
ARO, Inc.

July 1980

Final Report for Period June 18, 1976 — August 31, 1978

Approved for public release; distribution unlimited.

Property of U. S. Air Force  
AEDC LIBRARY  
F49620-77-C-0003

TECHNICAL REPORTS  
FINAL COPY

**ARNOLD ENGINEERING DEVELOPMENT CENTER  
ARNOLD AIR FORCE STATION, TENNESSEE  
AIR FORCE SYSTEMS COMMAND  
UNITED STATES AIR FORCE**

**NOTICES**

When U. S. Government drawings, specifications, or other data are used for any purpose other than a definitely related Government procurement operation, the Government thereby incurs no responsibility nor any obligation whatsoever, and the fact that the Government may have formulated, furnished, or in any way supplied the said drawings, specifications, or other data, is not to be regarded by implication or otherwise, or in any manner licensing the holder or any other person or corporation, or conveying any rights or permission to manufacture, use, or sell any patented invention that may in any way be related thereto.

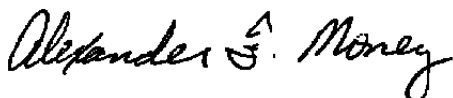
Qualified users may obtain copies of this report from the Defense Technical Information Center.

References to named commercial products in this report are not to be considered in any sense as an indorsement of the product by the United States Air Force or the Government.

This report has been reviewed by the Office of Public Affairs (PA) and is releasable to the National Technical Information Service (NTIS). At NTIS, it will be available to the general public, including foreign nations.

**APPROVAL STATEMENT**

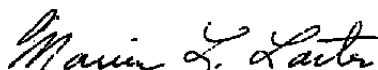
This report has been reviewed and approved.



ALEXANDER F. MONEY  
Project Manager  
Directorate of Technology

Approved for publication:

FOR THE COMMANDER



MARION L. LASTER  
Director of Technology  
Deputy for Operations



# UNCLASSIFIED

## 20. ABSTRACT (Continued)

noted were thought to be attributable either to improper store-to-aircraft alignment or to poor definition of inertial loads during maneuvering flight.

## PREFACE

The work reported herein was conducted in two phases: wind tunnel experiments, and a flight test program. The wind tunnel experiments were conducted by the Arnold Engineering Development Center (AEDC), Air Force Systems Command (AFSC), at the request of the Air Force Armament Laboratory (AFATL/DLJC). The AFATL project monitor was Maj. R. Van Putte. The flight test program was conducted by the Naval Air Test Center (NATC), Naval Air Systems Command (NASC), at the request of the Naval Weapons Center (NWC). The NATC project engineer was Ronald A. Wilson, and the pilot for the entire flight program was Robert C. Springer, Major, USAF. The NWC project monitor was Dr. Arthur R. Maddox. The results of the research were obtained by ARO, Inc., AEDC Division (a Sverdrup Corporation Company), operating contractor for the AEDC, AFSC, Arnold Air Force Station, Tennessee, under ARO Project Number P34A-S7A. Data analysis was completed in September 1978, and the manuscript was submitted for publication on December 21, 1978.

## CONTENTS

	<u>Page</u>
1.0 INTRODUCTION . . . . .	7
2.0 EXPERIMENTAL APPARATUS	
2.1 Test Facility . . . . .	8
2.2 Models . . . . .	8
2.3 Model Instrumentation . . . . .	9
2.4 Flight Test Equipment . . . . .	10
3.0 DESCRIPTION OF TESTS	
3.1 Wind Tunnel Flow Conditions and Procedure . . . . .	13
3.2 Corrections to Wind Tunnel Data . . . . .	13
3.3 Precision of Wind Tunnel Data . . . . .	14
3.4 Flight Procedures and Conditions . . . . .	14
3.5 Precision of the Inflight Data . . . . .	15
4.0 DISCUSSION OF RESULTS	
4.1 Constant Mach Number, Level Flight . . . . .	15
4.2 Flight with Moderate Maneuvers . . . . .	17
4.3 Altered Afterbody, AB 2 . . . . .	20
4.4 Comparison with Other Wind Tunnel Data . . . . .	21
5.0 CONCLUSIONS . . . . .	22
REFERENCES . . . . .	23

## ILLUSTRATIONS

### Figure

1. Schematic Illustration of a Typical Model Installation in Tunnel 4T . . . . .	25
2. Outline Drawing of the 1/20-Scale Model of the F-4C Aircraft . . . . .	26
3. Details of the 1/20-Scale Models of the F-4C Pylons . . . . .	27
4. Details of the 1/20-Scale Model of the Triple Ejector Rack (TER) . . . . .	28
5. Details of the 1/20-Scale Model of the MK 83 Store . . . . .	29
6. Sketch of the 1/20-Scale MK 83/TER Model Installation . . . . .	30

<u>Figure</u>	<u>Page</u>
7. Photograph of the F-4/MK 83 (AB 2) Flight Test Installation . . . . .	31
8. Photographs of the UK-Sponsored Installation on the Right Wing . . . . .	32
9. Photograph of the MK 83/TER/Left-Wing Inboard Pylon Installation, Inert Stores Removed . . . . .	35
10. Photographs of the Flight-Ready MK 83/TER Installation . . . . .	36
11. Closeup View of the MK 83/TER/Pylon Installation . . . . .	38
12. Details of the Full-Size MK 83 Store . . . . .	39
13. Photograph of the Nose-Mounted, Instrumented Boom . . . . .	41
14. Photographs of the NWC Flight-Rated Balance . . . . .	42
15. Statistical Precision Intervals for Flight Condition Parameters . . . . .	44
16. Statistical Precision Intervals for Inflight Force and Moment Coefficients . . . . .	46
17. Comparison of Wind Tunnel and Inflight Data for Constant Mach Number, Level Flight, AB 1 . . . . .	51
18. Comparison of Wind Tunnel and Inflight Data for Low-g Maneuvering Flight, AB 1 . . . . .	57
19. Comparison of Wind Tunnel and Inflight Data for Maneuvering Flight, AB 1 . . . . .	63
20. Comparison of Wind Tunnel and Inflight Data for Constant Mach Number, Level Flight, AB 2 . . . . .	69
21. Comparison of Wind Tunnel and Inflight Data for Low-g Maneuvering Flight, AB 2 . . . . .	75
22. Comparison of Wind Tunnel and Inflight Data for Maneuvering Flight, AB 2 . . . . .	81
23. Comparison of Wind Tunnel and Inflight Data for Constant Mach Number, Level Flight plus Low-g Maneuvering Flight, AB 1 . . . . .	87
24. Comparison of Wind Tunnel and Inflight Data for Constant Mach Number, Level Flight plus Low-g Maneuvering Flight, AB 2 . . . . .	93

#### TABLES

1. Data-Precision Intervals for Force and Moment Coefficients from Aerodynamic Tunnel (4T) . . . . .	99
--	----

<u>Figure</u>	<u>Page</u>
2. Data-Precision Intervals for Fundamental Flight Instrumentation Systems . . . . .	99

#### APPENDIX

A. Single-Store Configuration (Flight 1) . . . . .	101
NOMENCLATURE . . . . .	113

## 1.0 INTRODUCTION

An evaluation of methods and techniques used in wind tunnel experiments to measure static aerodynamic loading of captive stores was initiated during FY72 at the Propulsion Wind Tunnel Facility (PWT) of the Arnold Engineering Development Center (AEDC). Several associated experiments were conducted in Aerodynamic Wind Tunnel (4T) of the PWT complex, and the results were published in four technical reports (Refs. 1 through 4). As one result of the evaluation, it was observed that all conventional techniques of supporting external store models in the captive position on an aircraft model could be identified as applications of one of two general methods: either internal bracket support (store model attached to aircraft model), or dual external support (aircraft and store models supported with separate stings or blades). However, it was also observed during the evaluation studies that in some cases there were differences between respective measurements of captive store loads taken using the two methods of supporting the store model (Ref. 3). Consequently, to aid in establishing the relative validity of the techniques used, it was considered desirable to obtain inflight measurements of static aerodynamic loads acting on a captive store over a range of Mach number and angle of attack.

During the period FY74 through FY76, discussions took place between the Naval Weapons Center (NWC), China Lake, California, the Air Force Armament Laboratory (AFATL), Eglin Air Force Base, Florida, and the AEDC that ultimately resulted in a joint USN/USAF flight test program. Early in the discussions, it was revealed that the NWC possessed a MK 83 low-drag bomb casing that had been emptied of explosives, fuze, etc., and equipped internally with a strain-gage balance and accelerometers for a flight test program some ten years earlier. Hence, to allow for possible future correlation with inflight loads measurements, the MK 83 was selected as one of the configurations to be used in the wind tunnel experiments mentioned above. Over the period of time during which the experiments were being conducted in the wind tunnel, approval was secured by the NWC to use the special MK 83/balance configuration once more in a flight test program to measure the static aerodynamic loads acting on the MK 83 in a captive position on an F-4 fighter aircraft. In final format, the flight tests involved flights conducted at the Naval Air Test Center (NATC), Patuxent River, Maryland, and calibration of the balance and reduction of the inflight data at the AEDC.

A correlation between the flight test and wind tunnel data sets is made herein. As a supplement to the primary comparisons, limited data from the flight program are correlated with corresponding measurements made during experiments conducted in the United Kingdom (UK) at the Bedford, England facilities of the Aircraft Research

Association (ARA). The UK data are an indirect result of the simultaneous installation on the flight test aircraft of the MK 83/balance configuration on the left-wing inboard pylon, and an independent store loads experiment conducted by the Cranfield Institute of Technology and the Royal Aircraft Establishment (RAE) on the right-wing inboard pylon. The primary purpose of the UK wind tunnel program at the ARA was to generate data for correlation with their inflight data, but models of the MK 83/balance installation were included to establish full geometric similitude. Since the scale factor used in the ARA experiments was different from that of the AEDC models, the UK data for the MK 83 were considered useful for a first-order evaluation of scale effects and are included herein.

## 2.0 EXPERIMENTAL APPARATUS

### 2.1 TEST FACILITY

Experiments were conducted in the AEDC Aerodynamic Wind Tunnel (4T), a closed-circuit tunnel in which continuous flow can be maintained at various density settings. Mach number in the free stream can be set at any value from 0.1 to 1.3, and nozzle blocks can be installed to provide discrete Mach numbers of 1.6 and 2.0. Stagnation pressure can be maintained at any value from 300 to 3,700 psfa. The test section is 4 ft square and 12.5 ft long with perforated, variable porosity (0.5- to 10-percent open) walls. It is completely enclosed in a plenum chamber from which the air can be evacuated, allowing part of the tunnel airflow to be removed through the perforated walls of the test section.

Models are supported in the test section with a conventional strut-sting system. A model can be pitched from approximately -12 to 28 deg with respect to the centerline of the tunnel. A capability of rolling a model from -180 to 180 deg about the centerline of the sting is also available. An illustration showing a typical model installed for testing is presented in Fig. 1.

### 2.2 MODELS

#### 2.2.1 Aircraft

Experiments in Tunnel 4T were conducted with 1/20-scale models. A model of the F-4C aircraft was used with tail surfaces removed. Airflow was allowed to enter the model engine intakes, pass through internal ducting, and exit the model through cruise configuration exhaust ports. An outline drawing of the F-4C model is presented in Fig. 2.

### 2.2.2 Pylons

During all wind tunnel experiments, inboard and outboard pylons were installed on both the right and left wings of the aircraft model. All pylons were empty except the left-wing inboard pylon, on which the experiments were conducted. An empty weapons adaptor was also installed on the centerline fuselage station. All model pylons were of the conventional USAF configuration. Details of the pylon models are presented in Fig. 3.

### 2.2.3 Triple Ejector Rack

To support the stores on the left-wing inboard pylon, a model of the USAF Triple Ejector Rack (TER), Type TER-9A, was used. Sway braces and ventilating slots existing on full-size racks were simulated on the model. Dimensions and details of the TER model are presented in Fig. 4. Throughout the experiments, dummy store models were mounted on the shoulder stations of the TER, and an instrumented store model was mounted on the bottom, or center, station.

### 2.2.4 Store

A low-drag bomb of the 1,000-lb class, the MK 83, was the only store configuration included in the study. The exact contour of the airfoil of the fins was not simulated on the 1/20-scale model, although it was possible to include the 2-deg incidence of the fins. Details of the store model are shown in Fig. 5. A sketch of the store installed on the TER is presented in Fig. 6. The axis of symmetry of the store was aligned in an attitude parallel to the lower surface of the pylon (i.e., 1 deg nose-down with respect to the reference waterline of the aircraft, and 2 deg nose-down with respect to the wing chord reference plane).

## 2.3 MODEL INSTRUMENTATION

A strain-gage balance was used to sense and resolve the six customary components of aerodynamic forces and moments acting on the store model. In the shape of a cylinder 0.3 in. in diameter and 3.05 in. long, the balance was mounted entirely within the store model, as depicted in Fig. 6. With the store model attached at the nose to the live end of the balance, necessary physical support for the grounded end of the balance was provided by a rigid bracket protruding through a slot in the upper surface of the store model and securely fastened to the TER model. The slot was so cut that sufficient clearance was allowed between the bracket and the adjacent model surfaces to prevent fouling of the balance outputs. In addition to the force and moment measurements for the store model, the gravimetric angle of attack of the aircraft model was sensed with an oil-damped pendulum equipped with strain gages and mounted in the nose of the aircraft model.

## 2.4 FLIGHT TEST EQUIPMENT

### 2.4.1 Aircraft and Pylons

Flights were made with an F-4J aircraft assigned to the NATC, number F-4J-153077. The aircraft was of conventional USN configuration, but the model used in the earlier wind tunnel experiments was of a USAF F-4C configuration. Alterations of the pylon-TER installation on the left wing of the flight test aircraft were made to more nearly match the configuration of the wind tunnel model. Despite the alterations, at least five features of the flight test aircraft configuration were different from the model configuration: 1) a research boom was installed on the nose of the aircraft to accurately sense the angles of attack and yaw; 2) the missile wells in the fuselage were empty rather than filled and faired, as in the case of the model; 3) the outboard pylons on both the left and right wings, and the inboard pylon the right wing, were of USN design, with weapons adapters attached; 4) no weapons adapter was installed on the centerline station; and 5) a totally different store/TER combination was installed on the right-wing inboard pylon. A photograph of the left-wing installation is presented in Fig. 7, in which a visual comparison of the leading-edge shapes of the USAF pylon (foreground) and the USN pylon (background) can be made.

By far the most noticeable difference between the flight-test and AEDC wind tunnel configurations was the presence of the UK store and TER on the right-wing inboard pylon of the F-4J aircraft (Section 1.0). Photographs of the UK installation are presented in Fig. 8. The presence of the UK installation on the right wing was estimated to have little or no influence on the loads acting on the MK 83 on the left wing.

### 2.4.2 Triple Ejector Rack

A TER-9A was attached to the left-wing inboard pylon to carry the MK 83 stores. Again, to match the wind tunnel model, the TER was of USAF specification. Further, the specific TER used had been equipped with instrumentation on Station 1 (bottom center station) to measure store loads, namely load cells in the place of conventional pads at the store contact points of the sway brace screws, and strain gages attached to the store suspension hooks. Sway brace arms approximately 2-1/2 in. greater in span than standard arms were required on the bottom station of the TER, since the location of the store contact points for the sway brace pads was not standard for the TER-9A used. Figures 9 and 10 are photographs of the store/TER installation on the aircraft, and Fig. 11 is a closeup of the store-to-TER interface. The instrumented TER was furnished by the Air Force Armament Laboratory (AFATL), Eglin Air Force Base, Florida.

### 2.4.3 Store

The TER on the left inboard pylon of the aircraft was fully loaded with three stores of the MK 83 low-drag bomb shape: two inert stores on the "shoulder" stations, and an instrument-equipped store on the bottom center station. Both the casing and the internal strain-gage balance of the instrument-equipped store were furnished by the NWC and had been used in a previous flight test program, as described in Section 1.0. Installation of the balance inside the MK 83 involved cutting holes through the casing to allow attachment of suspension lugs and sway brace screws to the grounded upper platform of the balance. Sufficient clearance existed between the MK 83 casing and the upper platform to prevent fouling.

Two afterbody configurations were used: AB1, the conventional shape, and AB 2, an altered shape. The AB 2 shape was fabricated by superimposing a cylindrical body on a conventional afterbody, as shown in Fig. 12. As altered, AB 2 matched the configuration of the sting-supported MK 83 model used in the wind tunnel (Section 2.2.4).

No attempt was made to match the mass or center of gravity specifications for a production version of the MK 83. The weight of the store casing was approximately 556 lb, and the weight of the balance was about 360 lb, for a total of 916 lb, about 7 percent less than a conventional MK 83. For data reduction purposes, in calculating the inertial load (i.e., the static tare correction), only the weights of the casing and lower platform of the balance, approximately 105 lb, were included. Therefore, the inertial load to which the balance was exposed was 661 lb per g of acceleration.

Other than the holes in the casing, the configuration of the store with AB 1 was correct. Dimensions of the store are presented in Fig. 12a, and photographs are shown in Figs. 9 and 10 (AB 1), and 7 and 12b (AB 2).

### 2.4.4 Instrumentation

#### 2.4.4.1 Aircraft Attitude

A slender boom of the type customarily used for research and development flight programs was mounted on the nose of the aircraft to provide accurate determination of aircraft attitude. Angles of attack and sideslip of the aircraft were sensed with vane potentiometers attached to the boom. Appropriate pressure transducer ports and hot-wire sensors were also housed on the boom for interference-free sensing of static pressure and total temperature, respectively. A photograph of the boom is presented in Fig. 13.

#### 2.4.4.2 Strain-Gage Balance

The NWC strain-gage balance mounted inside the MK 83 casing was developed in 1966 at the Aerial Measurements Laboratory of Northwestern University, Evanston, Illinois. In Refs. 5 and 6, the balance is referred to as the "AML" balance, or the "Pastushin" balance. Photographs of the balance, showing the general arrangement of the gaged elements and the massive upper and lower structural platforms, are presented in Fig. 14. The upper platform is the mechanically grounded component of the balance, which provides attachment points for the suspension lugs and contact points for the sway brace pads. The upper platform is also the supporting structure for the strain-gaged elements, or flexures. Moments are transmitted to the flexures through ball-end rods attached to the lower platform, to which the store casing is securely bolted. From the moments, the six conventional components of forces and moments acting on the store are resolved. Maximum allowable loads for linear response of the balance are at least four times the predicted inflight aerodynamic loads, a margin required to accommodate the inertial loading that occurs during maneuvering flight. The balance was calibrated in the PWT facility of the AEDC.

#### 2.4.4.3 Accelerometers

Three accelerometers were mounted on the lower platform of the balance to detect and give a quantitative indication of acceleration of the balance in the longitudinal, lateral, and vertical directions of the store-body axis system. Operating ranges for the X-, Y-, and Z-axis accelerometers were  $\pm 5$ ,  $\pm 5$ , and  $\pm 10$  g, respectively. Thermostat-commanded resistance heaters in the accelerometer housings were used in an attempt to assure a uniform thermal environment for the accelerometers. An output disturbance resulted, however, from use of the heaters (for example, shifts of 0.007, 0.010, and 0.045 g were observed during calibration of the X-, Y-, and Z-accelerometers, respectively, at the AEDC). Accelerometers were also mounted near the center of gravity of the aircraft but were not calibrated at the AEDC.

#### 2.4.4.4 Data-Recording System

A fourteen-track MARS 2000 Intermediate Band magnetic tape recorder with a frequency response of 250 kHz at a tape speed of 60 in./sec was used to record all data. A tape speed of 30 in./sec was selected to accommodate the data bandwidth requirement of the various instrumentation systems. Approximately 30 min of recording time was available for each flight. The pilot initiated recording by pressing the bomb release button on the control column.

Data were recorded using either a pulse code-modulated (PCM) or frequency-modulated (FM) format, depending on the parameter. For PCM data, a bit rate of 88K bits/sec was used, allowing a sample rate of 100 per second, and reconstruction of the data up to 20 Hz. Instruments were scanned at the rate of 100 per second, but values were recorded only ten times each second. All data channels were either filtered or designed not to exceed the 20-Hz limit. The FM/FM system consisted of constant band voltage-controlled oscillators and a 100-kHz crystal oscillator. Constant band was used rather than proportional band because of a 1-kHz filtering of the balance outputs.

Synchronization of data, event markers, and time signals was accomplished with a system consisting of a time code generator, a cockpit time display, a pilot's event marker, the bomb button firing pulse, a tone generator, and a UHF radio. Time synchronization with NATC time signals was accomplished via the UHF radio.

All signal conditioning, such as voltage monitoring, filtering, amplification, etc., was accomplished through appropriate circuitry in a special interface system. Signal conditioning was not required for static pressure, airspeed, altitude, and outside air temperature, all sensed from the boom, or for the TER instrumentation outputs. All aircraft instrumentation was designed, fabricated, calibrated, and installed by the NATC.

### **3.0 DESCRIPTION OF TESTS**

#### **3.1 WIND TUNNEL FLOW CONDITIONS AND PROCEDURE**

Static aerodynamic forces and moments acting on the store model were measured at nominal free-stream Mach numbers of 0.6, 0.7, 0.8, and 0.9. (Data were recorded at other Mach numbers but are not reported herein. See Ref. 7 for additional data). Reynolds number was maintained at approximately  $3.5 \times 10^6$  per foot for all Mach numbers.

During the experiments, flow conditions were first established, and then a pitch-pause technique was used, in which the attitude of the aircraft model was set and maintained for approximately 3 sec at each value of a specified sequence of attitudes. Data were recorded at the end of each phase, after which the attitude of the aircraft was changed to the next sequential value. The process was reported for each Mach number.

#### **3.2 CORRECTIONS TO WIND TUNNEL DATA**

To account for the influence of balance flexibility during the experiments, the balance calibration data were used in the online data reduction equations to calculate the correct gravimetric angle of attack of the store model. Calibration data were also used to correct the force and moment measurements for tare contributions attributable to the weight of the store model.

### 3.3 PRECISION OF WIND TUNNEL DATA

For the fundamental flow parameters  $P_{t_{\infty}}$  and  $M_{\infty}$ , statistical precision intervals containing 95 percent of the data were estimated from knowledge of both the calibrations of the instruments used to sense the pressure and temperature of the airflow in the wind tunnel, and the repeatability and uniformity of the free-stream flow in the test section during tunnel calibration. Statistical precision intervals for the instrumentation systems were estimated from repeated calibrations of the systems using secondary standards with accuracies traceable to the National Bureau of Standards. Statistical precision intervals for values of forces and moments derived from the output of the balance gages were determined from a root-mean-square analysis of the calibration data for the balance. Values of the above intervals and estimates of instrument bias were combined using the Taylor series method of error propagation to determine the precision intervals for the force and moment coefficients. Values of the precision intervals for the coefficients of forces and moments acting on the model used in the wind tunnel experiments are presented in Table 1. For all flow conditions, the precision interval for angle of attack was  $\pm 0.15$  deg, and for Mach number was  $\pm 0.004$ .

### 3.4 FLIGHT PROCEDURES AND CONDITIONS

All instrumentation systems were operated during preflight checkout procedures to establish reference zero readings, analogous to "wind-off" values recorded before wind tunnel experiments. At the command of the pilot (by pressing the bomb-release button, see Section 2.4.4.4) both preflight and inflight data were recorded in analog form on magnetic tape at the rate of ten points per second (a "point" is defined as one complete scan of the instrument outputs). After the flights, the analog data were translated into digital form by the NATC. Reduction of the digital data to engineering units and coefficient form was subsequently accomplished at the AEDC.

Data were recorded during several types of maneuvers. Most fundamental was the unaccelerated, "straight and level" pass, during which the pilot attempted to maintain constant altitude, attitude, and Mach number for several tens of seconds. Straight and level passes were made at two altitudes, 3,000 and 5,000 ft. To increase the range of aircraft attitude for which data were recorded, pushovers, dives, pullouts, coordinated turns, wind-up turns, and rudder doublets were also performed. Typical dives were initiated at 14,000 ft, with pullouts near 2,000 ft. Turns and rudder doublets were performed at 4,000 ft. All flights took place in the 0- to 15,000-ft range of altitude.

### 3.5 PRECISION OF THE INFLIGHT DATA

Statistical precision intervals (i.e., intervals centered on a mean value of a parameter and including, statistically, 95 percent of the appropriate data from the experiment) were calculated using information furnished by the NATC and recorded during calibration of the aircraft and store instrumentation systems (see Table 2). Since Mach number and dynamic pressure were calculated using values of static pressure, total temperature, and indicated velocity recorded from aircraft instruments, statistical precision intervals were calculated using the Taylor Series method of error propagation to combine the uncertainties of the various aircraft instruments involved. Figure 15 presents a graph of the statistical precision intervals for Mach number and dynamic pressure as a function of altitude. No corrections were attempted for atmospheric turbulence.

Statistical precision intervals for the store force and moment coefficients that were derived from the outputs of the strain-gage balance were also calculated using the Taylor Series method of error propagation, combining both the precision of the outputs and the estimated bias in the instrumentation systems. The primary influence on the precision intervals for the store force and moment coefficients was the large inertial loading attributable to the very heavy store shell and lower balance platform compared to the relatively weak static aerodynamic loads acting on the store. Poor resolution in the value of aircraft acceleration resulted in large uncertainty in the force data. Values of the statistical precision intervals for the force and moment coefficients as a function of altitude are presented in Fig. 16.

## 4.0 DISCUSSION OF RESULTS

### 4.1 CONSTANT MACH NUMBER, LEVEL FLIGHT

For nominal Mach numbers of 0.6, 0.7, 0.8, and 0.9, the data from wind tunnel experiments, including average statistical precision intervals for the entire range of angle of attack, are compared in Fig. 17 with all data recorded during unaccelerated, level flight, with AB 1 installed on the MK 83. Depending on Mach number, from approximately 570 to 3,880 data points were recorded during three different sorties on two days of flying. (Note: In all figures, the light, or faded, regions in the midst of the patterns of inflight data represent a very dense population of data points. The photographic process used to reproduce the original graph caused these regions to fade and appear devoid of data points.)

Clearly, because of the requirement to maintain level, unaccelerated flight, the inflight data were acquired in a limited range of angle of attack, corresponding to trim values for the aircraft weight and altitude. A few constant Mach number, low-g terms (g

< 1.5) were included in the flight program, serving two purposes: 1) to assess the performance of the balance during maneuvering flight, and 2) to extend the range of angle of attack over which store loads were recorded. The data recorded during these gentle maneuvers are presented in Fig. 18 and do, in fact, extend over a greater range of angle of attack. The sets of data presented in both Figs. 17 and 18 may be considered together in view of the low-g flight conditions of each set.

In the pitch plane, the agreement between wind tunnel and inflight normal-force and pitching-moment coefficients, respectively, while good for Mach number 0.6, deteriorates with increasing Mach number (Figs. 17a, 17e, 18a, and 18e). The trends with angle of attack are essentially the same for both wind tunnel and inflight data sets, with greater precision (less scatter) evident for tunnel data - a natural result of the tighter control of flow conditions and model attitude maintained in a wind tunnel experiment. Also, the tunnel data were recorded at a near-constant unit Reynolds number ( $3.5 \times 10^6$  per foot), while the inflight unit Reynolds number varied from  $3.5$  to  $5.5 \times 10^6$  per foot. Since an increase in Reynolds number generally correlates with an increase in normal force, the trend of inflight data away from the wind tunnel data is not consistent with a Reynolds number effect.

In the yaw plane, the trend of agreement between wind tunnel and inflight data with Mach number at first appears to be the opposite of that in the pitch plane (i.e., as Mach number is increased, the agreement between wind tunnel and inflight side-force coefficient appears to improve) (Figs. 17b and 18b). For the wind tunnel experiments, side-force coefficient was essentially independent of Mach number throughout the subsonic regime. If the inflight data are superimposed without regard to Mach number, as in Fig. 19, it becomes clear that the coincidence of wind tunnel and inflight data for Mach number 0.9 (compare Figs. 17b and 19b) is simply the intersection of two curves that are independent of Mach number - one curve fitting the wind tunnel data for side-force coefficient, and one curve fitting the inflight data for side-force coefficient - each representing slightly different functions of angle of attack of the store. (A more complete discussion of Fig. 19 is presented in Section 4.2.) The different functional relationships between side-force coefficient and angle of attack for wind tunnel and in-flight data is unexplained, but see Section 4.3 for a brief consideration of store-to-aircraft misalignment.

Axial-force and rolling-moment coefficient data for both the wind tunnel and flight experiments agree extremely well. Both magnitudes and trends with angle of attack match well throughout the subsonic regime (Figs. 17c, 17d, 18c, and 18d).

## 4.2 FLIGHT WITH MODERATE MANEUVERS

Several maneuvers such as climbs, pushovers, dives, and wind-up turns were included in the flight program, providing the opportunity to acquire data over a wider range of angle of attack than could be achieved in trimmed flight. During these maneuvers, Mach number, angle of attack, altitude, and acceleration of the aircraft varied. To gain as much use of the inflight data as possible, all data points recorded during maneuvering flight have been superimposed on one set of axes in Fig. 19, together with all data from the wind tunnel experiments. Inflight data are presented as individual points, recorded at the rate of ten per second. As described in Section 4.1, the "core" regions in the pattern of data points that appear to be devoid of points are, in fact, totally filled with points, and should have been reproduced as completely black. These improperly-reproduced regions are useful, however, in visually defining the trend of the data. The wind tunnel data are presented as a band of all data for Mach numbers 0.6 to 0.9, the same range of Mach number as for flight, with the data precision intervals for the extreme Mach numbers serving as bounding curves. The relatively weak dependence of the static aerodynamic load coefficients upon Mach number is apparent.

Two comparisons are made on each page of Fig. 19. At the top of each graph, all inflight data are presented, irrespective of aircraft acceleration in the  $Z_B$  direction. [Note: Balance gage and accelerometer outputs were nulled on the ground prior to flight (i.e., in an equilibrium state); hence, any similar straight-and-level, unaccelerated, equilibrium flight condition would be considered to be 0-g flight, not the customary 1-g description. All references to flight condition g's are made in this context.] The range of aircraft acceleration for the flight program was approximately -1.5 to 4.5 g's. At the bottom of each graph in Fig. 19, the wind tunnel data are again displayed just as at the top, but only those inflight data points recorded when the aircraft acceleration in the  $Z_B$  direction was less than 1.3 g's are presented, for reasons discussed below.

For normal-force coefficient (Fig. 19a), a scattering of inflight data points is noted in the range  $2 \text{ deg} < \alpha_S < 6 \text{ deg}$ , well outside the trend established by the overwhelming majority of other points. These points correspond to those portions of the maneuvering flights during which the acceleration of the aircraft (and store) in the  $Z_B$  direction was greater than 1.3 g's, an acceleration derived in the following manner.

In the middle of the range of angle of attack for which the discrepancy occurs (i.e.,  $\alpha_S = 4 \text{ deg}$ ), the value of  $C_N$  indicated by both the wind tunnel data and the trend of adjacent low-g flight data is approximately  $C_N \approx 0.1$ . For this flight condition, it was noted that  $q = 800 \text{ psf}$ ; hence, the static, aerodynamic normal force that should have been sensed by the balance was

$$\begin{aligned}
 F_N &= C_N q_\infty A \\
 &\approx (0.1) (800) (1.069) \\
 &\approx 85 \text{ lb}
 \end{aligned}$$

In Section 2.4.3, it was noted that because of the mass of the store shell and lower platform of the balance, the strain gages were subjected to an inertial load of 661 lb per g of acceleration. Hence, when  $A_z = 1.3$  g, the inertial load was

$$\begin{aligned}
 F_{N_{ST}} &= A_z W_N \\
 &\approx (1.3) (661) \\
 &\approx 860 \text{ lb}
 \end{aligned}$$

Since the cited uncertainty in the accelerometer output was  $\pm 0.1$  g (Table 2), then the uncertainty in the inertial tare load for normal force was

$$\begin{aligned}
 \Delta(F_{N_{ST}}) &\approx \Delta A_z F_{N_{ST}} \\
 &\approx (\pm 0.1) (860) \\
 &\approx \pm 86 \text{ lb}
 \end{aligned}$$

Therefore, when  $A_z$  was greater than 1.3, the uncertainty in the inertial tare load for normal force exceeded, in many cases (depending on  $q$  and  $\alpha_S$ ), the expected static aerodynamic normal force. Hence, if the inflight data points recorded when  $A_z > 1.3$  are ignored as inaccurate, the correlation of the remaining data points is improved, as indicated by the curves presented on the lower halves or lower graphs in Fig. 19. Significant improvement in correlation is noted for rolling-moment coefficient, Fig. 19d, for which many of the inflight data points in the upper graph appear to have been recorded at a constant value of  $C_l \approx 0$ , representing a saturation of strain-gage output and/or mechanical fouling. Such data are clearly invalid. Data points in the range  $\alpha_S > 6$  deg were, for the most part, recorded during high-g maneuvers and therefore were ignored. However, those points that remain were recorded during a low-g approach to landing, the only such low-g, high angle-of-attack "maneuver" during which the data tape recorder was allowed to run.

An additional source of uncertainty in the inertial loading was the heater system used to maintain a constant temperature range inside the accelerometers. As mentioned in

Section 2.4.4.3, a 0.045-g shift in the output of the Z-axis accelerometer was noted when the heater operated during calibration at the AEDC. Such a shift would appear as an inertial tare variation of

$$\begin{aligned}\Delta F_{N_{ST}} &= \Delta A_Z W_N \\ &= (0.045) (661) \\ &\approx 30 \text{ lb}\end{aligned}$$

which was larger than the expected static aerodynamic load in many cases, especially near  $\alpha_S = 5$  deg.

As an explanation of some of the observed discrepancies between wind tunnel and flight data, the quality of the aerodynamic simulation in the wind tunnel was considered, specifically with respect to the boundary-layer development over the store model. On the basis of some inflight data recorded during the first flight, however, such an explanation was rejected as inadequate. The first flight was a system checkout flight, during which the only store mounted on the TER was the instrument-equipped store on the bottom center TER station. With a fully loaded TER, a rather constricted flow passage is created between the three stores, in which some regions of locally supersonic flow could exist. If the character of the boundary layer were not simulated properly in the wind tunnel because of discrepancy between wind tunnel and flight Reynolds numbers, then the interaction of the store boundary layers with any pressure disturbances attributable to the supersonic flow, or with other boundary layers, could result in different pressure distributions over the stores and different store loading as compared with the flight configuration. However, without the two inert store casings mounted on the "shoulder" stations of the TER, there was no constricted flow passage, and little probability of regions of supersonic flow. A comparison of data from the first flight with some available wind tunnel data was therefore undertaken and is presented in Appendix A.

Two other explanations for the discrepancies between tunnel and flight data, especially in the longitudinal plane, were considered. First, since angle of attack of the store was assumed to be simply one deg less than the angle of attack of the aircraft, the validity of the measurement of aircraft angle of attack could be questioned. Specifically, in a 3- or 4-g pullout, the boom supporting the aircraft attitude vanes was suspected of deflecting, creating a bias in the measurement of angle of attack. However, even though such deflection was possible, an inspection of the pitching- and yawing-moment coefficient data indicated that such an explanation was not satisfactory. For example, according to Fig. 19e, a shift of the flight data by an angle of attack of +2 deg would be

required to improve the correlation. However, it can be seen in Fig. 19 that a shift of -2 deg would be required. An improvement in the correlation for one component would be accompanied by a deterioration in the correlation for another component. Hence, although deflections of the boom are possible, they cannot be cited as the complete explanation of tunnel-flight discrepancies.

The flight path during maneuvers is curved, whereas "flight" in the wind tunnel is always straight. However, the radius of curvature of the flight paths was quite large during most maneuvers, on the order of 10,000 ft. Hence, the contribution of the local flight path angle to the aircraft angle of attack over the 60-ft length of the aircraft is negligible.

### 4.3 ALTERED AFTERBODY, AB 2

Two sorties were flown with the instrumented MK 83 store casing fitted with the altered afterbody configuration, AB 2 (Fig. 12). Correlation with wind tunnel data is presented in Figs. 20 and 21 for constant Mach number, level flight, and in Fig. 22 for maneuvering flight. As for AB 1 (Section 4.1), Figs. 20 and 21 can be considered together, since the only difference between the two sets of data relates to a relatively minor difference in maneuvers represented. In Fig. 20, only data for trimmed, level attitude flight are included, but in Fig. 21, data for some low-g turns and pushovers, all within  $\pm 500$  ft of the entry altitude, are presented.

Correlation between wind tunnel and inflight data is of the same character as for AB 1. Since the AB 2 can be considered simply another store configuration, fundamental fidelity in the modeling process is probable. The discrepancies between wind tunnel and inflight data could be attributed to a bias in either store attitude or fin attitude. The former is more likely, since in both wind tunnel and flight procedures for store installation the forebody, centerbody, and balance components of the configuration were undisturbed when the change was made from AB 1 to AB 2 or vice versa. Both full-size and scale-model afterbody shapes were of one-piece construction and were attached to the centerbody with screws. It is unlikely that a bias between afterbody and aircraft could be repeated when such a change in configuration was made. A bias in the centerbody/balance/TER alignments, however, would have remained throughout the experiments and could contribute to an explanation of the tunnel-flight discrepancies. Indeed, a constant shift of the force and moment data at zero angle of attack for all Mach numbers, for both afterbody shapes, would result in an extraordinary correlation. For example, at  $M_\infty = 0.6$ ,  $C_{N_\alpha} \approx -0.09$  (Fig. 20a). A shift of -0.15 in  $C_N$  at  $\alpha_S = 0$  would improve the correlation at all Mach numbers. The bias in angular alignment required to cause such a shift would be

$$\begin{aligned}\delta (\alpha_S) &= \frac{\delta (C_N)}{C_{N\alpha}} \\ &\approx \frac{-0.15}{-0.09} \\ &= 1.7 \text{ deg}\end{aligned}$$

It is conceivable that a bias of 1.7 deg could occur during installation of the store and/or store model. As an example of the latitude in geometric fidelity allowed among randomly selected samples of the same store configuration, the stores of this flight program should be considered. The distances measured between nosetips and tail tips of the same two stores, as installed on the aircraft, differed by as much as 1.5 in., indicating a "camber" in an off-the-shelf store of perhaps 3/4 of a degree. This type of routine bias, existing as it apparently does among mass-produced items, could easily account for many of the observed tunnel-flight discrepancies.

#### 4.4 COMPARISON WITH OTHER WIND TUNNEL DATA

Comparisons of all constant Mach number, level-flight data, including turns, with other wind tunnel data (in addition to the AEDC/4T data) are presented in Figs. 23 and 24 for AB 1 and AB 2 configurations, respectively. A series of experiments was conducted at the ARA in 1977 with essentially the same configurations as those in the AEDC/4T experiments and in the flight program, but using 1/12-scale models (see Appendix A). Data were recorded for both AB 1 and AB 2 configurations, using both natural, or free, transition and artificially fixed transition techniques. Only the fixed-transition data are presented, since there is evidence that transition occurs early in Tunnel 4T because of noise generated at the holes in the perforated walls and/or because of contamination of the flow with particles that roughen the model surfaces on impact.

In addition to the ARA data, a few points were gleaned from experiments conducted in 1975 at the David Taylor Naval Ship Research and Development Center (DTNSRDC) at Carderock, Maryland (Ref. 8). One-tenth scale models were used in a series of grid studies (i.e., loads acting on the MK 83 store were measured at points of a spatial grid of locations beneath an F-4 aircraft model). The store model was mounted on a sting attached to the captive trajectory system (CTS) in the DTNSRDC 7- x 10-ft Transonic Wind Tunnel; therefore, the data were clearly AB 2 data. Comparisons were possible with the AEDC/4T and inflight data sets only at the point in the spatial grid corresponding to the captive position, and of course only for the same Mach numbers. Because of these constraints, only a few data points from the DTNSRDC experiments are presented in Fig. 24.

Except for the yawing-moment coefficient, all three sets of wind tunnel data are in fundamental agreement. (There are no ARA data for axial-force coefficients.) Magnitudes are in reasonable agreement, and the slopes of the coefficient curves as a function of angle of attack are well matched between the AEDC, ARA, and flight data. The discrepancies in coefficient values at zero angle of attack could be attributed to store attitude bias, as discussed in Section 4.3. No explanation is offered for the shape of the ARA yawing-moment coefficient curve at low angle of attack. No trends with scale factor can be established, because of insufficient data.

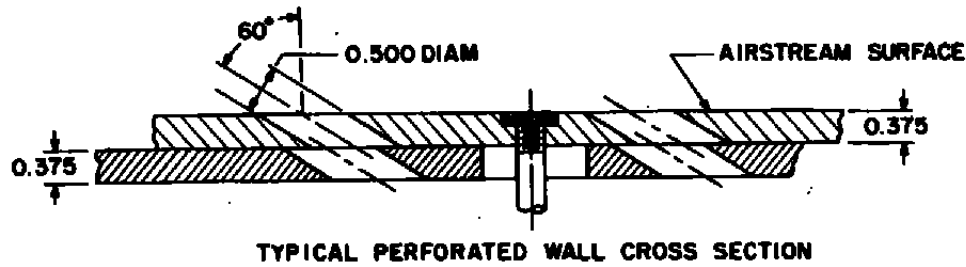
## 5.0 CONCLUSIONS

In a coordinated set of experiments, static aerodynamic loads acting on a low-drag bomb shape mounted in the captive position under the wing of a contemporary fighter aircraft were measured in three different wind tunnels with models of three different scale factors, as well as in flight with full-size articles. Efforts were made to maintain geometric similitude despite the differences in scale. Unit Reynolds numbers were matched, as well as nominal Mach numbers. From an analysis of the corresponding data, the following conclusions have been drawn:

1. Fundamental agreement of the trends of captive store loads with angle of attack was established for experiments with 1/20- and 1/12-scale models in wind tunnels, and with full-size hardware in flight. Insufficient data were acquired to make a definitive assessment of scale effects on captive store load measurements.
2. Differences between flight and wind tunnel measurements of store load coefficients at zero angle of attack of the store may be attributed to differences in geometric store alignment between flight and wind tunnel installations.
3. In any flight test program in which it is necessary to isolate static aerodynamic loads from the sum of aerodynamic plus inertial loads attributable to accelerated motion of the aircraft, care should be taken to measure acceleration with instrumentation of appropriate resolution (i.e., the uncertainty of the inertial loads should not be of the same order of magnitude as the aerodynamic loads).
4. The strain-gage balance used in the flight tests was capable (with the caution discussed in item 3 above) of sensing, with appropriate response, store loads in flight with maneuvers of up to 5 g's.

## REFERENCES

1. Dix, R. E. "A Review of Methods of Measuring Aerodynamic Forces and Moments Acting on Captive Stores in Wind Tunnel Tests." AEDC-TR-72-108 (AD902816L), August 1972.
2. Dix, R. E. "Influences of Sting Support on Aerodynamic Loads Acting on Captive Store Models." AEDC-TR-76-1, AFATL-TR-76-25 (ADA022257), March 1976.
3. Dix, R. E. "Comparison of Two Methods Used to Measure Aerodynamic Loads Acting on Captive Store Models in Wind Tunnel Tests." AEDC-TR-76-122 (ADA030208), September 1976.
4. Dix, R. E. "Evaluation of an Internal Balance-Supporting Bracket Simulating Lug Suspension for Captive Stores in Wind Tunnel Tests." AEDC-TR-76-117 (ADA030603), October 1976.
5. Smith, R. E. "Measured Air Loads for a Free-Fall Weapon on an A-4 Aircraft." NWC TP 4804 (AD863534L), October 1969.
6. Smith, R. E. "Prediction of Store-Separation Motion Using Initial Captive Loads." NWC TP 5261 (AD890671L), October 1971.
7. Dix, R. E. "Influence of Sway Braces and Mounting Gaps on the Static Aerodynamic Loading of External Stores." AEDC-TR-77-117 (ADA054963), February 1978.
8. Cooper, G. F., Maddox, A. R., Marshall, J. R., and McCabe, E. F. "Store Separation: State of the Art Review." Proceedings of the 10th Navy Symposium on Aeroballistics, 15-17 July, 1975, Fredricksburg, Virginia.
9. Marsden, P. "Results of Tests on a One-Twelfth Scale F-4K Phantom Model Fitted with MK 83 1,000-lb Low Drag Bombs Supported on a Variety of USAF and RAF Triple Ejector Release Unit Configurations in the ARA 9 ft x 8 ft Transonic Wind Tunnel." Model Test Note M 48/6, Aircraft Research Association, Bedford, Hants, United Kingdom, December 1978.



DIMENSIONS AND TUNNEL STATIONS IN INCHES

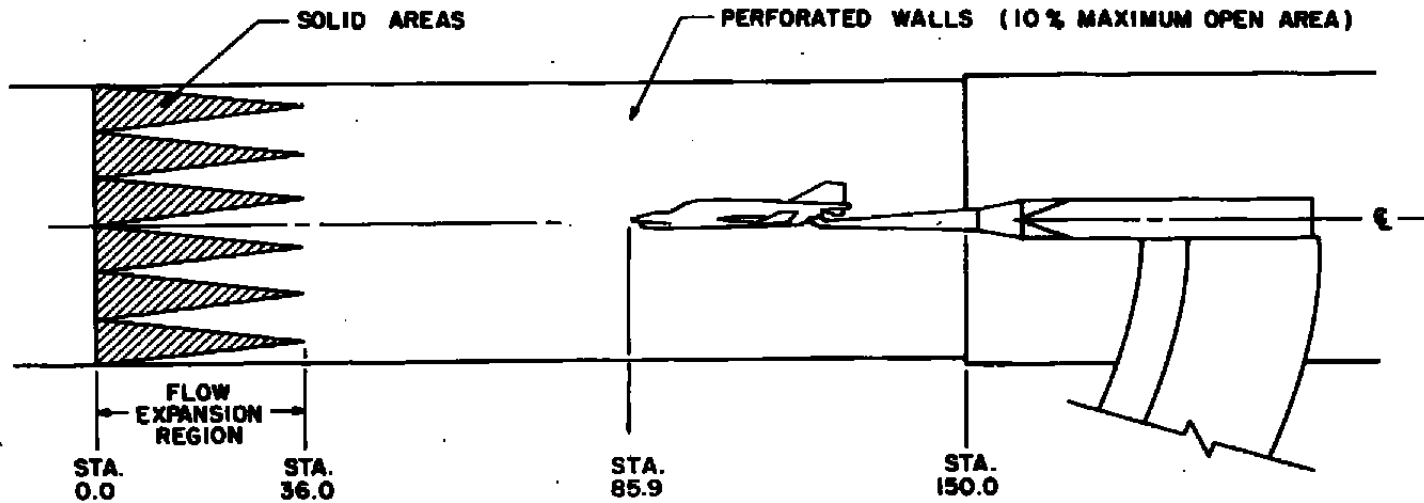


Figure 1. Schematic illustration of a typical model installation in Tunnel 4T.

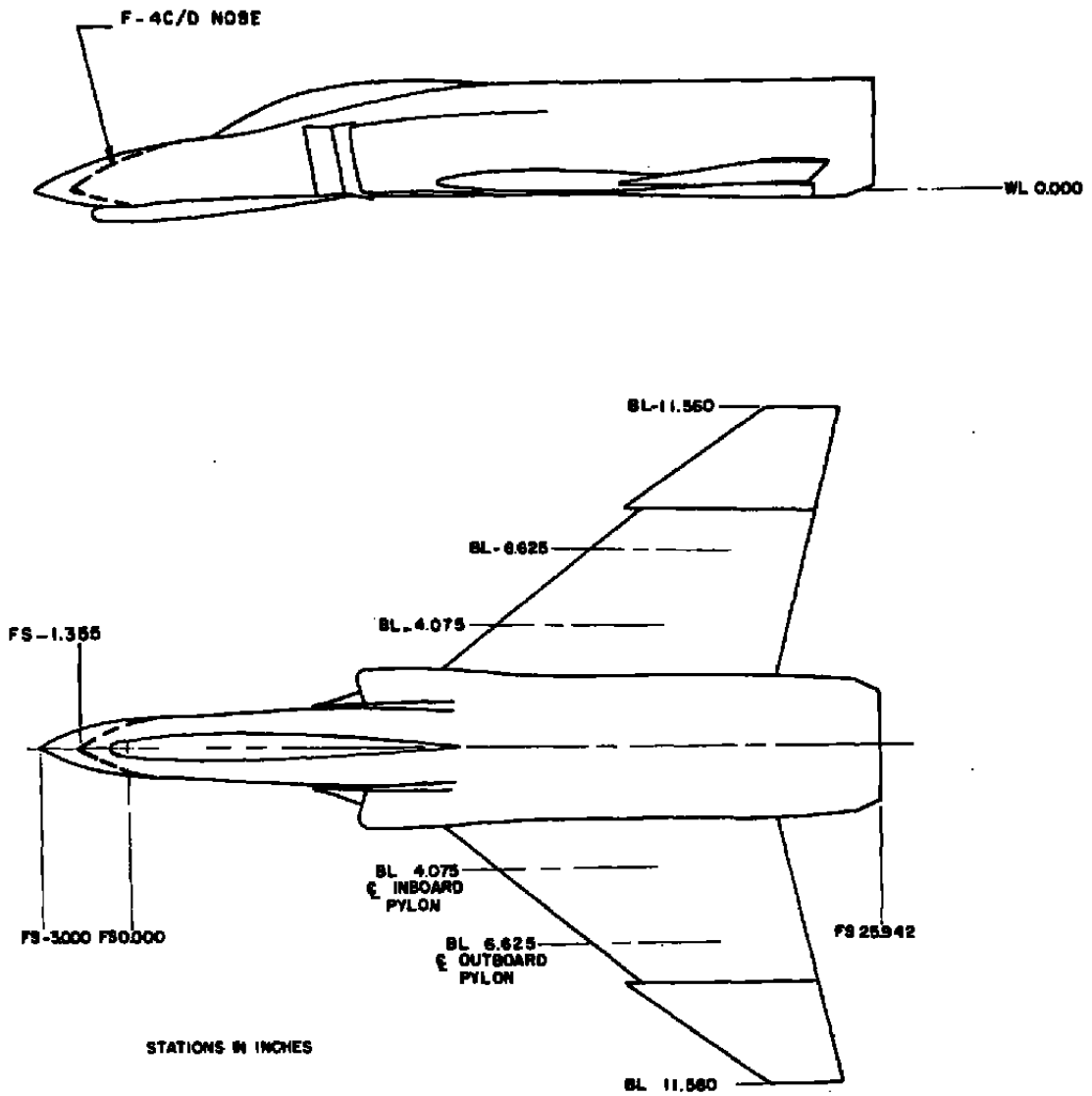


Figure 2. Outline drawing of the 1/20-scale model of the F-4C aircraft.

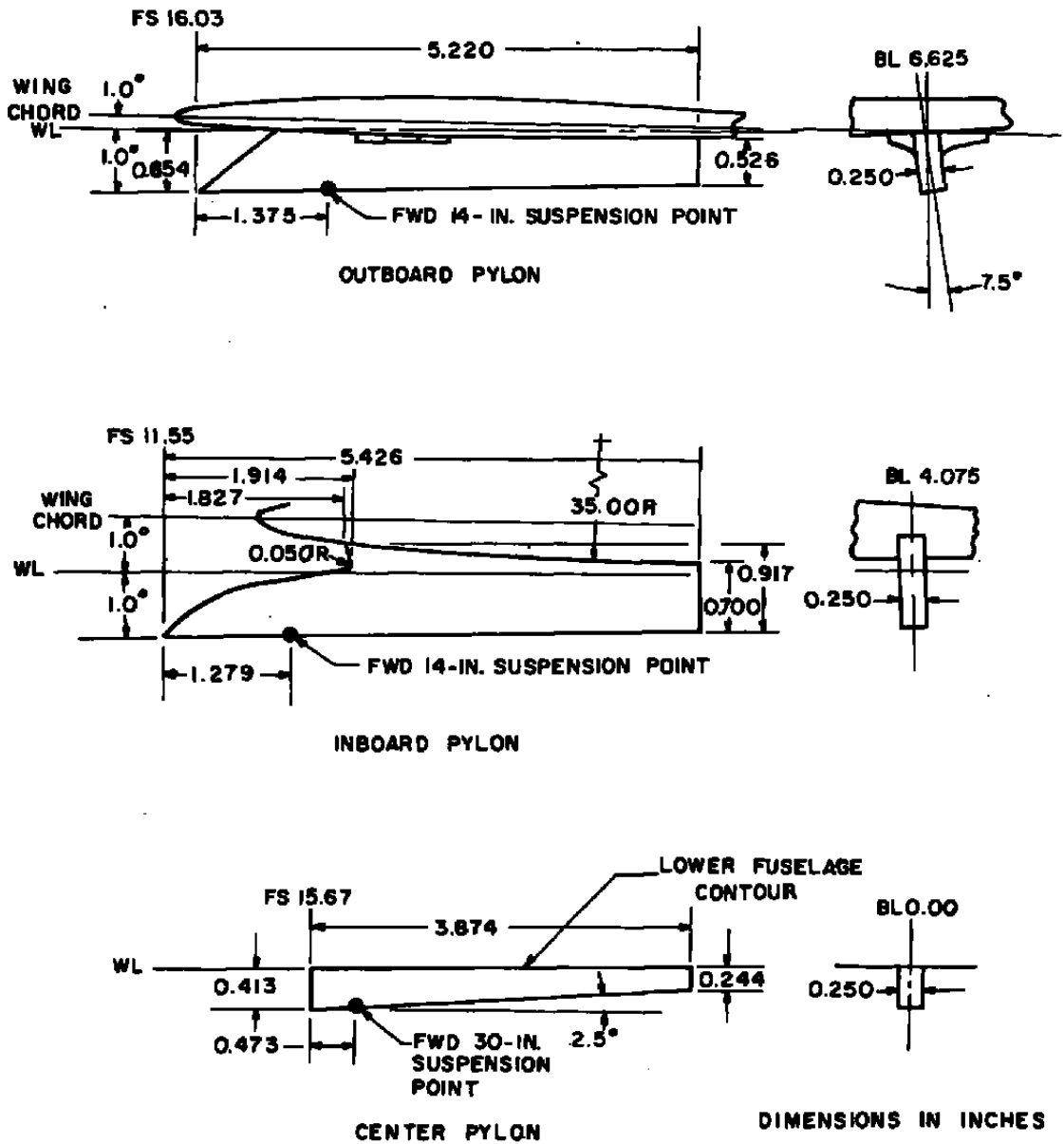
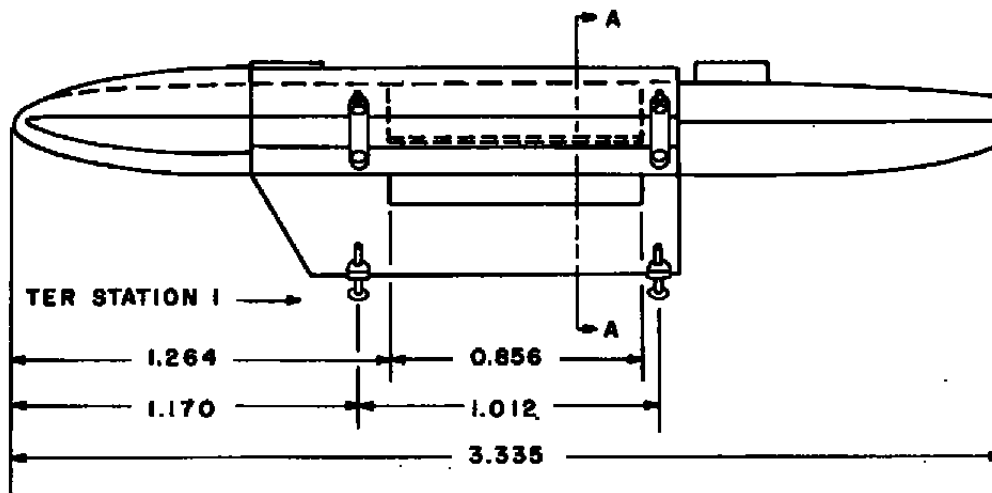
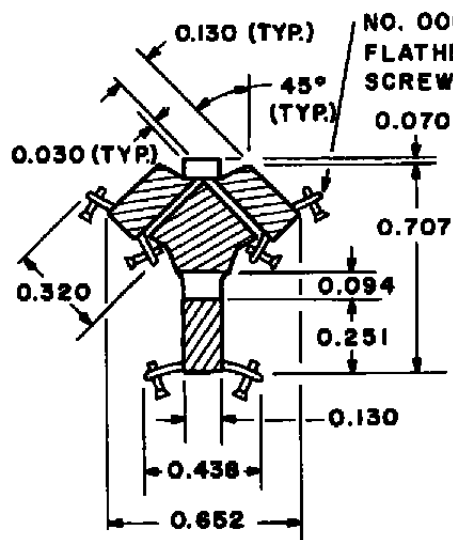
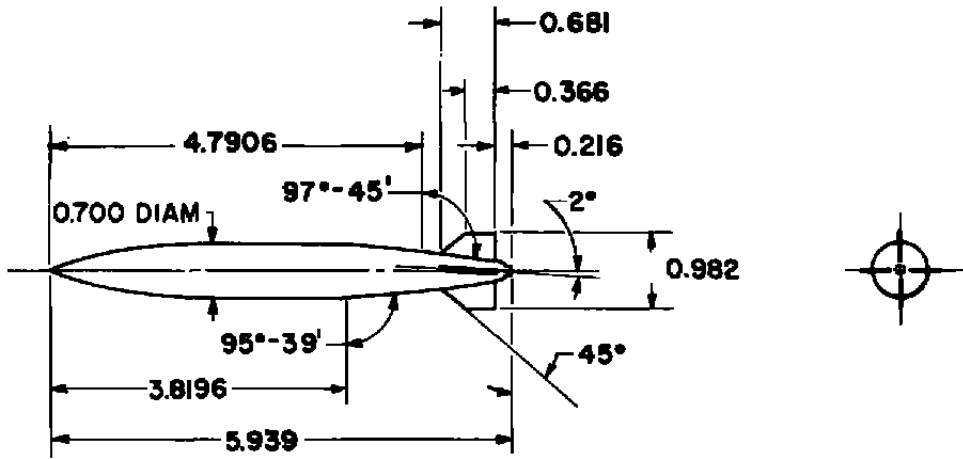


Figure 3. Details of the 1/20-scale models of the F-4C pylons.

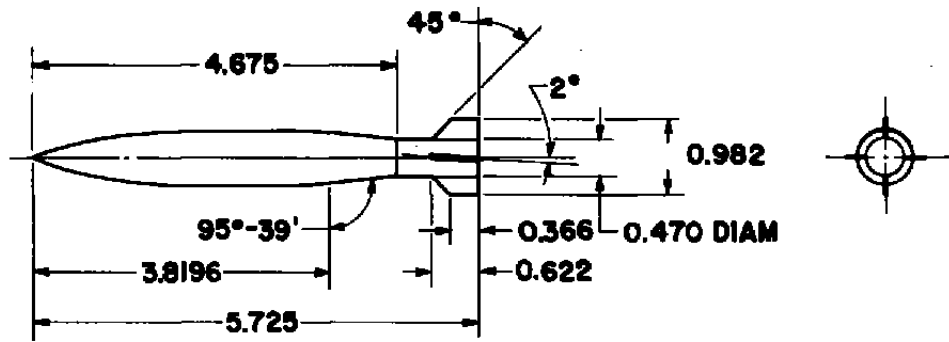


DIMENSIONS IN INCHES

Figure 4. Details of the 1/20-scale model of the triple ejector rack (TER).



ACTUAL CONFIGURATION



CONFIGURATION MODIFIED FOR STING SUPPORT

DIMENSIONS IN INCHES

Figure 5. Details of the 1/20-scale model of the MK 83 store.

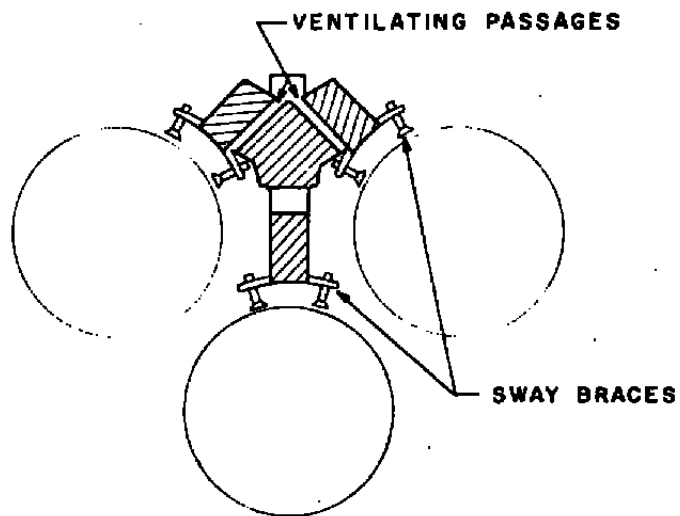
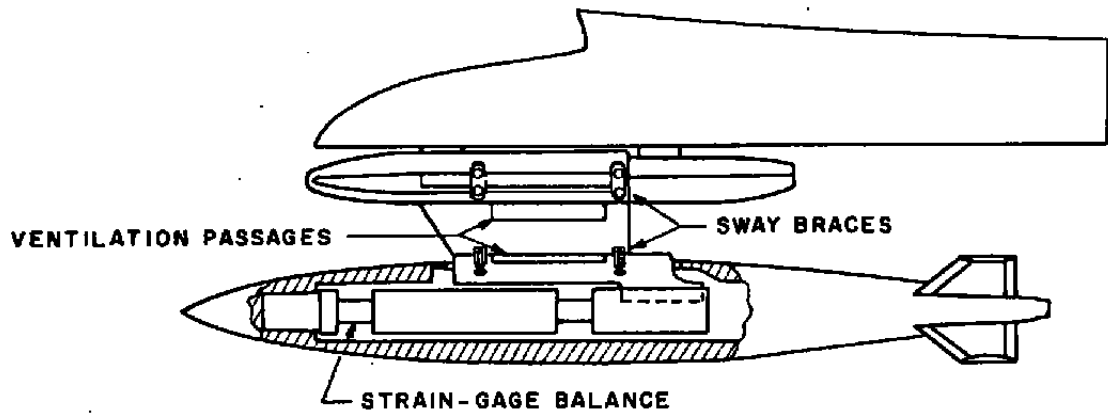


Figure 6. Sketch of the 1/20-scale MK 83/TER model installation.

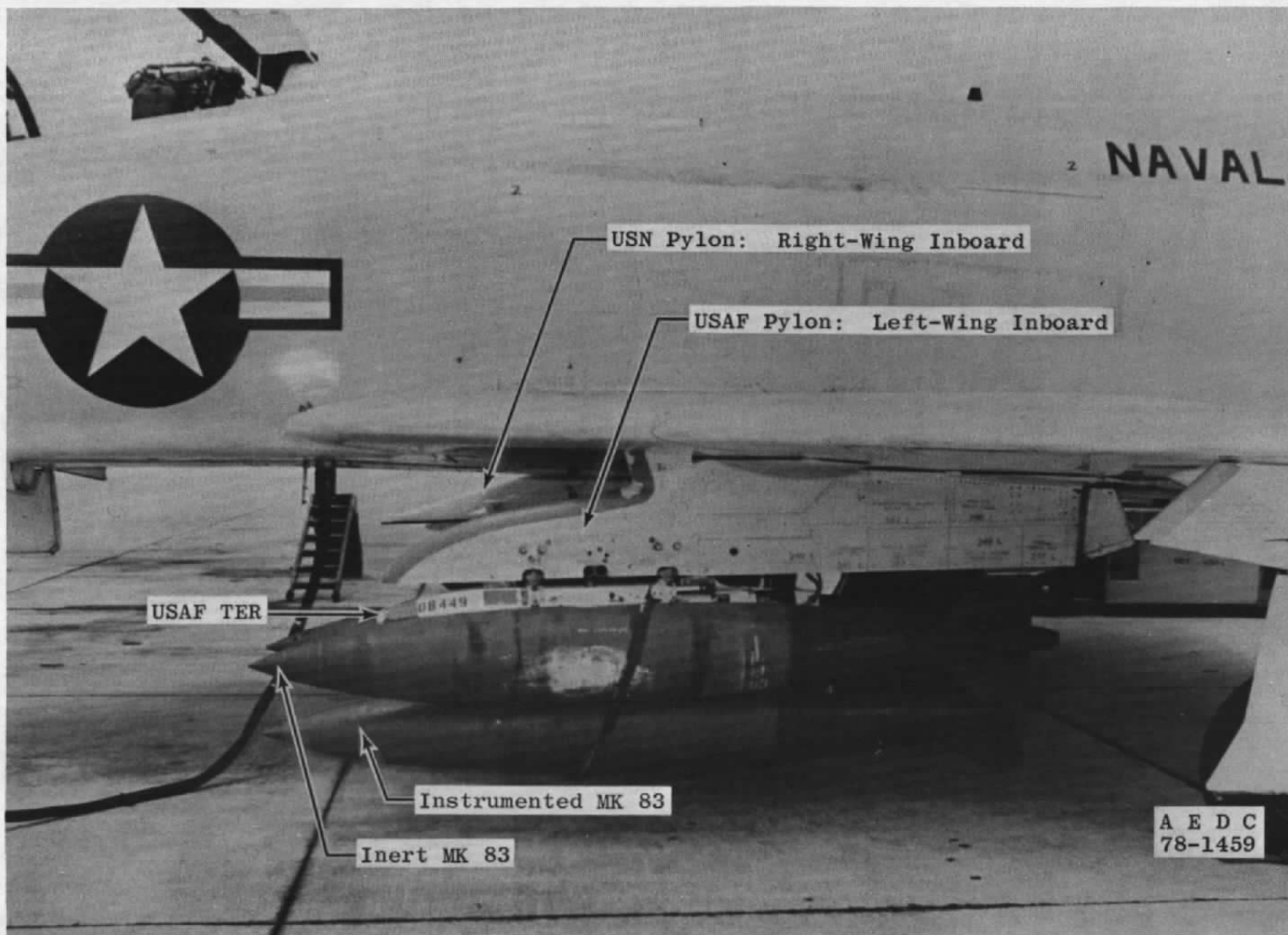
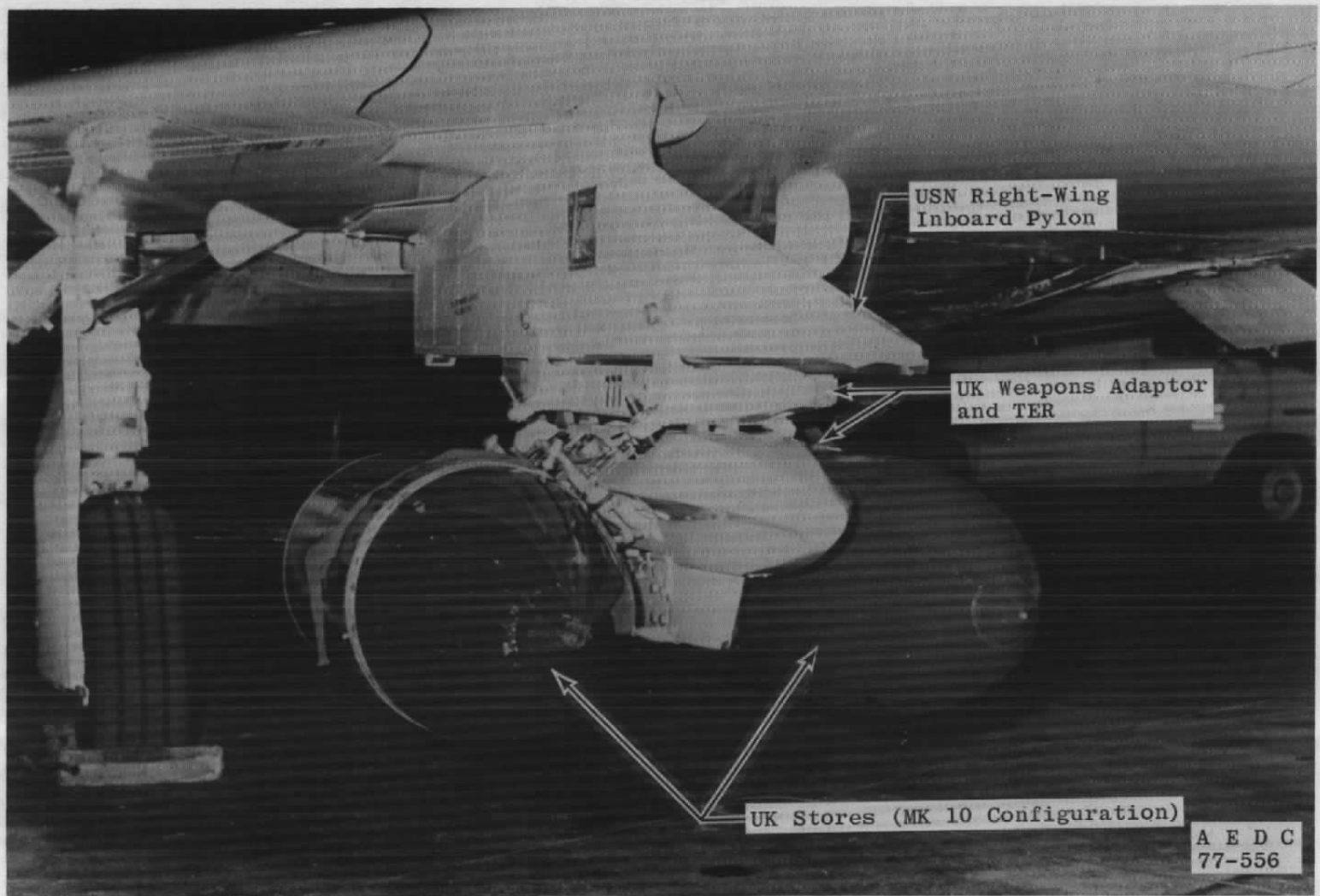
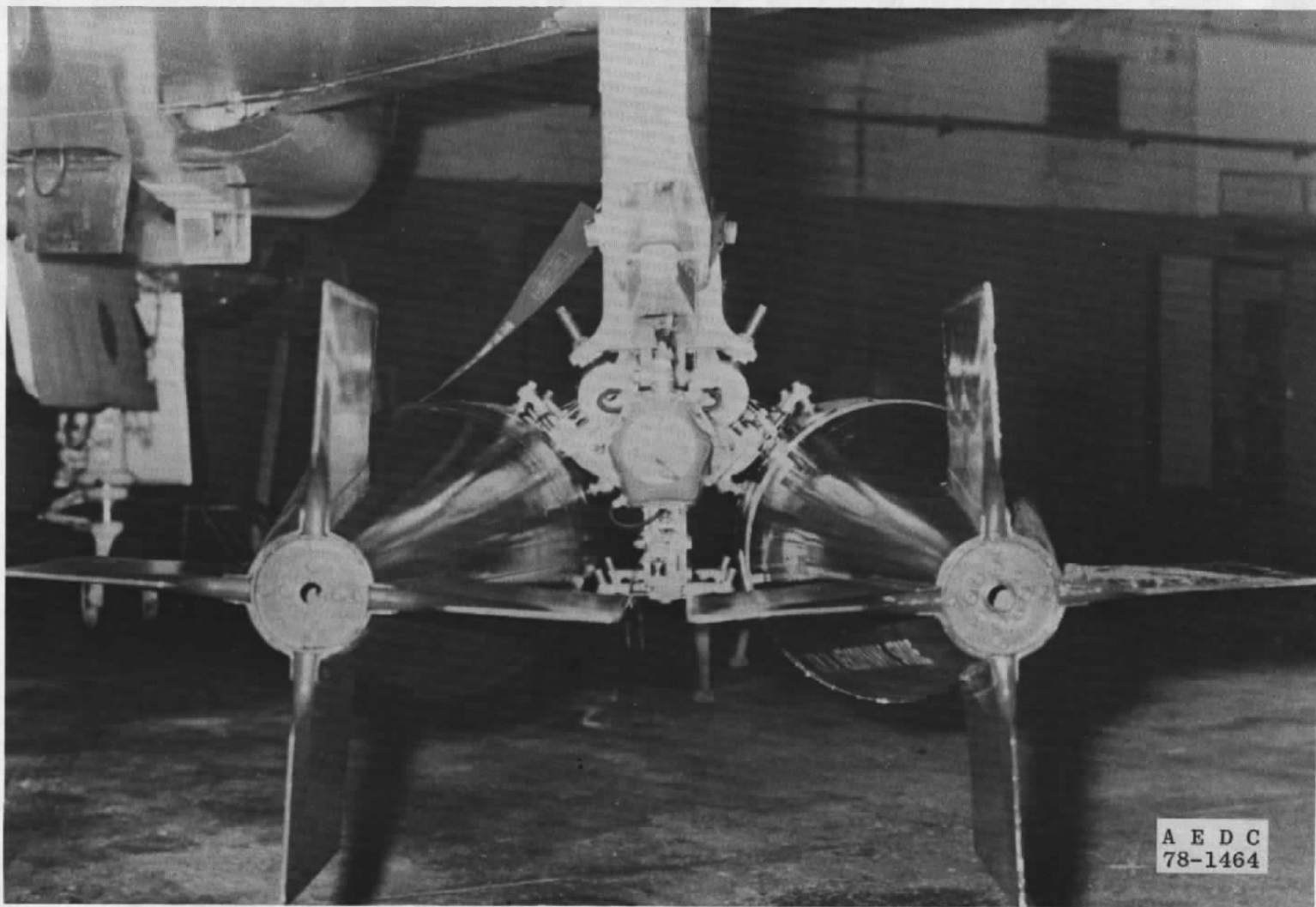


Figure 7. Photograph of the F-4/MK 83 (AB 2) flight test installation.

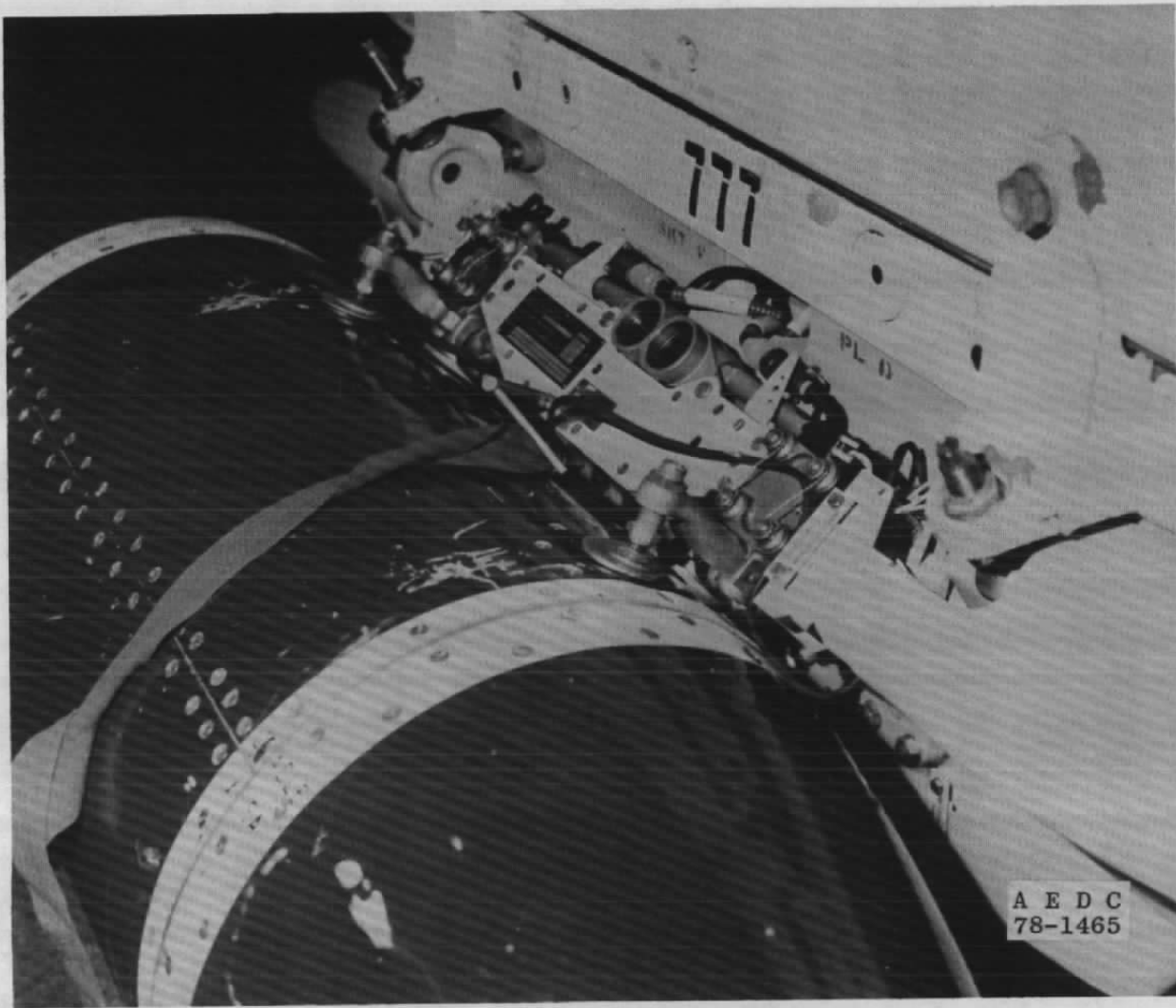


a. Right-wing inboard pylon

Figure 8. Photographs of the UK-sponsored installation on the right wing.



b. View looking forward  
Figure 8. Continued.



c. Closeup of store-TER installation  
Figure 8. Concluded.

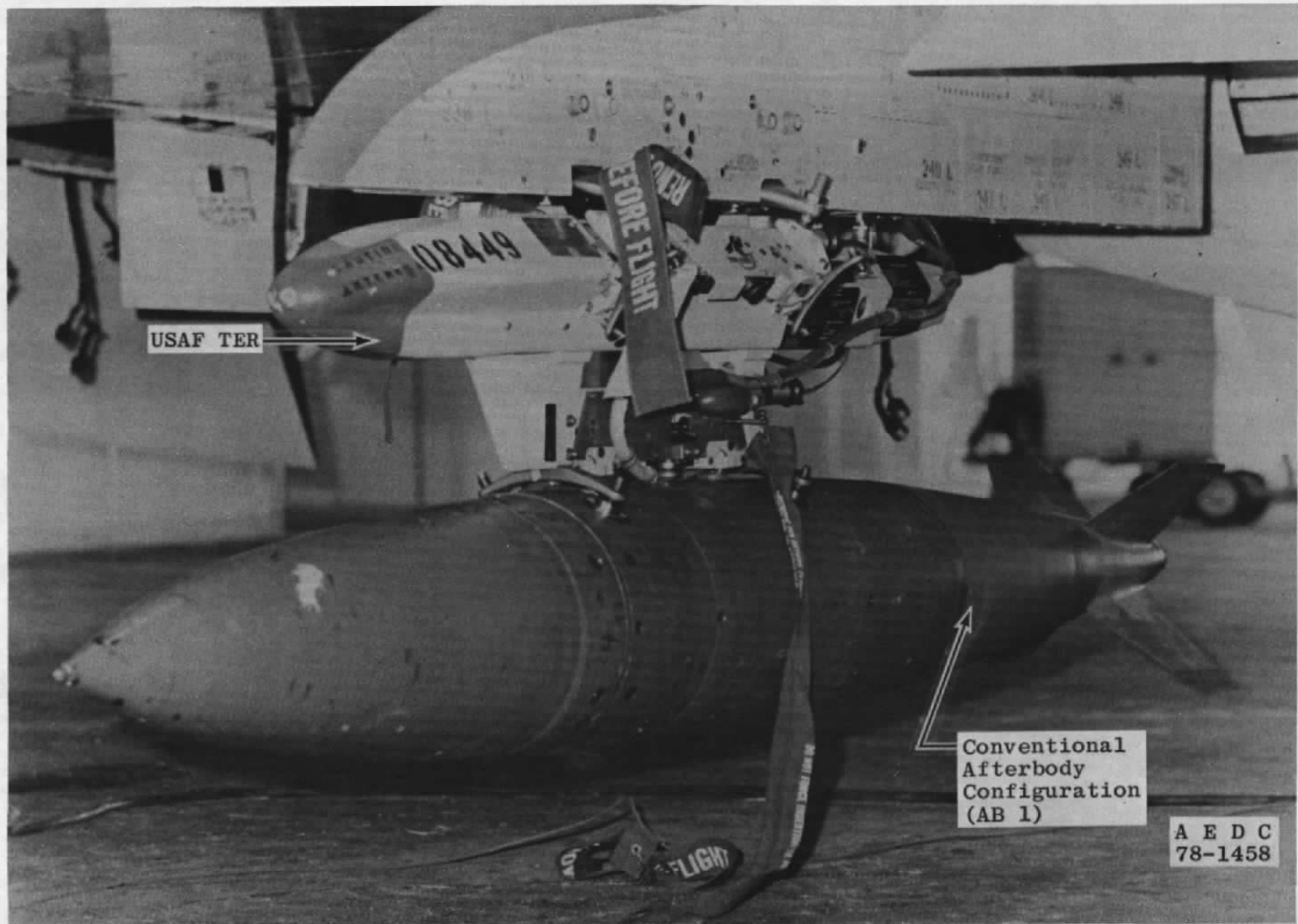
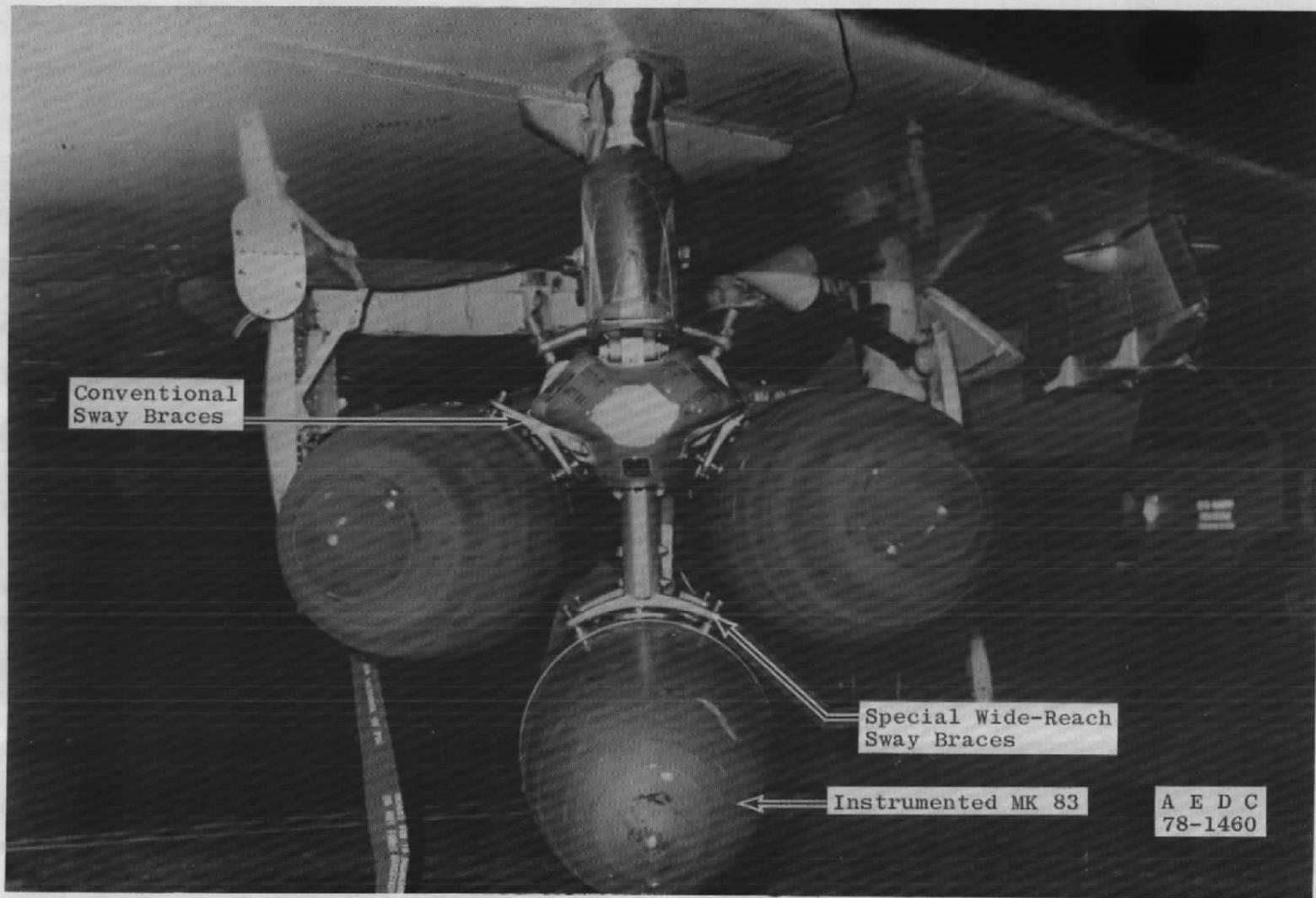
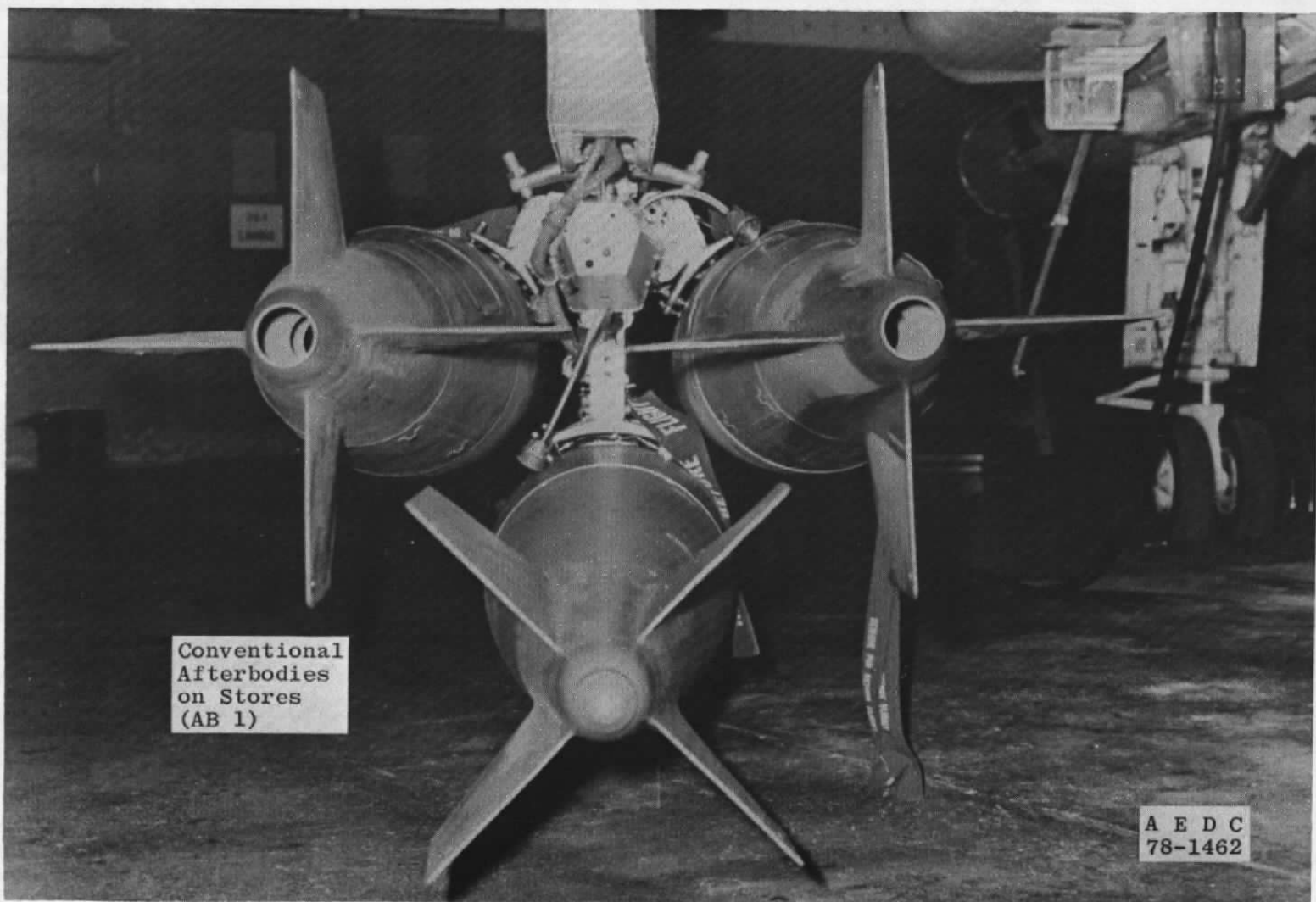


Figure 9. Photograph of the MK 83/TER/left-wing inboard pylon installation, inert stores removed.



a. View looking aft  
Figure 10. Photographs of the flight-ready MK 83/TER installation.



b. View looking forward  
Figure 10. Concluded.

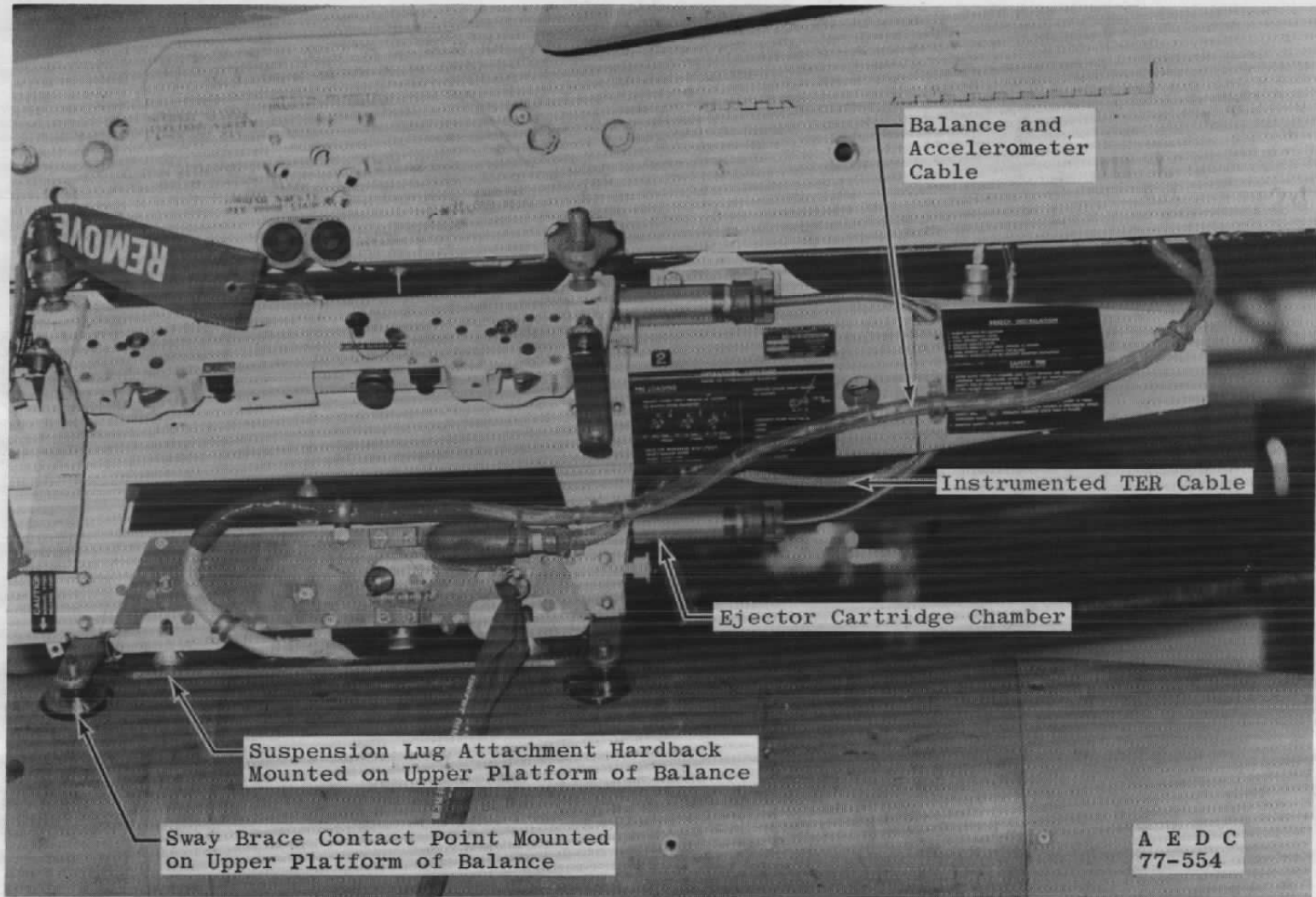
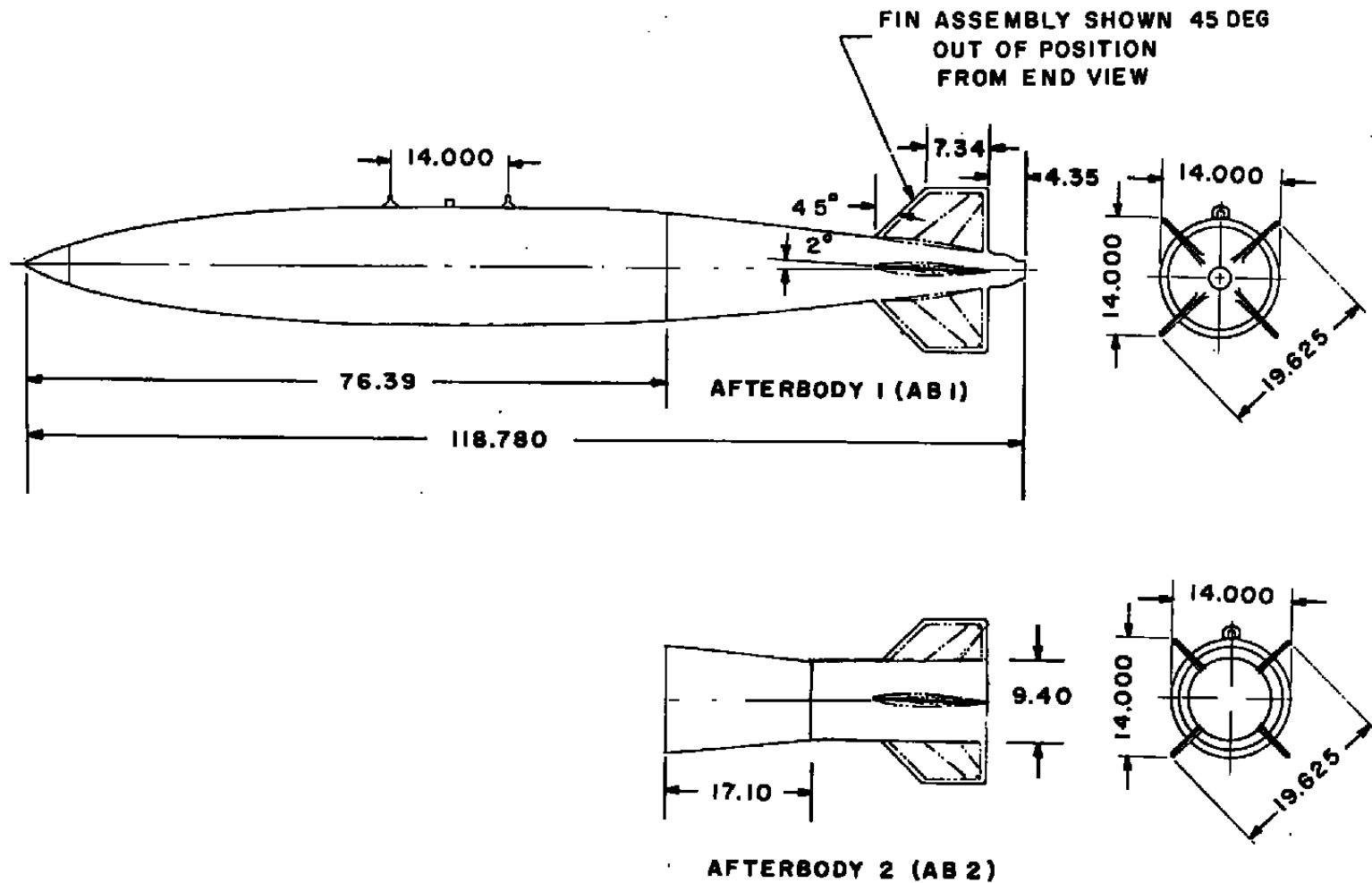
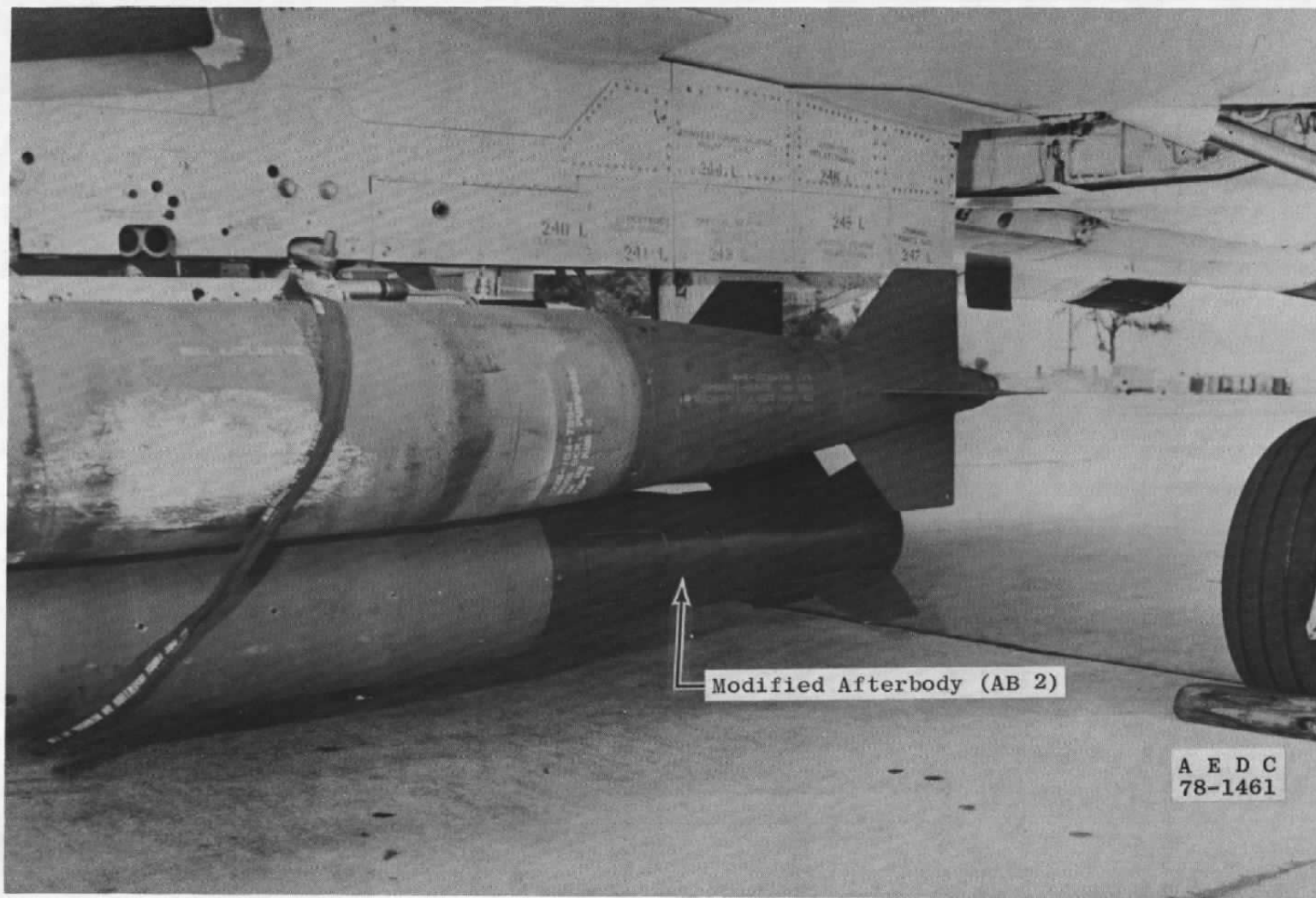


Figure 11. Closeup view of the MK 83/TER/pylon installation.



a. Sketch

Figure 12. Details of the full-size MK 83 store.



b. Photograph  
Figure 12. Concluded.

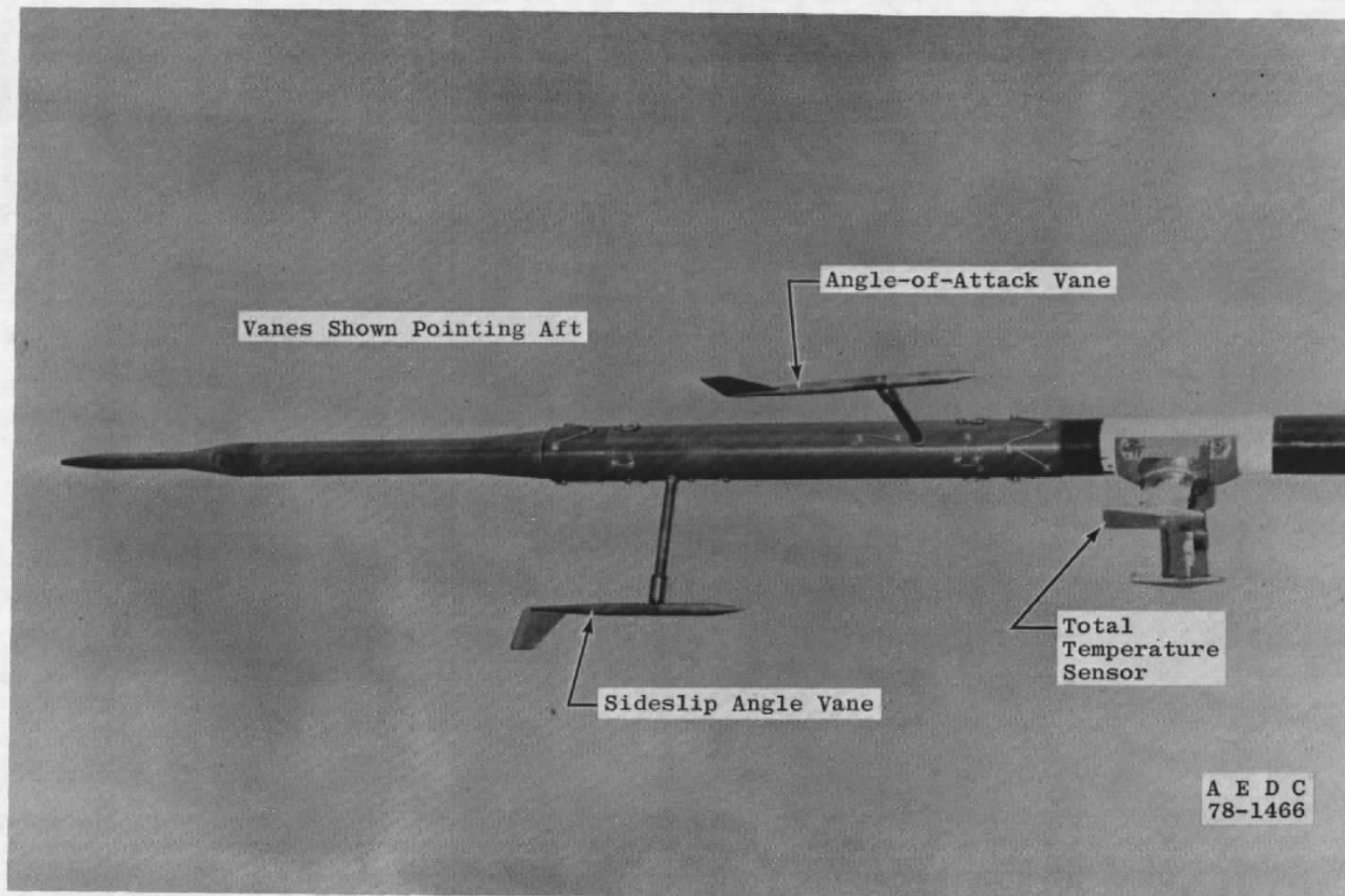
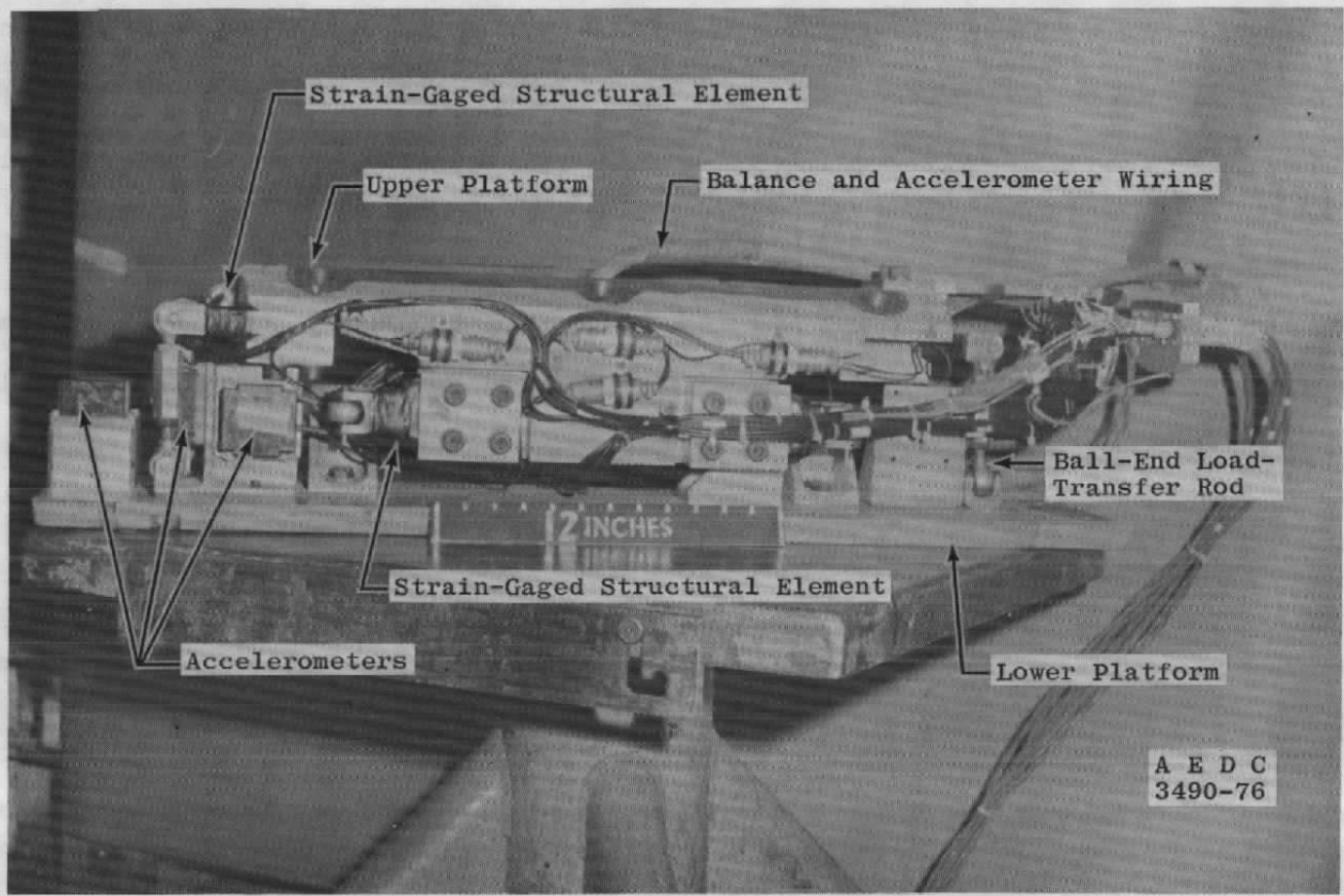
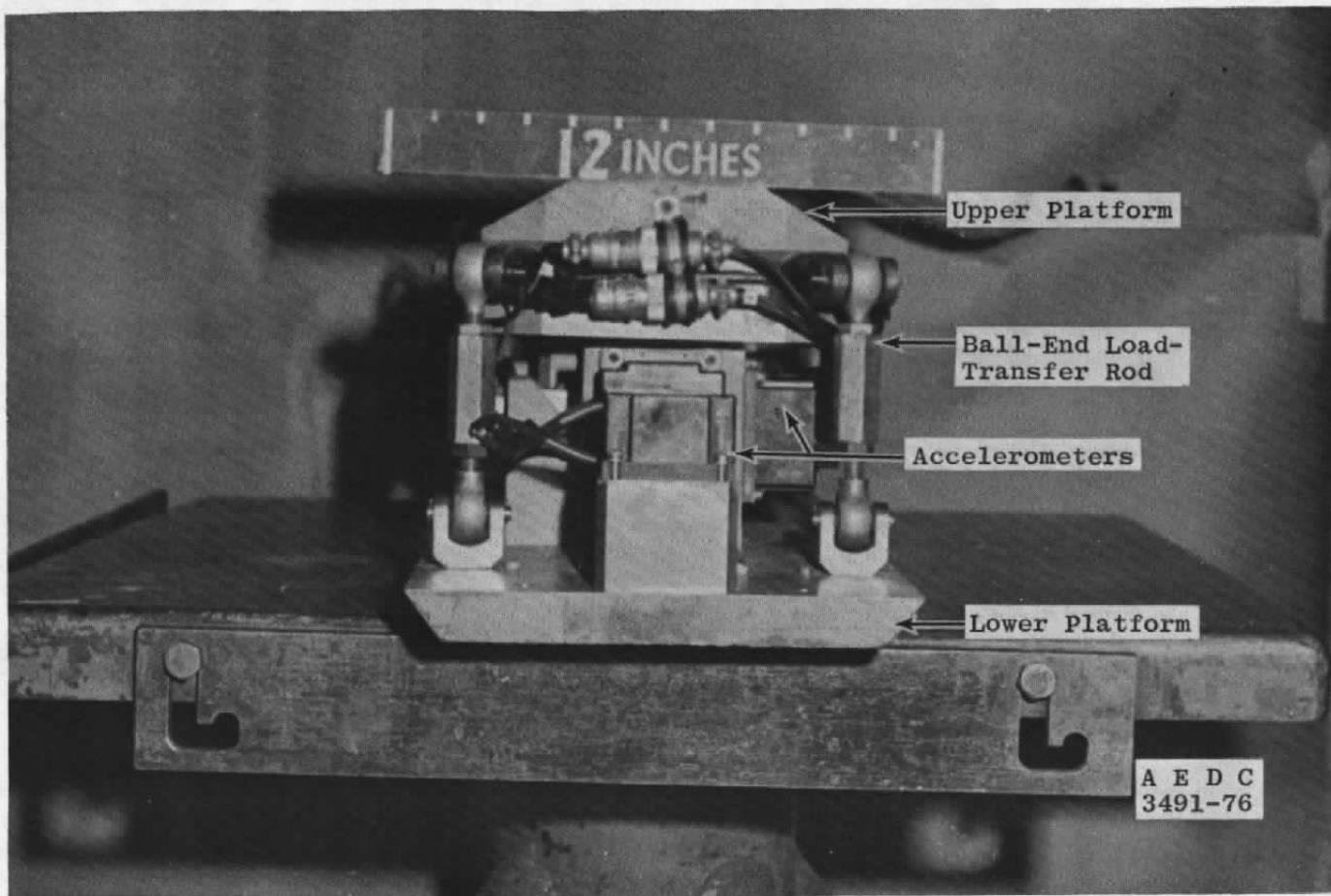


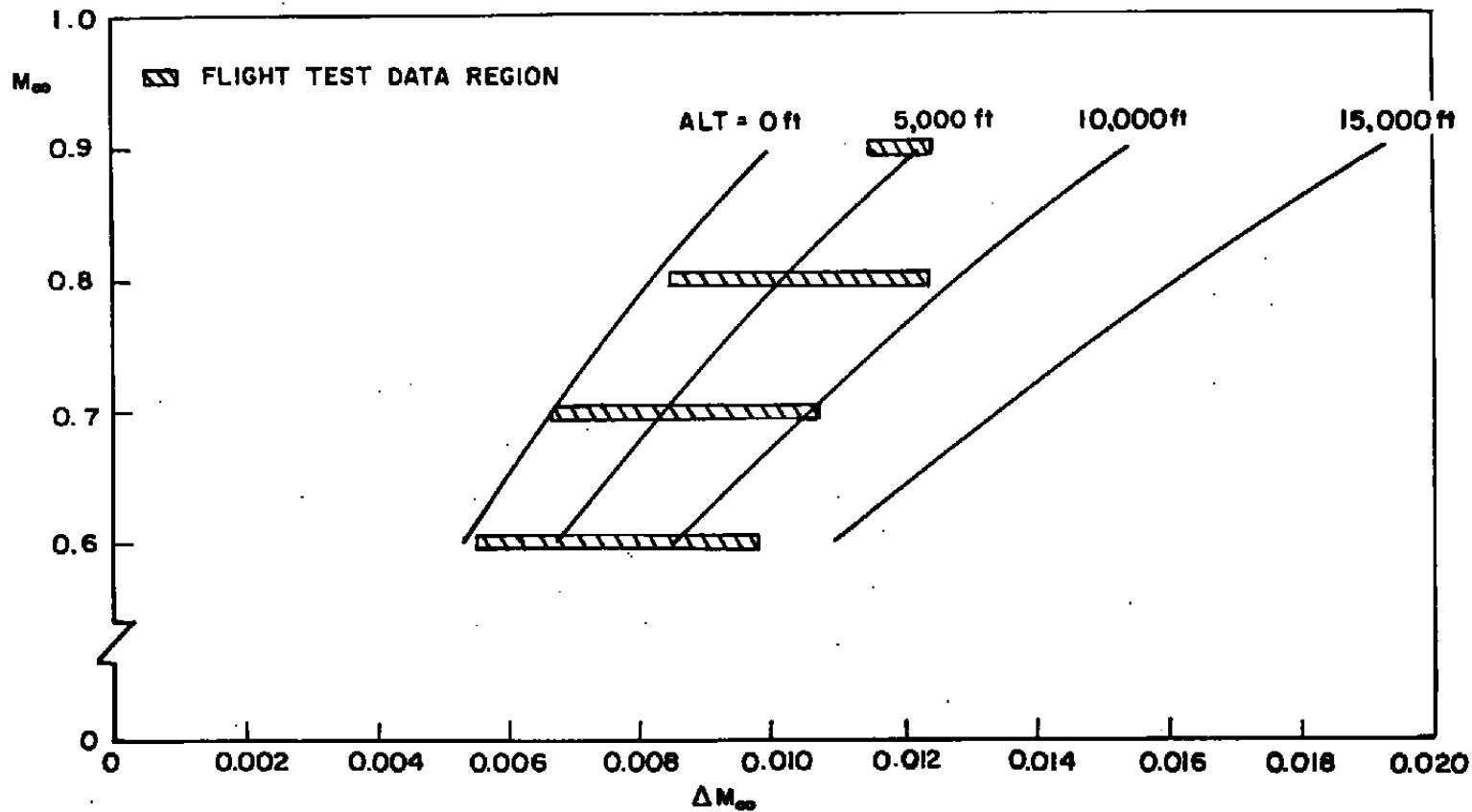
Figure 13. Photograph of the nose-mounted, instrumented boom.



a. Left-side view  
Figure 14. Photographs of the NWC flight-rated balance.



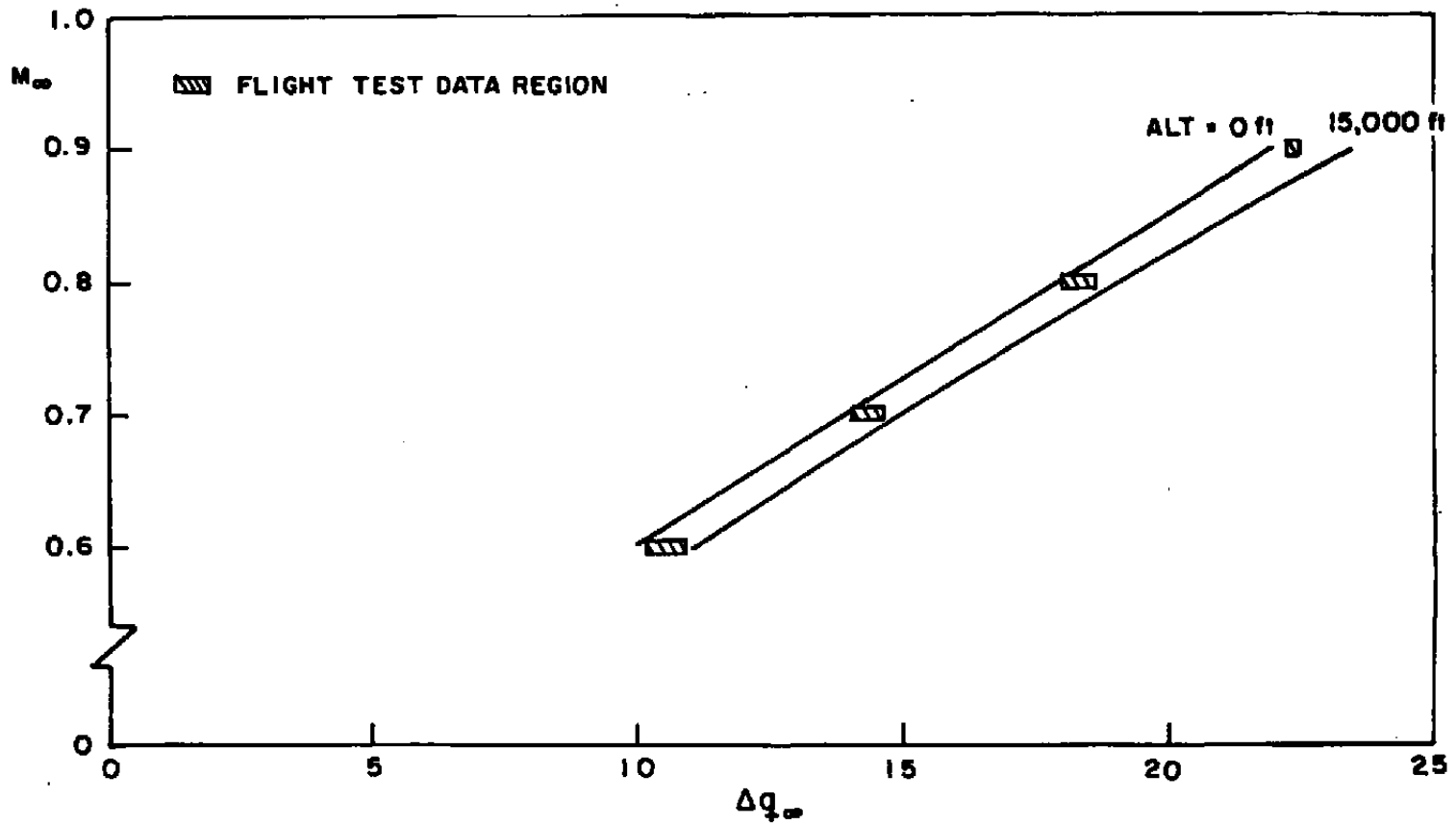
b. Front view  
Figure 14. Concluded.



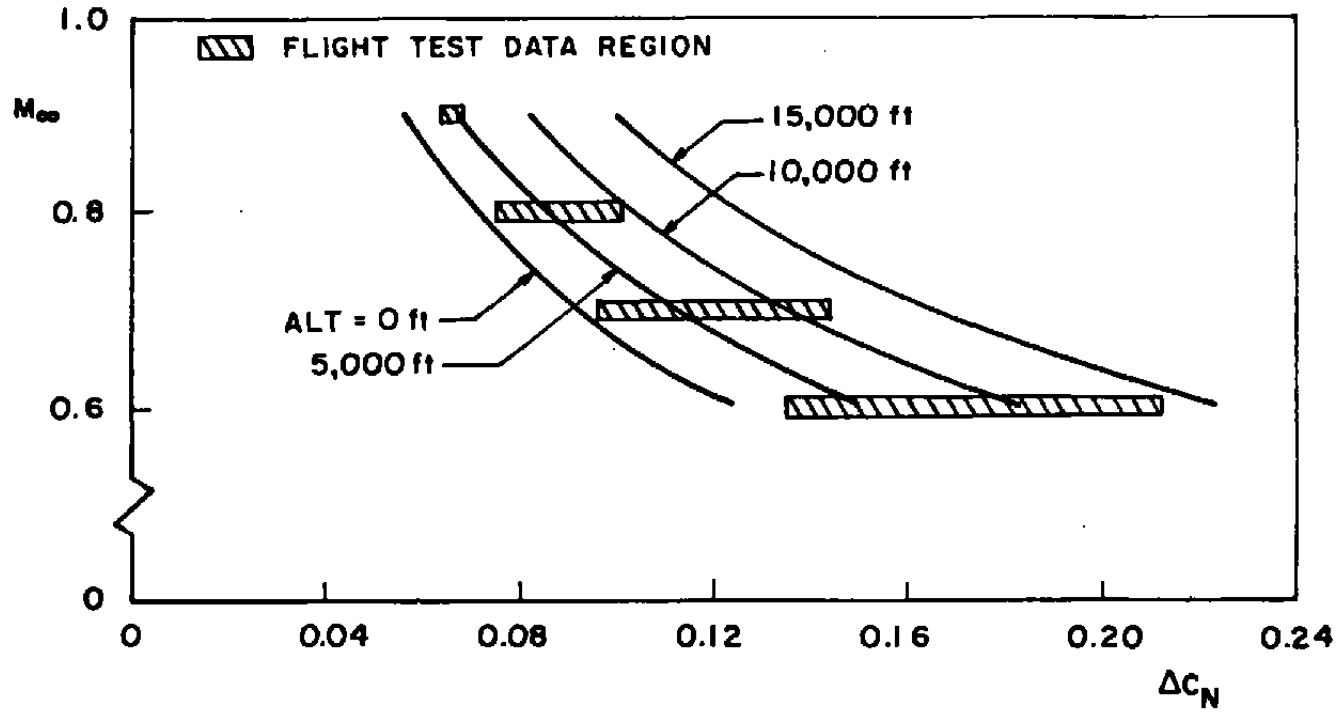
44

a. Mach number

Figure 15. Statistical precision intervals for flight condition parameters.

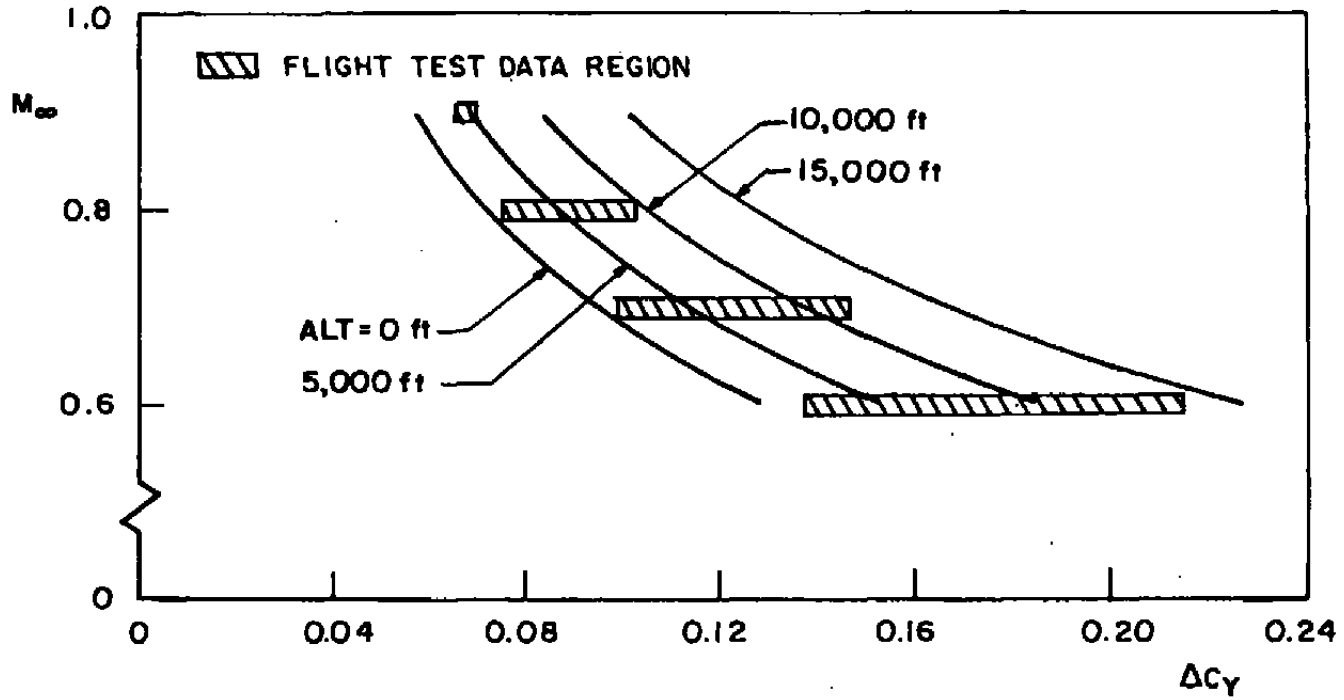


b. Dynamic pressure  
Figure 15. Concluded.

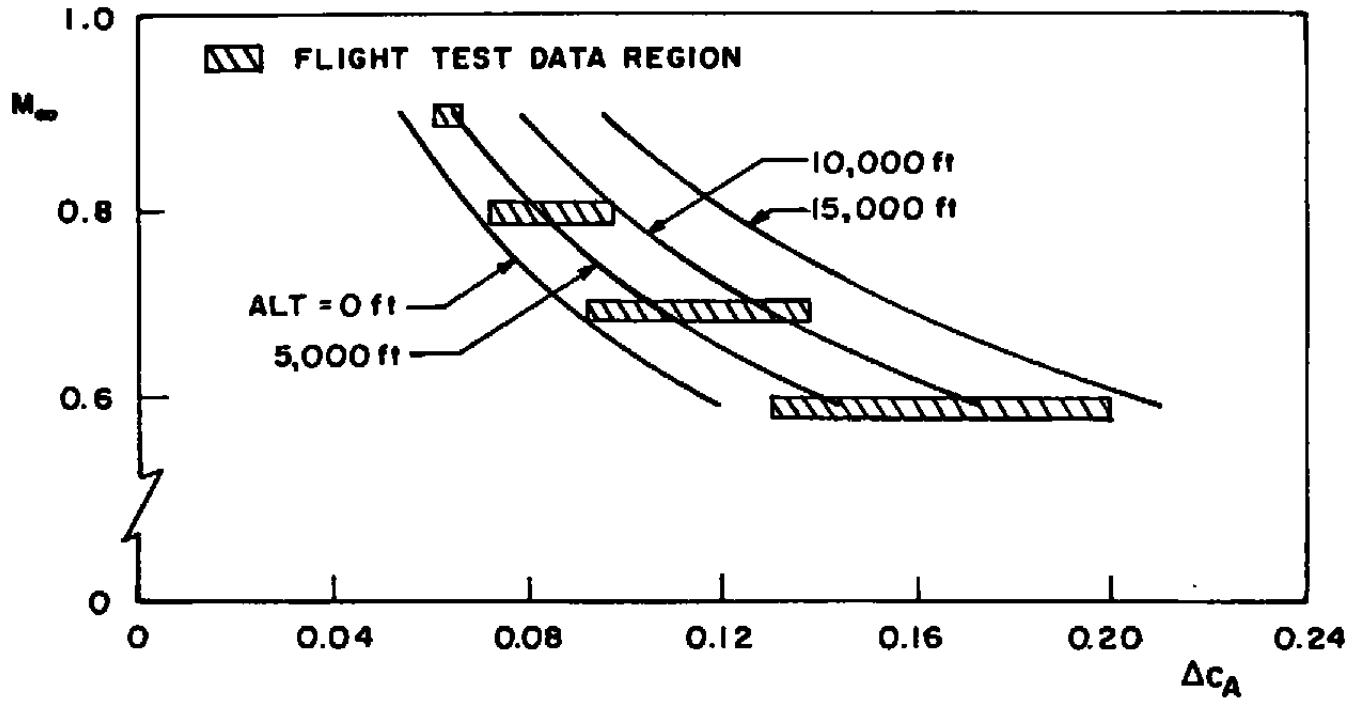


a. Normal-force coefficient

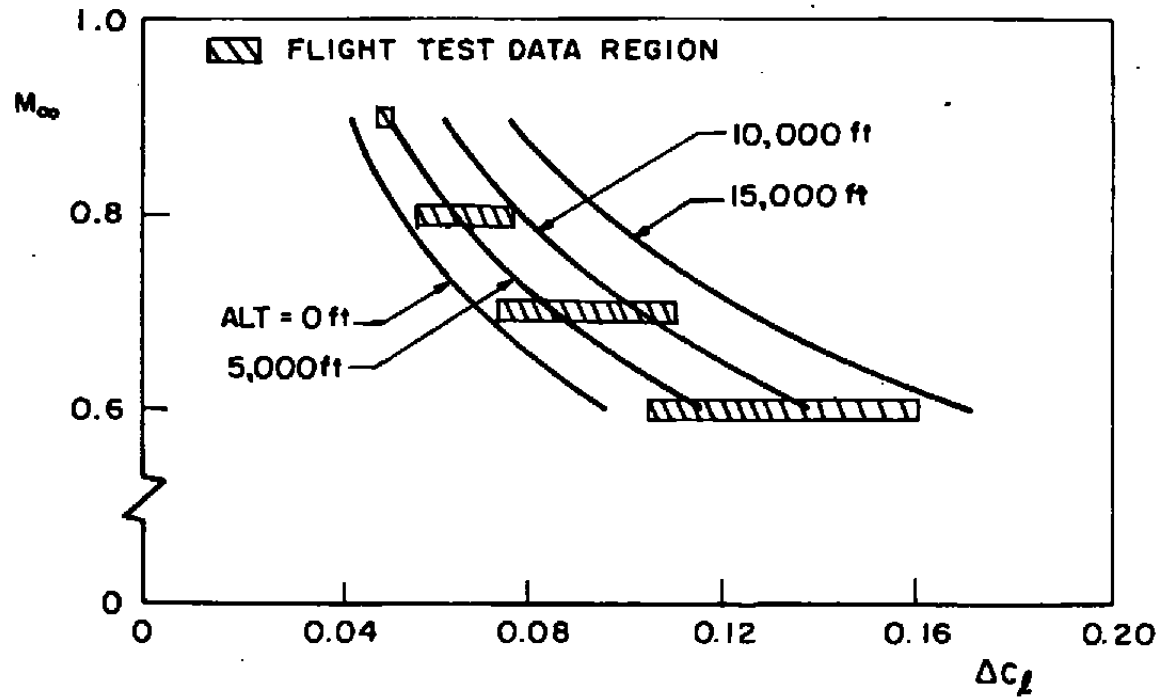
Figure 16. Statistical precision intervals for in-flight force and moment coefficients.



b. Side-force coefficient  
Figure 16. Continued.

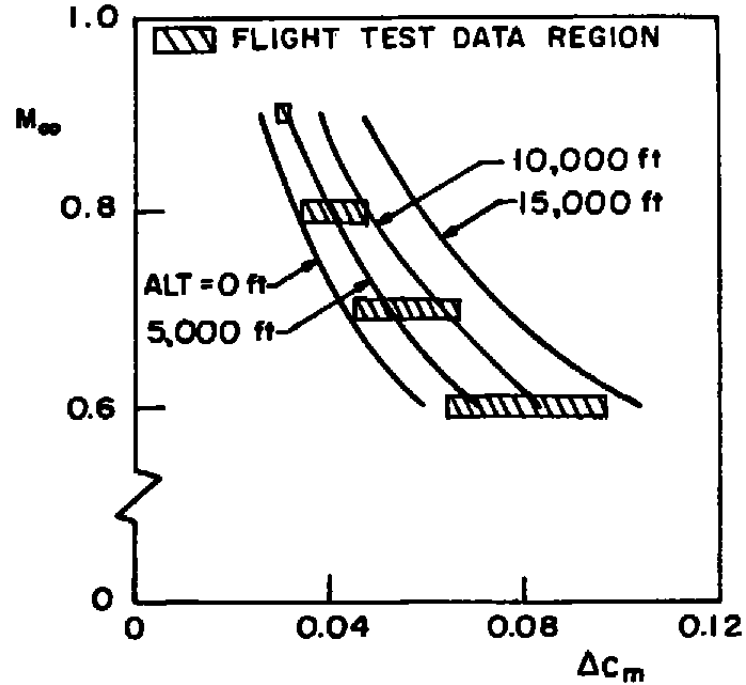


c. Axial-force coefficient  
Figure 16. Continued.

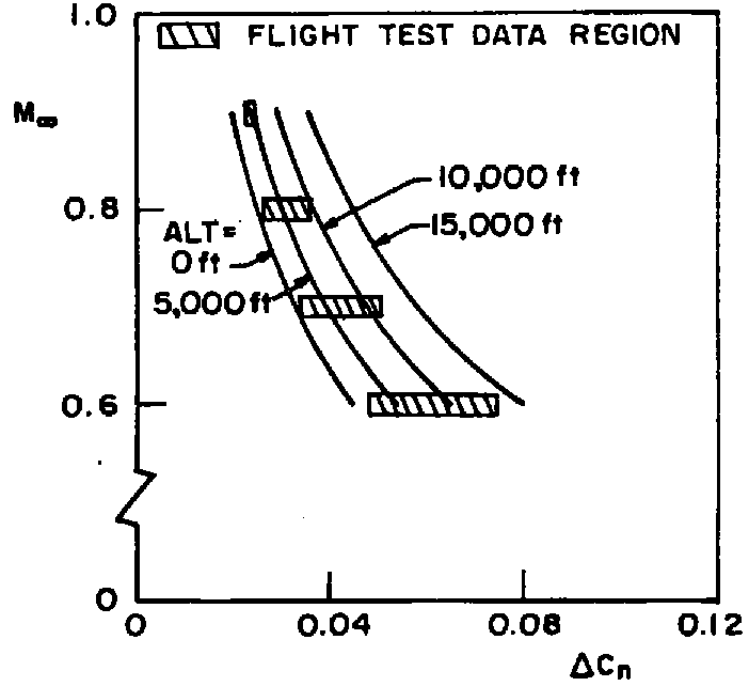


d. Rolling-moment coefficient  
Figure 16. Continued.

50

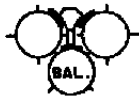


e. Pitching-moment coefficient  
Figure 16. Continued.



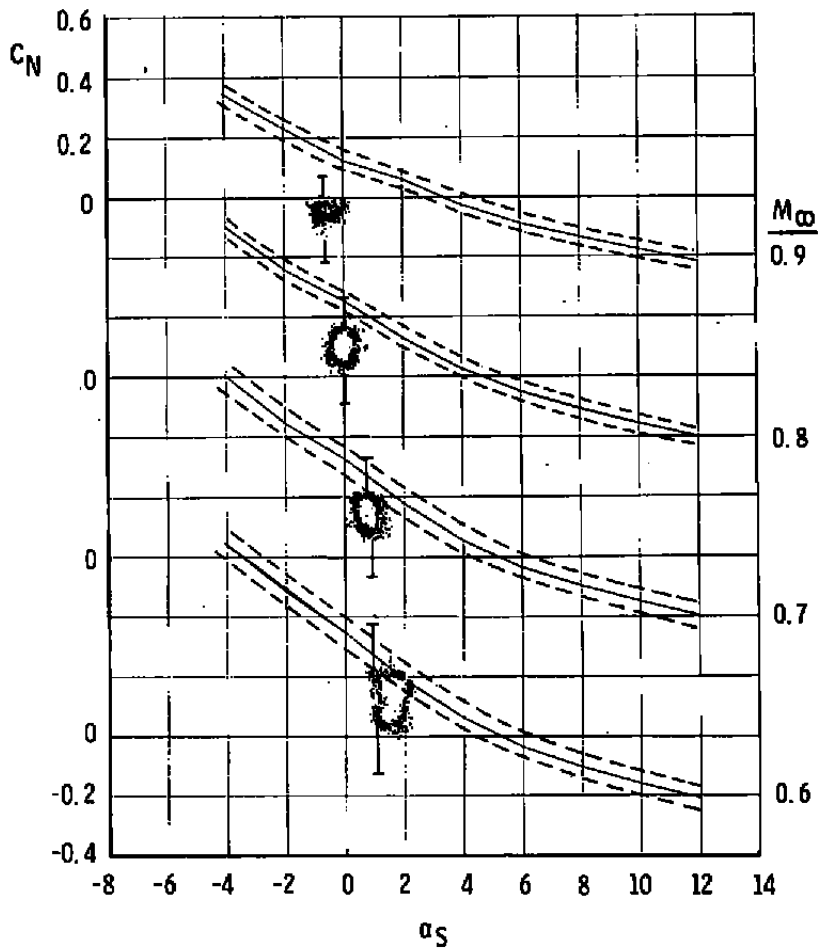
f. Yawing-moment coefficient  
Figure 16. Concluded.

MK 83, AB 1



In-Flight Data Points (Upper and Lower Data-Precision Bars Shown for Two Separate Points).

----- AEDC/4T, 1/20-Scale, Including Data-Precision Band (Ref. 7)



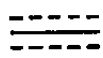
a. Normal-force coefficient

Figure 17. Comparison of wind tunnel and inflight data for constant Mach number, level flight, AB 1.

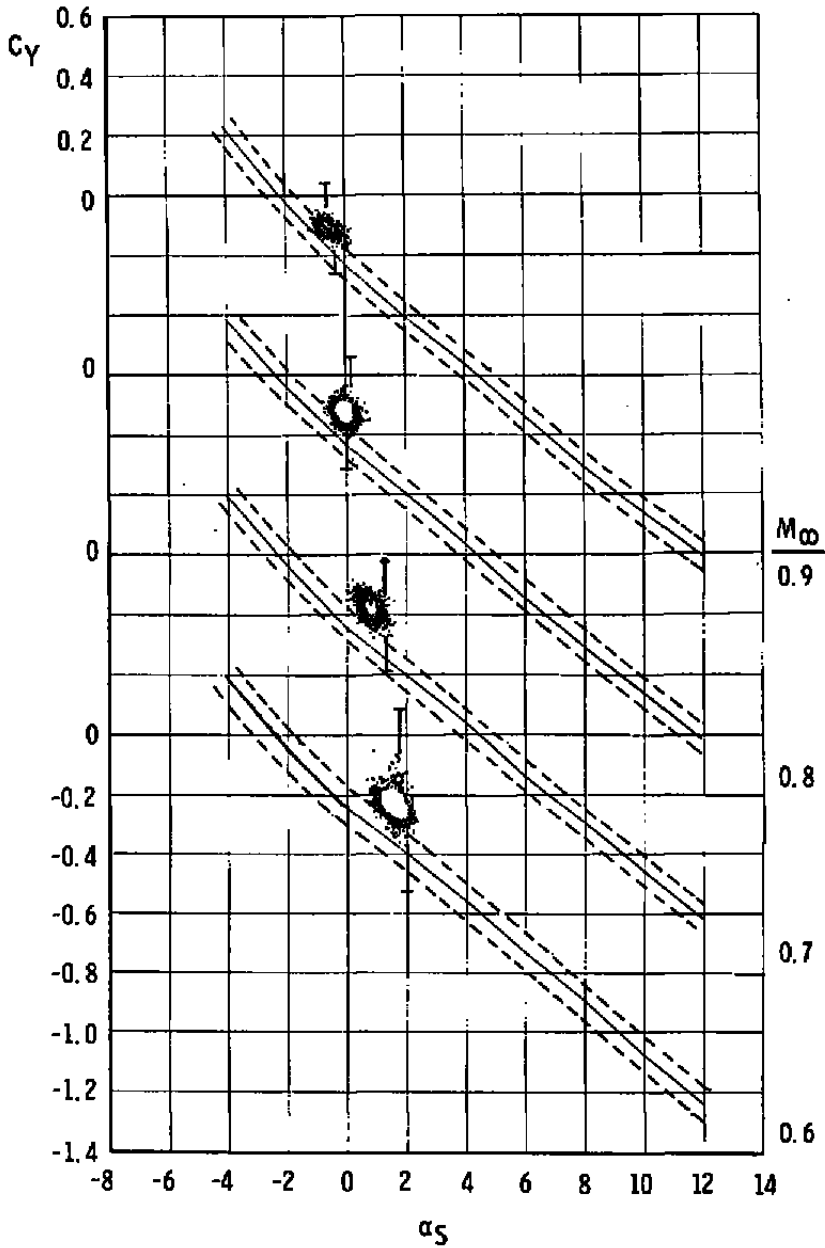
MK 83, AB 1



In-Flight Data Points (Upper and Lower Data-Precision Bars Shown for Two Separate Points).



AEDC/4T, 1/20-Scale, Including Data-Precision Band (Ref. 7)



b. Side-force coefficient  
Figure 17. Continued.

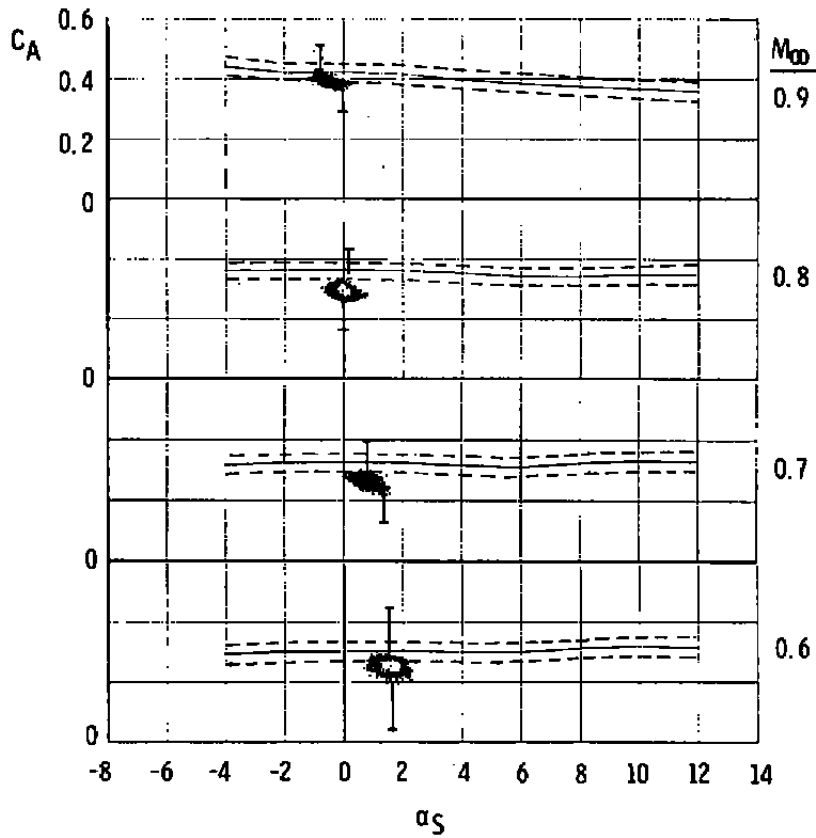
MK 83, AB 1



In-Flight Data Points (Upper and Lower Data-Precision Bars Shown for Two Separate Points).



AEDC/4T, 1/20-Scale, Including Data-Precision Band (Ref. 7)

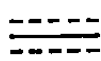


c. Axial-force coefficient  
Figure 17. Continued.

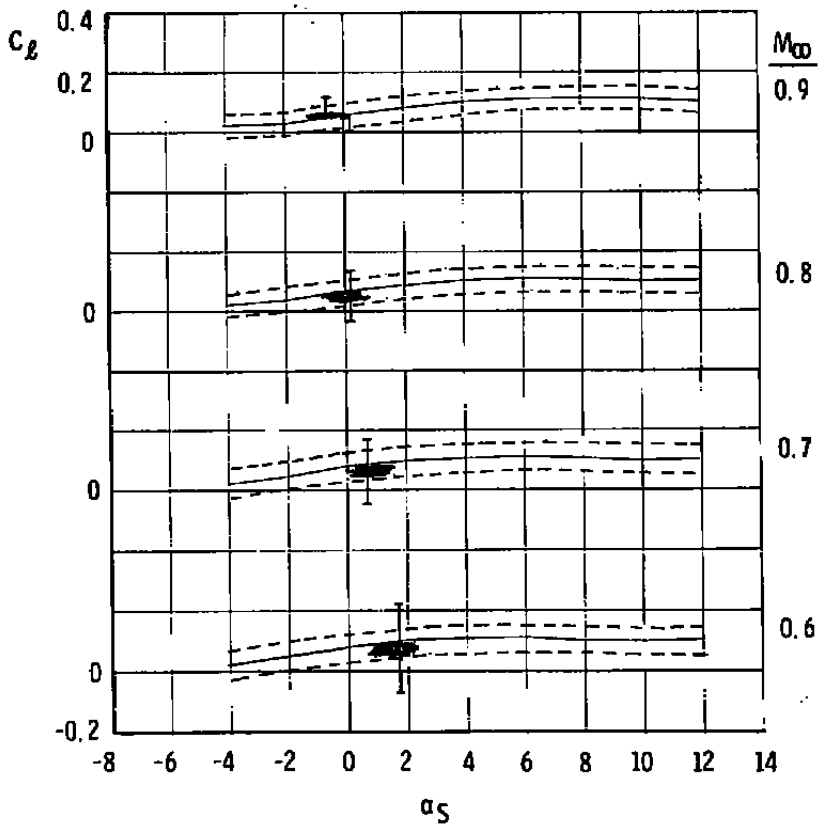
MK 83, AB 1



In-Flight Data Points (Upper and Lower Data-Precision Bars Shown for Two Separate Points).

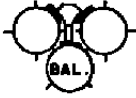


AEDC/4T, 1/20-Scale, Including Data-Precision Band (Ref. 7)



d. Rolling-moment coefficient  
Figure 17. Continued.

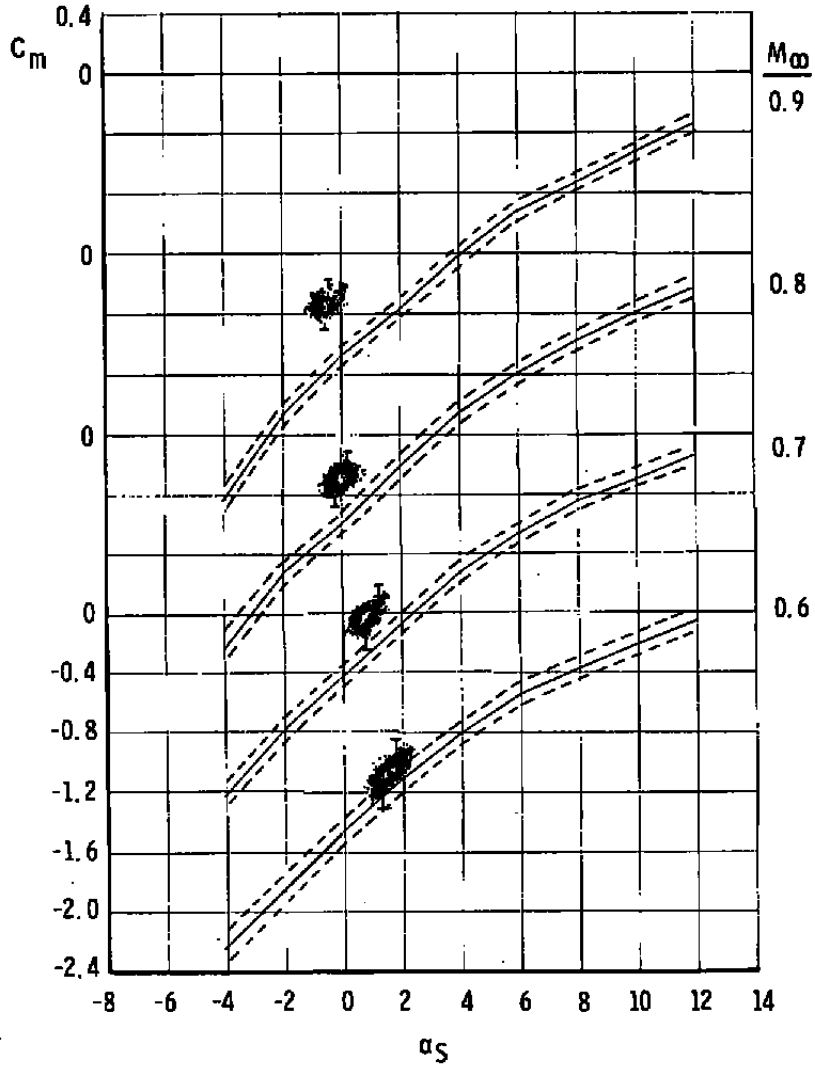
MK 83, AB 1



In-Flight Data Points (Upper and Lower Data-Precision Bars Shown for Two Separate Points).

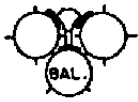


AEDC/AT, 1/20-Scale, Including Data-Precision Band (Ref. 7)

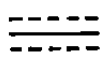


e. Pitching-moment coefficient  
Figure 17. Continued.

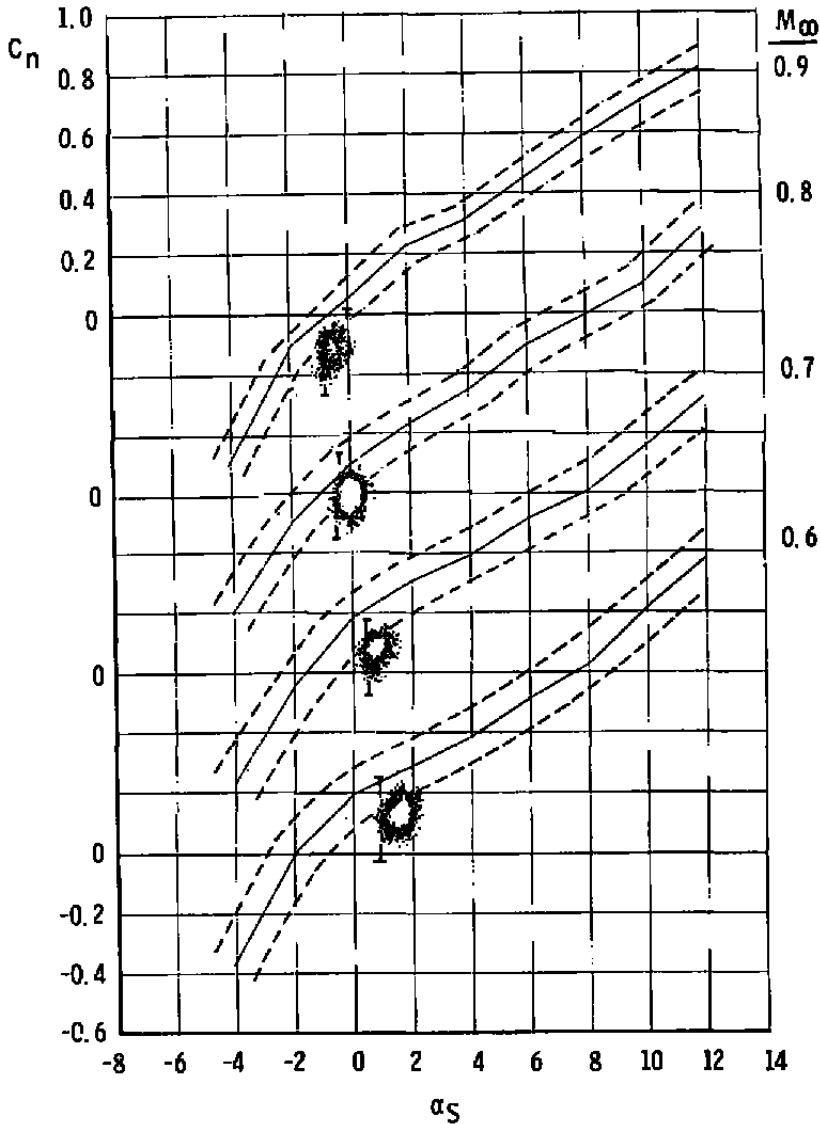
MK 83, AB 1



In-Flight Data Points (Upper and Lower Data-Precision Bars Shown for Two Separate Points).

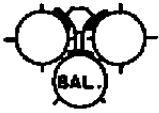


AEDC/4T, 1/20-Scale, Including Data-Precision Band (Ref. 7)

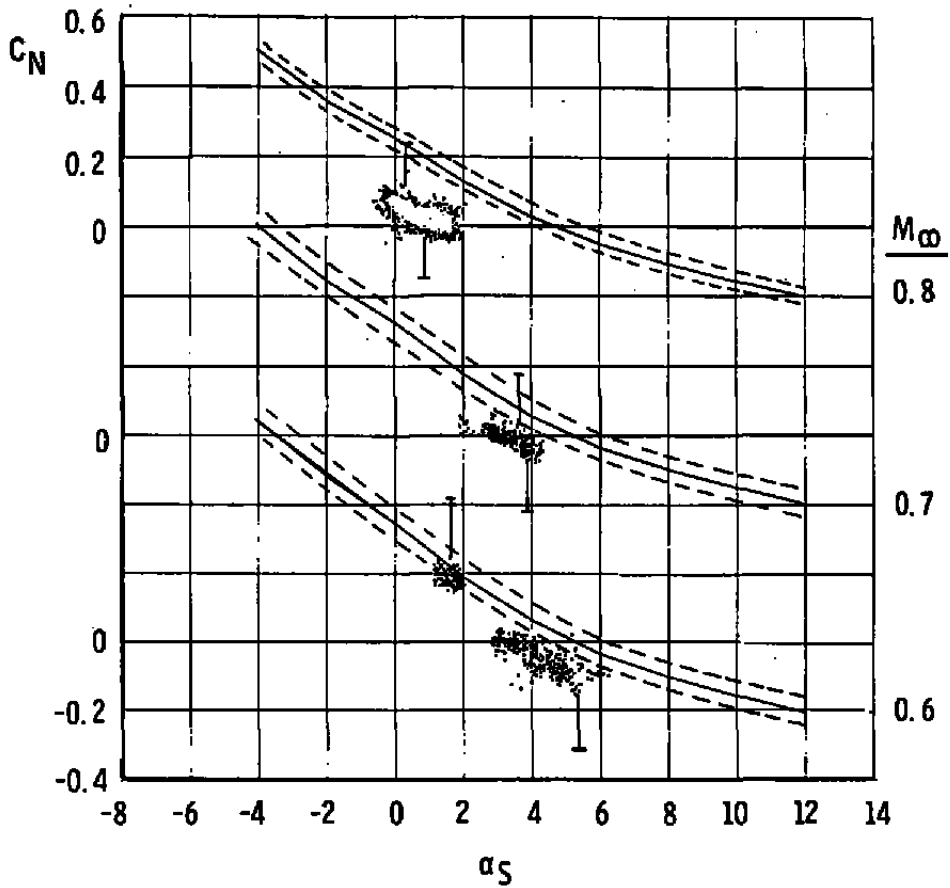


f. Yawing-moment coefficient  
Figure 17. Concluded.

MK 83, AB 1



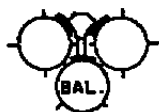
- 
 In-Flight Data Points (Upper and Lower Data-Precision Bars Shown for Two Separate Points).
- 
 AEDC/AT, 1/20-Scale, Including Data-Precision Band (Ref. 7)



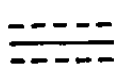
a. Normal-force coefficient

Figure 18. Comparison of wind tunnel and inflight data for low-g maneuvering flight, AB 1.

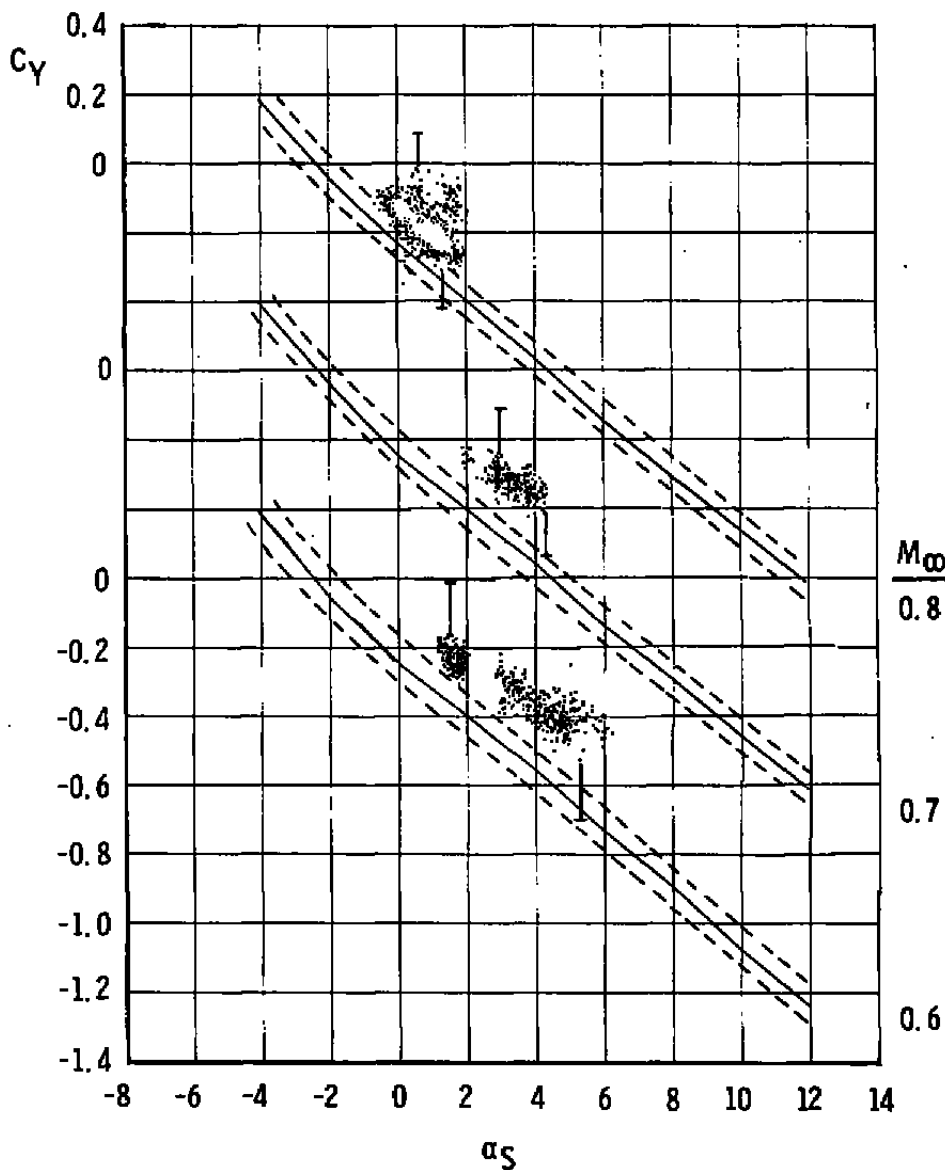
MK 83, AB 1



In-Flight Data Points (Upper and Lower Data-Precision Bars Shown for Two Separate Points).

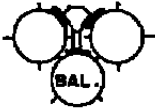


AEDC/4T, 1/20-Scale, Including Data-Precision Band (Ref. 7)

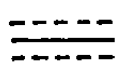


b. Side-force coefficient  
Figure 18. Continued.

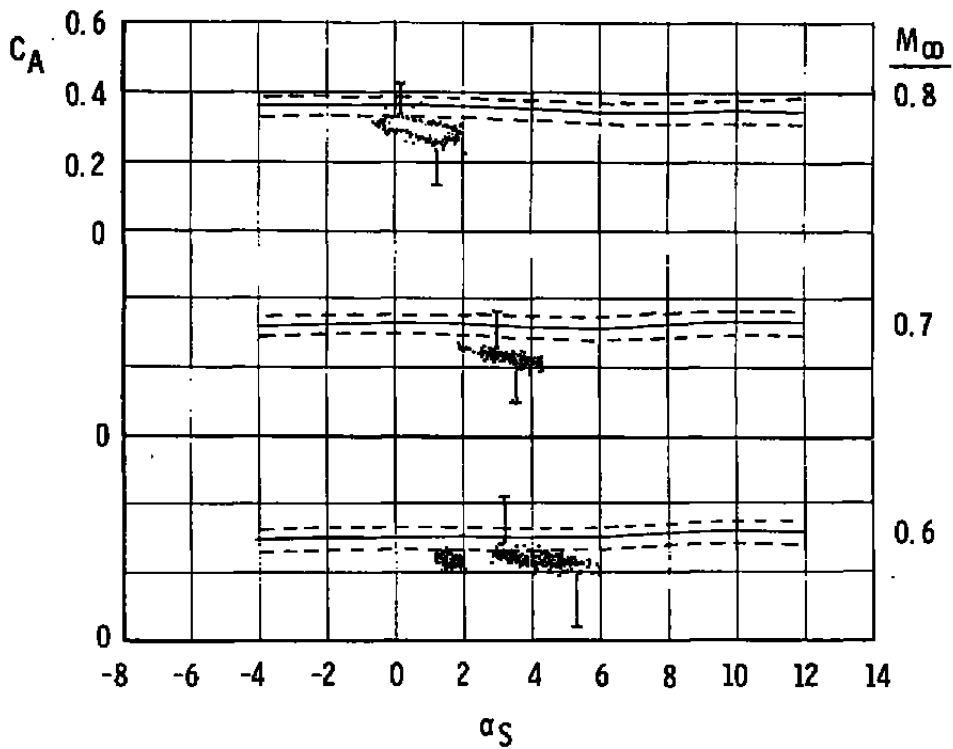
MK 83, AB 1



In-Flight Data Points (Upper and Lower Data-Precision Bars Shown for Two Separate Points).



AEDC/4T, 1/20-Scale, Including Data-Precision Band (Ref. 7)



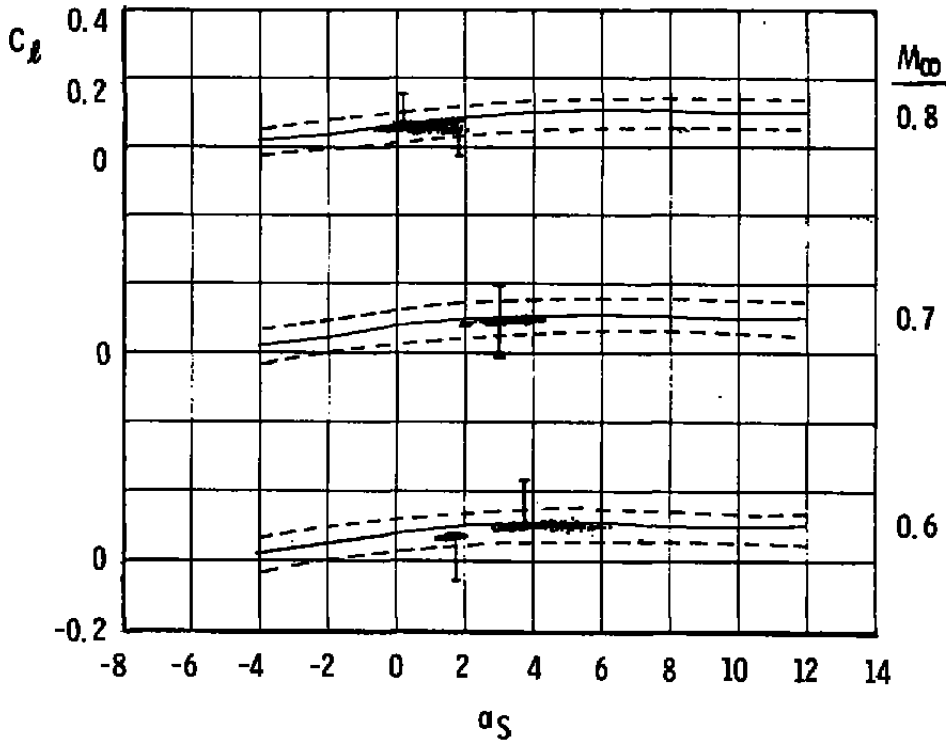
c. Axial-force coefficient  
Figure 18. Continued.

MK 83, AB 1



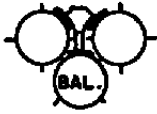
In-Flight Data Points (Upper and Lower Data-Precision Bars Shown for Two Separate Points).

----- AEDC/AT, 1/20-Scale, Including  
 ===== Data-Precision Band (Ref. 7)

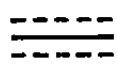


d. Rolling-moment coefficient  
 Figure 18. Continued.

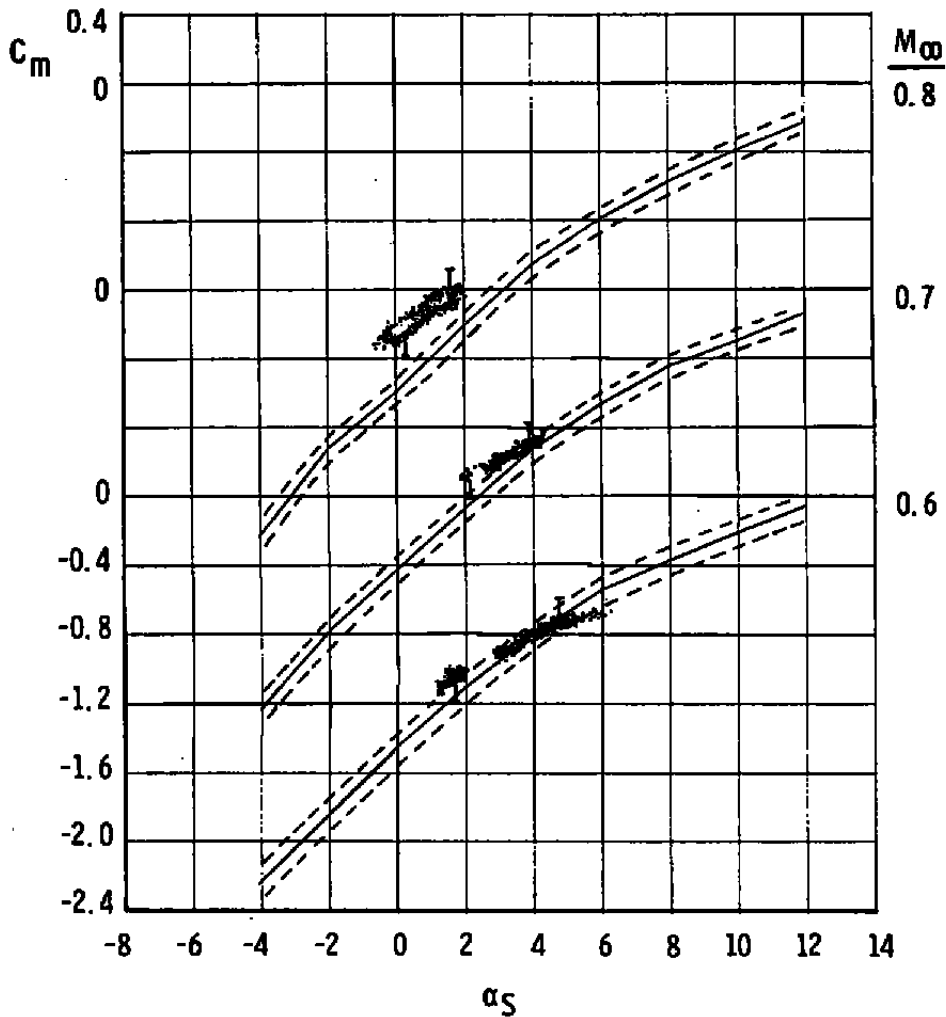
MK 83, AB 1



In-Flight Data Points (Upper and Lower Data-Precision Bars Shown for Two Separate Points).



AEDC/AT, 1/20-Scale, Including Data-Precision Band (Ref. 7)

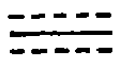


e. Pitching-moment coefficient  
Figure 18. Continued.

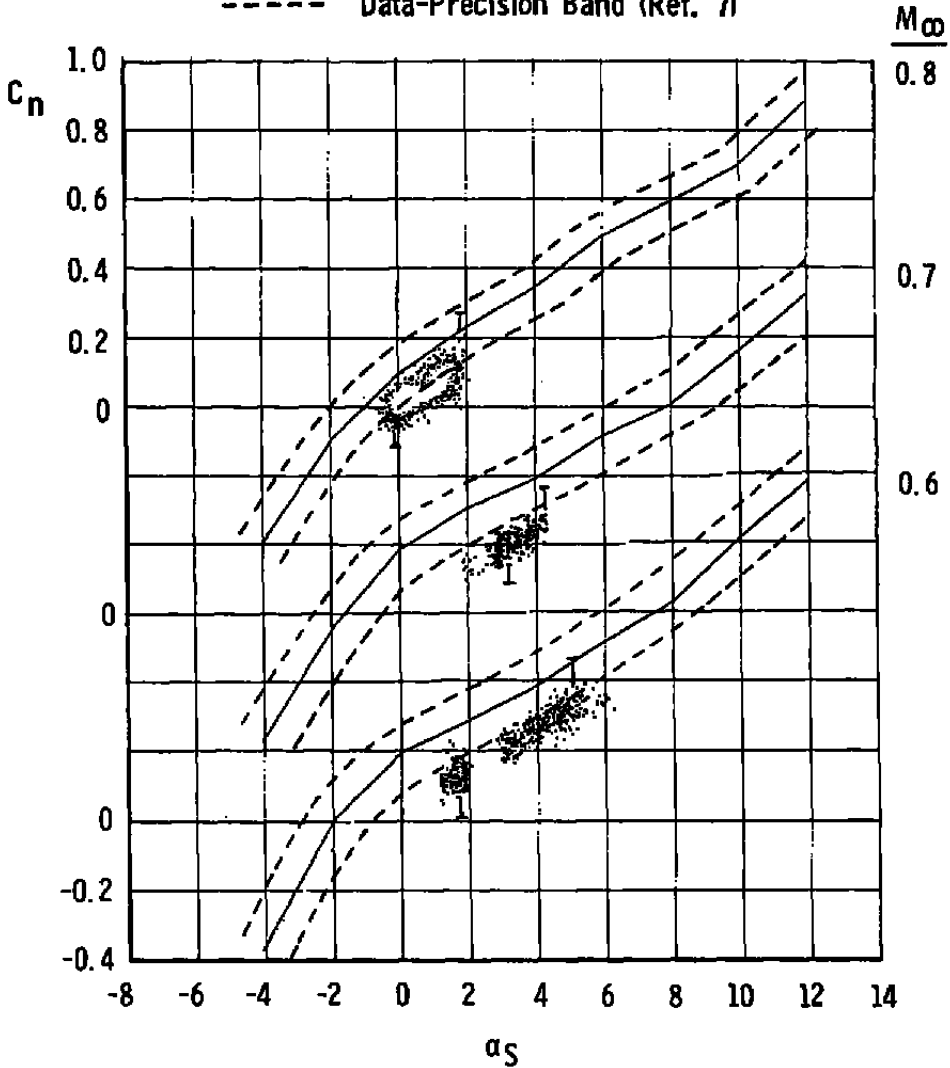
MK 83, AB 1



In-Flight Data Points (Upper and Lower Data-Precision Bars Shown for Two Separate Points).



AEDC/4T, 1/20-Scale, Including Data-Precision Band (Ref. 7)

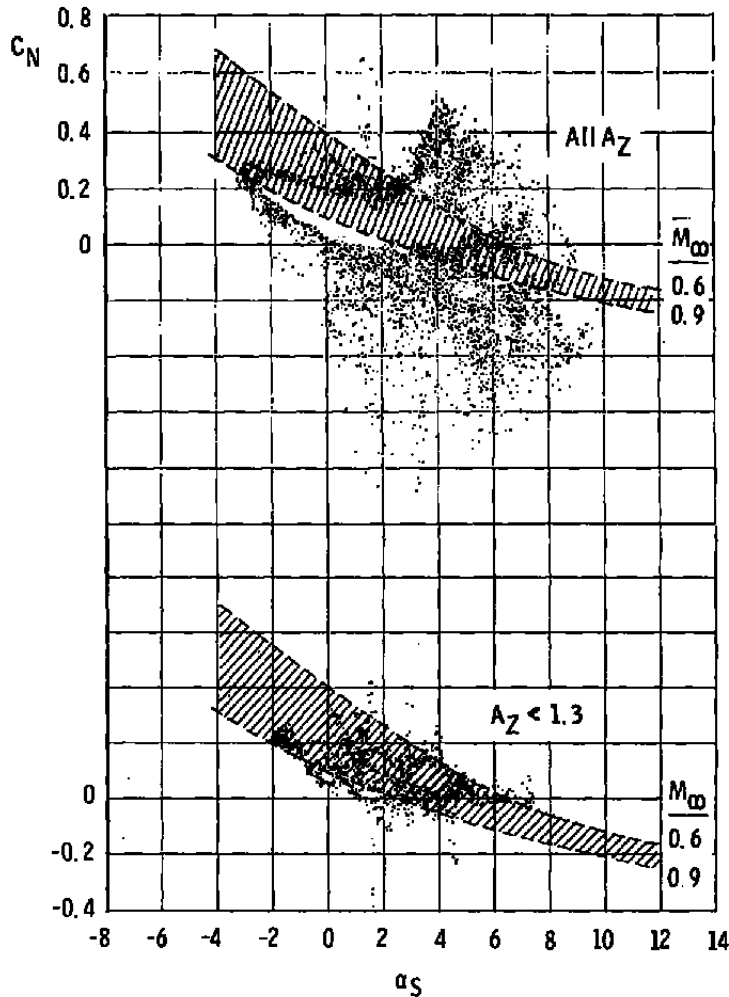


f. Yawing-moment coefficient  
Figure 18. Concluded.

MK 83, AB 1



-  In-Flight Data Points for Maneuvers with Variable Mach Number
-  AEDC/4T, 1/20-Scale, All Mach Numbers, Including Data-Precision Band (Ref. 7)



a. Normal-force coefficient

Figure 19. Comparison of wind tunnel and inflight data for maneuvering flight, AB 1.

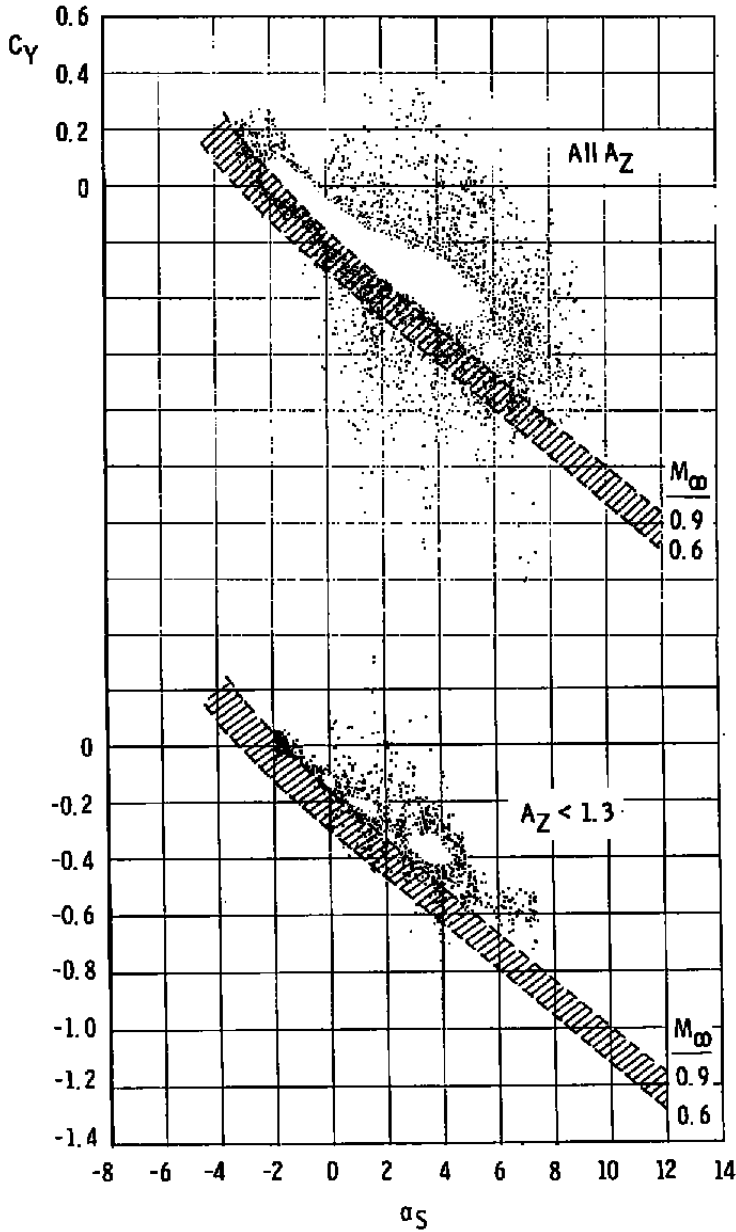
MK 83, AB 1



In-Flight Data Points for Maneuvers with Variable Mach Number



AEDC/4T, 1/20-Scale, All Mach Numbers, Including Data-Precision Band (Ref. 7)



b. Side-force coefficient  
Figure 19. Continued.

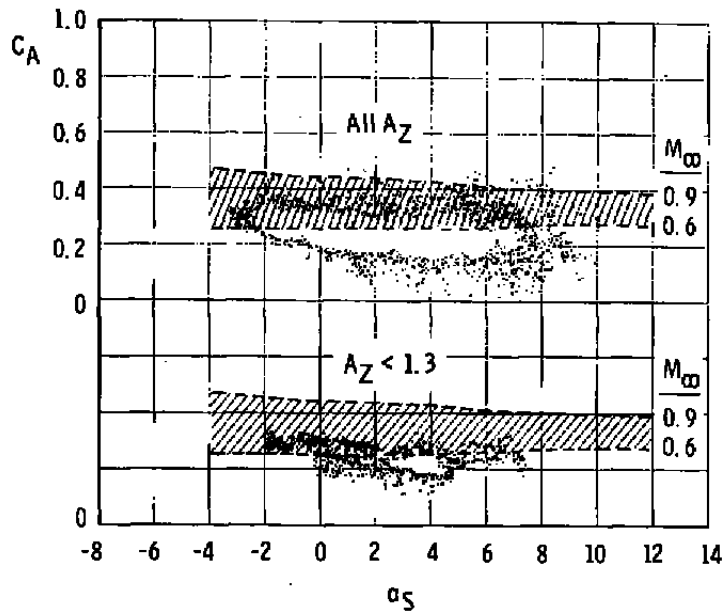
MK 83, AB 1



In-Flight Data Points for Maneuvers with Variable Mach Number



AEDC/4T, 1/20-Scale, All Mach Numbers, Including Data-Precision Band (Ref. 7)



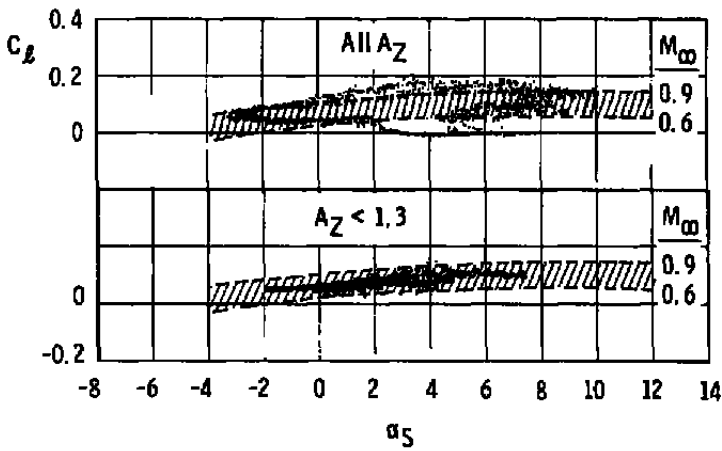
c. Axial-force Coefficient  
Figure 19. Continued.

MK 83, AB 1



 In-Flight Data Points for Maneuvers with Variable Mach Number

 AEDC/MT, 1/20-Scale, All Mach Numbers, Including Data-Precision Band (Ref. 7)



d. Rolling-moment coefficient  
Figure 19. Continued.

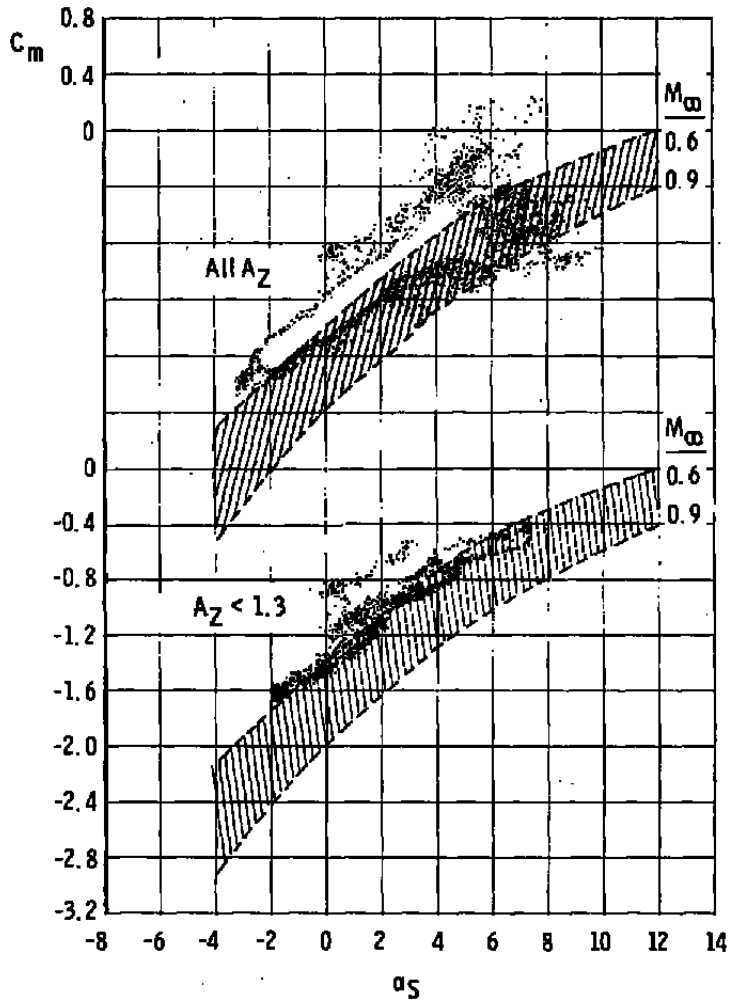
MK 83, AB 1



In-Flight Data Points for Maneuvers with Variable Mach Number



AEDC/4T, 1/20-Scale, All Mach Numbers, Including Data-Precision Band (Ref. 7)



e. Pitching-moment coefficient  
Figure 19. Continued.

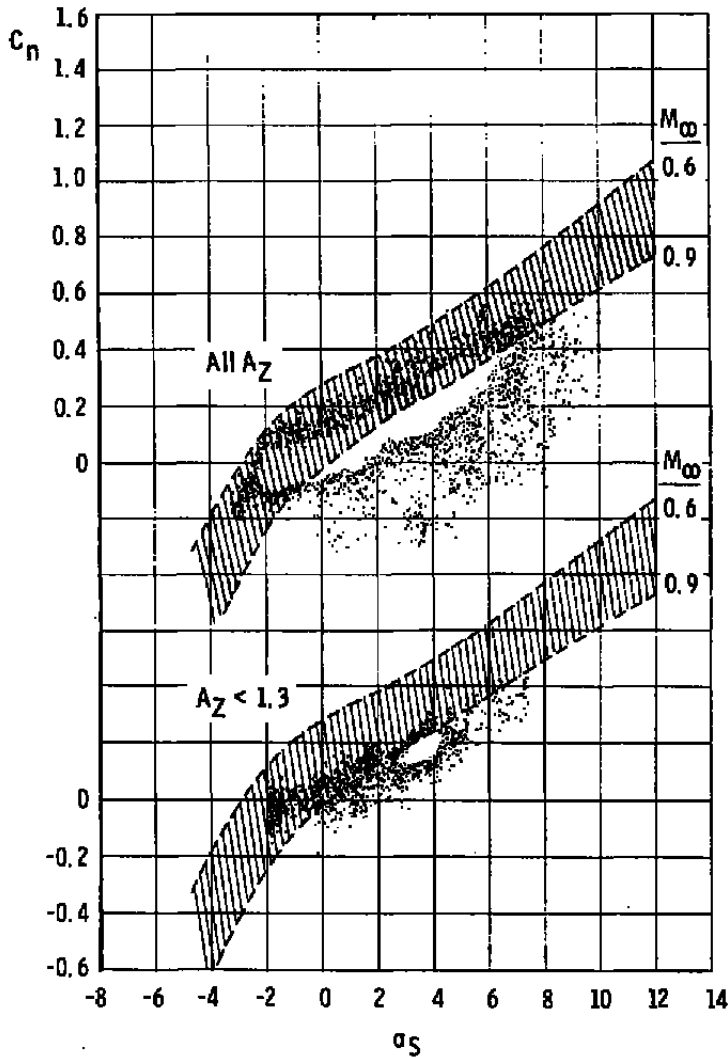
MK 83, AB 1



In-Flight Data Points for Maneuvers with Variable Mach Number



AEDC/AT, 1/20-Scale, All Mach Numbers, Including Data-Precision Band (Ref. 7)

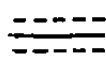


f. Yawing-moment coefficient  
Figure 19. Concluded.

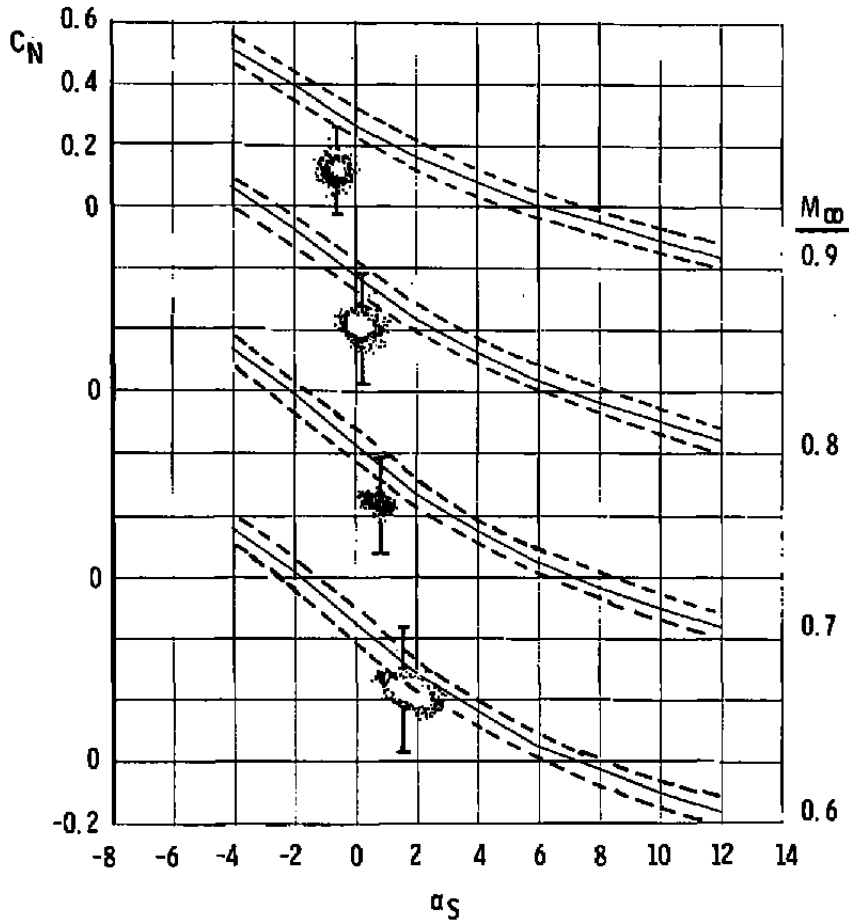
MK 83, AB 2



In-Flight Data Points (Upper and Lower Data-Precision Bars Shown for Two Separate Points).



AEDC/4T, 1/20-Scale, Including Data-Precision Band (Ref. 7)



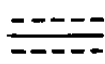
a. Normal-force coefficient

Figure 2D. Comparison of wind tunnel and inflight data for constant Mach number, level flight, AB 2.

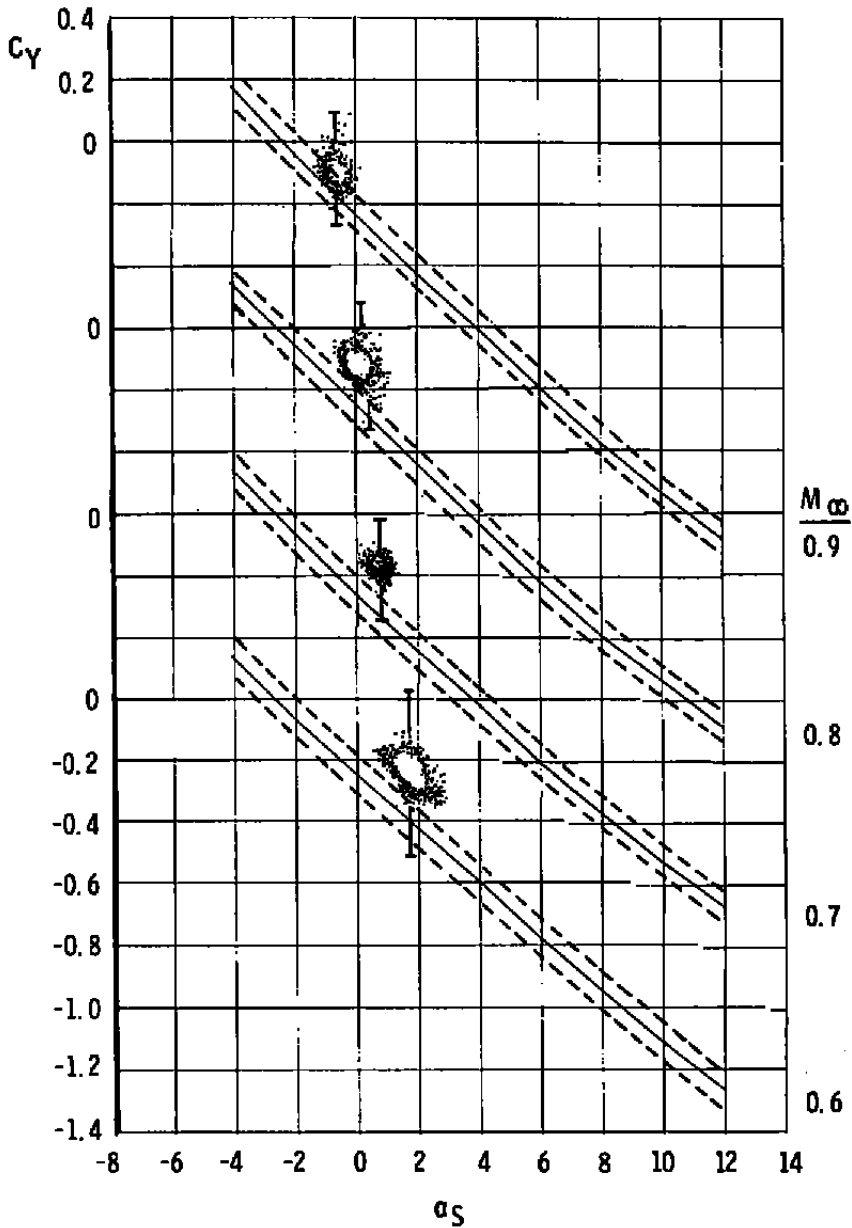
MK 83, AB 2



In-Flight Data Points (Upper and Lower Data-Precision Bars Shown for Two Separate Points).

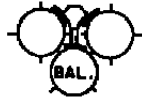


AEDC/MT, 1/20-Scale, Including Data-Precision Band (Ref. 7)

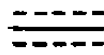


b. Side-force coefficient  
Figure 20. Continued.

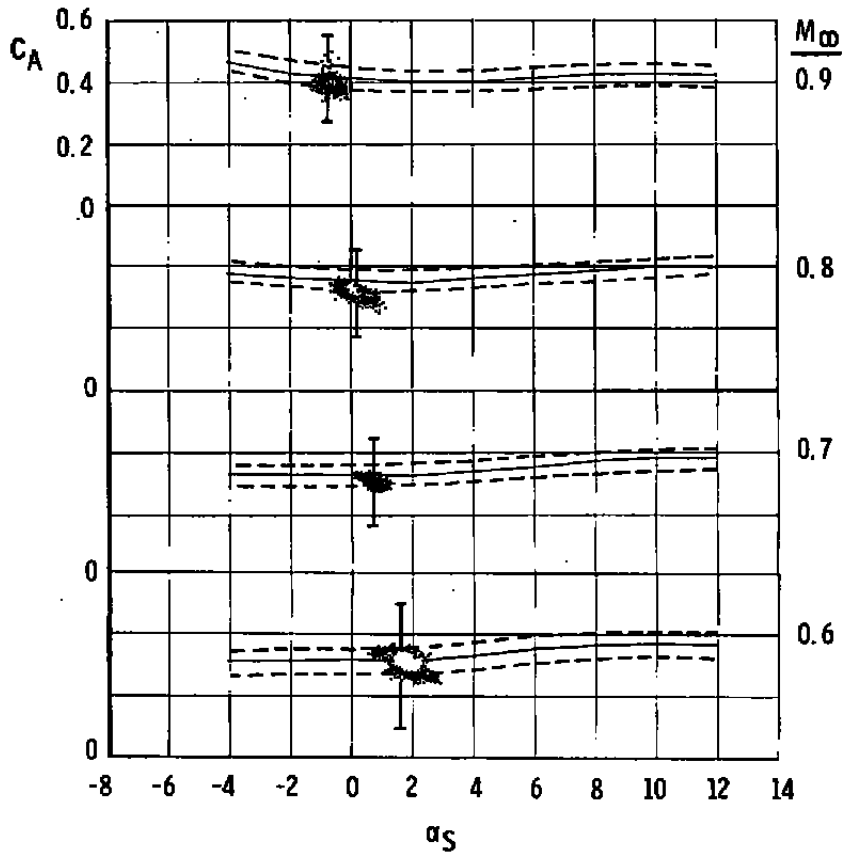
MK 83, AB 2



In-Flight Data Points (Upper and Lower Data-Precision Bars Shown for Two Separate Points).



AEDC/AT, 1/20-Scale, Including Data-Precision Band (Ref. 7)

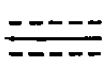


c. Axial-force coefficient  
Figure 20. Continued.

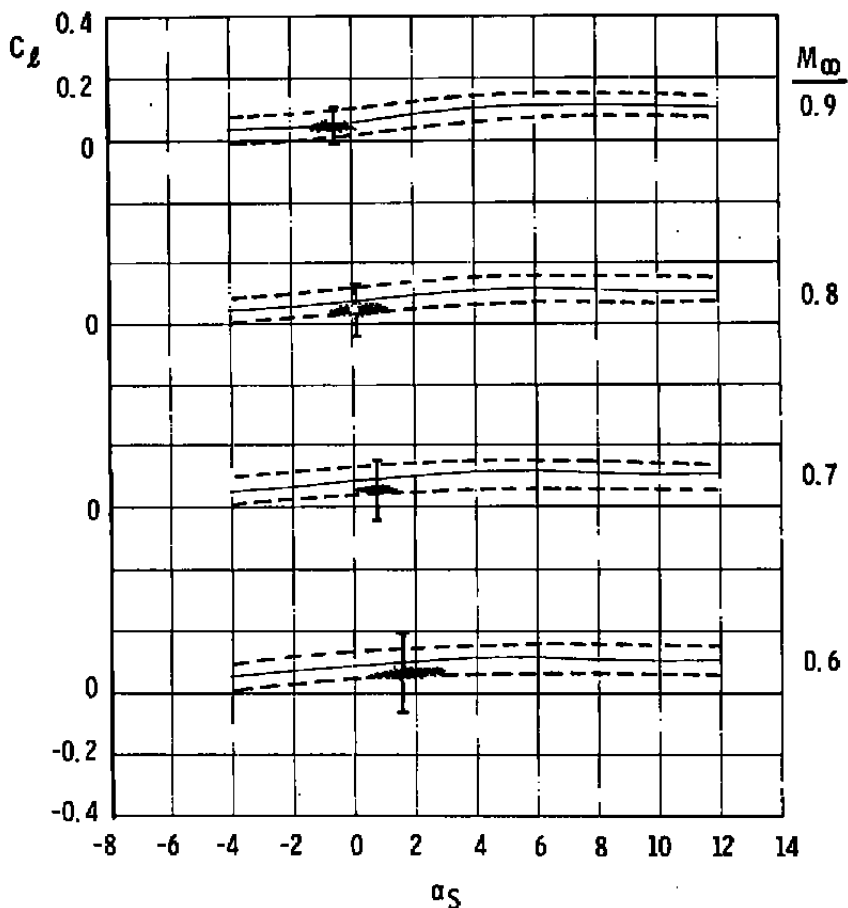
MK 83, AB 2



In-Flight Data Points (Upper and Lower Data-Precision Bars Shown for Two Separate Points).



AEDC/4T, 1/20-Scale, Including Data-Precision Band (Ref. 7)

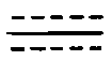


d. Rolling-moment coefficient  
Figure 20. Continued.

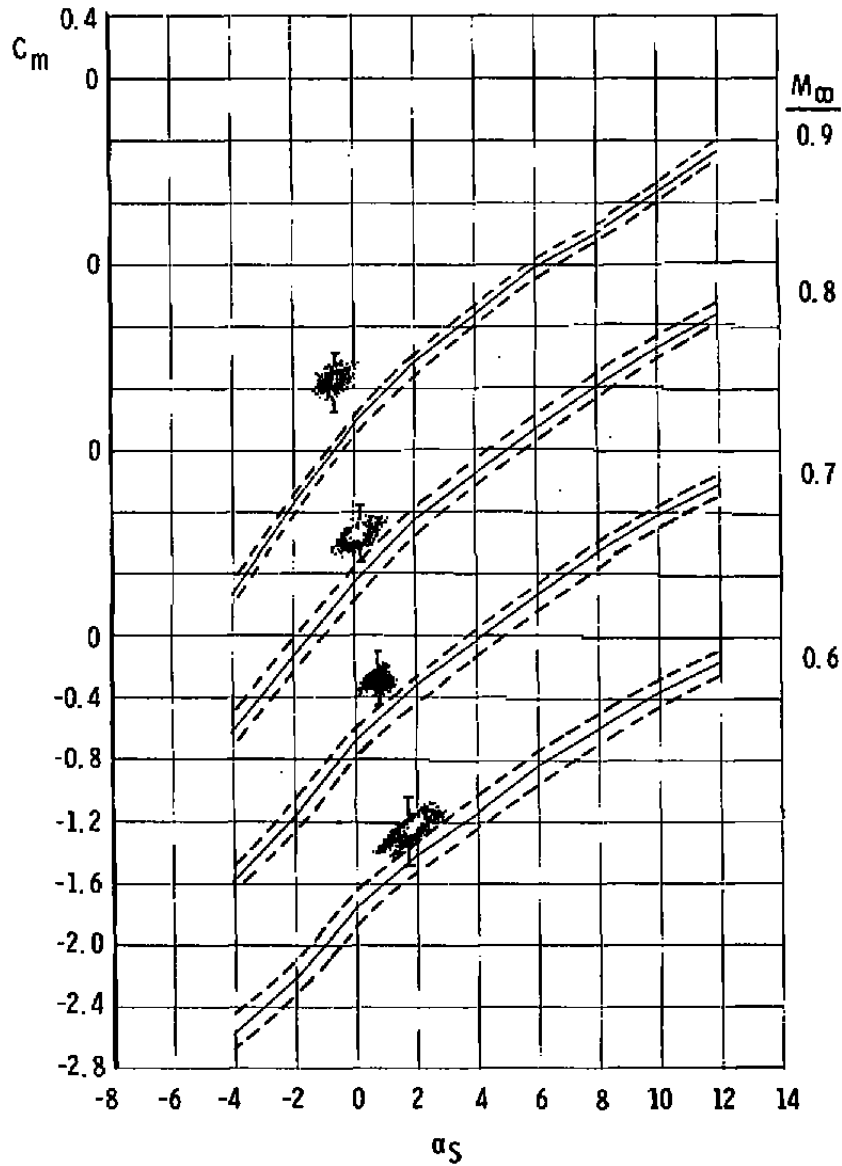
MK 83, AB 2



In-Flight Data Points (Upper and Lower Data-Precision Bars Shown for Two Separate Points).

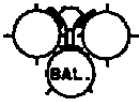


AEDC/AT, 1/20-Scale, Including Data-Precision Band (Ref. 7)

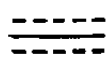


e. Pitching-moment coefficient  
Figure 20. Continued.

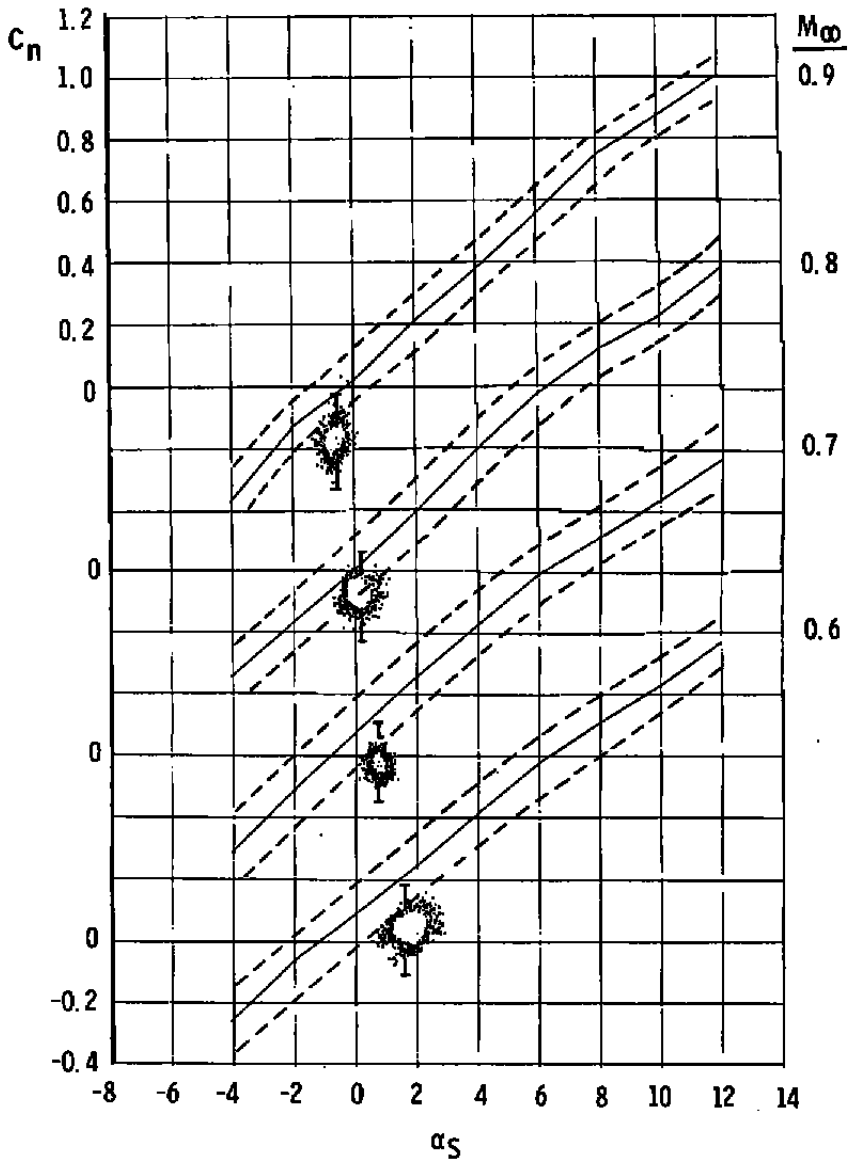
MK 83, AB 2



In-flight Data Points (Upper and Lower Data-Precision Bars Shown for Two Separate Points).

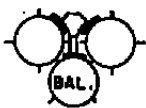


AEDC/4T, 1/20-Scale, Including Data-Precision Band (Ref. 7)



f. Yawing-moment coefficient  
Figure 20. Concluded.

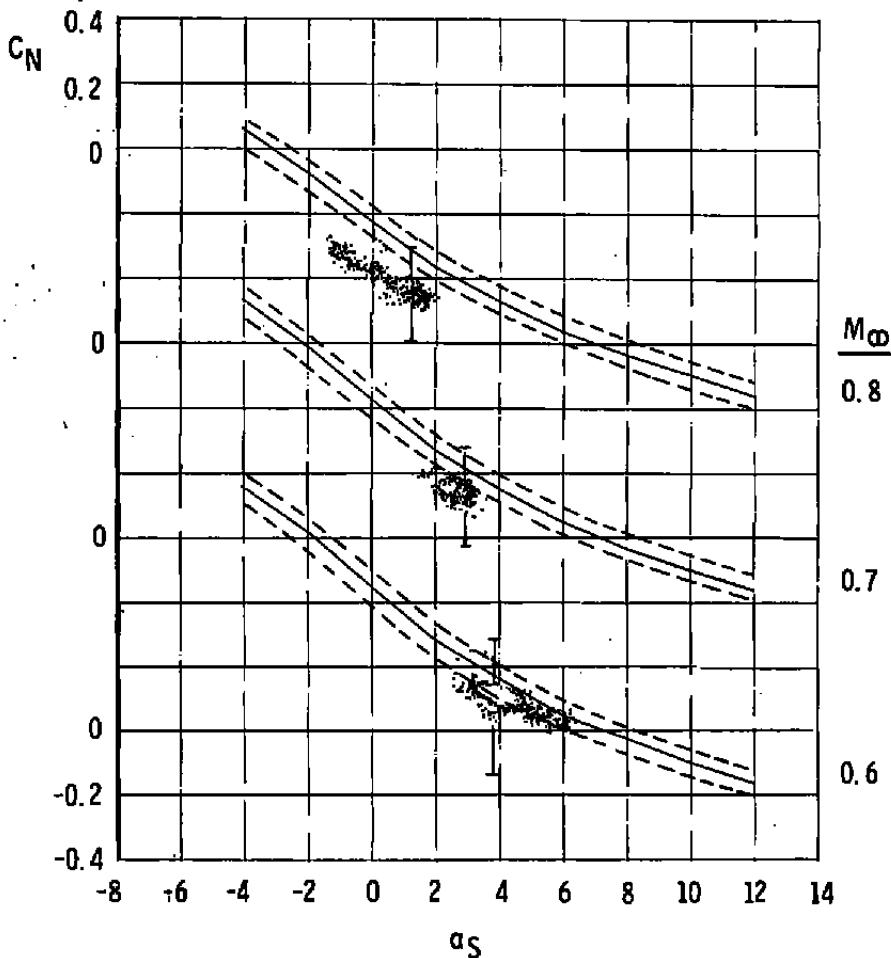
MK 83, AB 2



In-Flight Data Points (Upper and Lower Data-Precision Bars Shown for Two Separate Points).

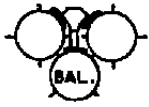


AEDC/4T, 1/20-Scale, Including Data-Precision Band (Ref. 7)

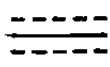


a. Normal-force coefficient  
 Figure 21. Comparison of wind tunnel and inflight data for low-g maneuvering flight, AB 2.

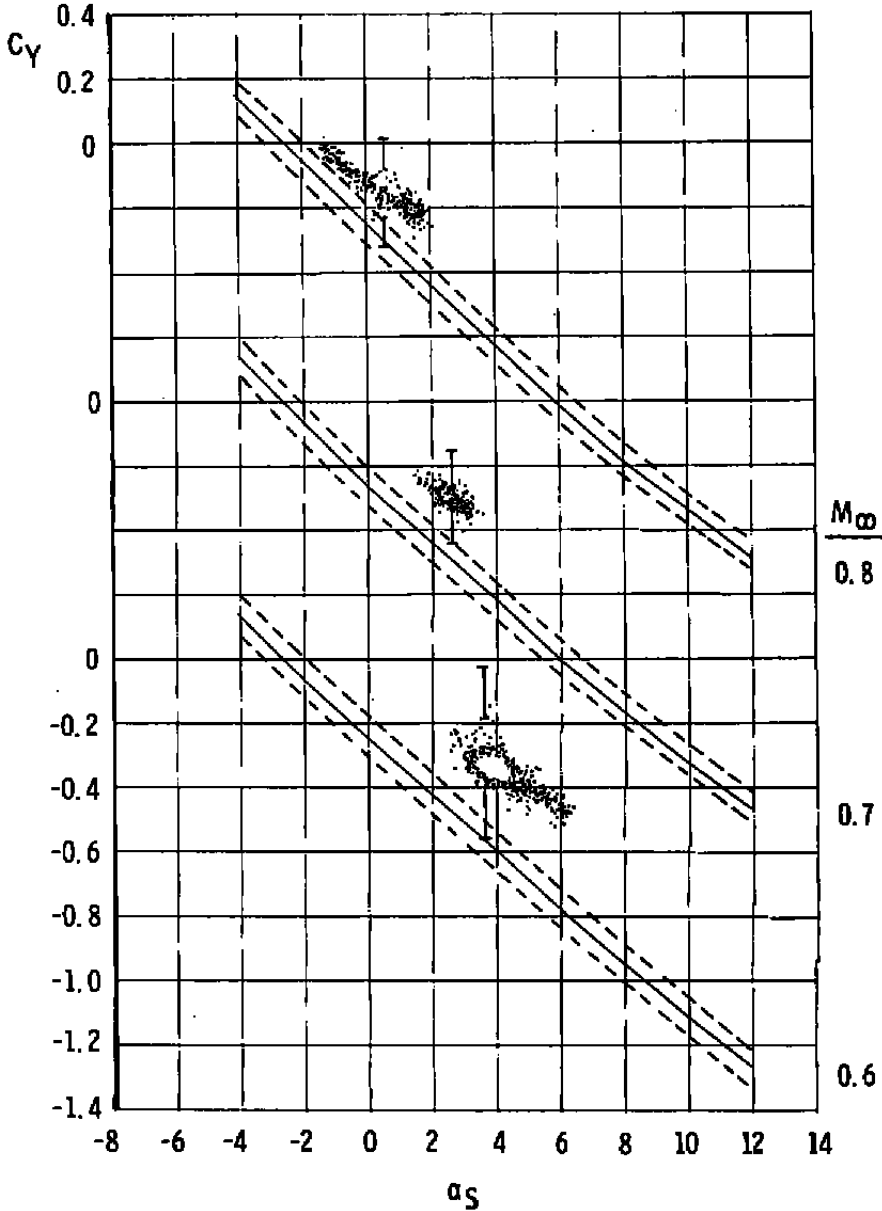
MK 83, AB 2



In-Flight Data Points (Upper and Lower Data-Precision Bars Shown for Two Separate Points).



AEDC/4T, 1/20-Scale, Including Data-Precision Band (Ref. 7)



b. Side-force coefficient  
Figure 21. Continued.

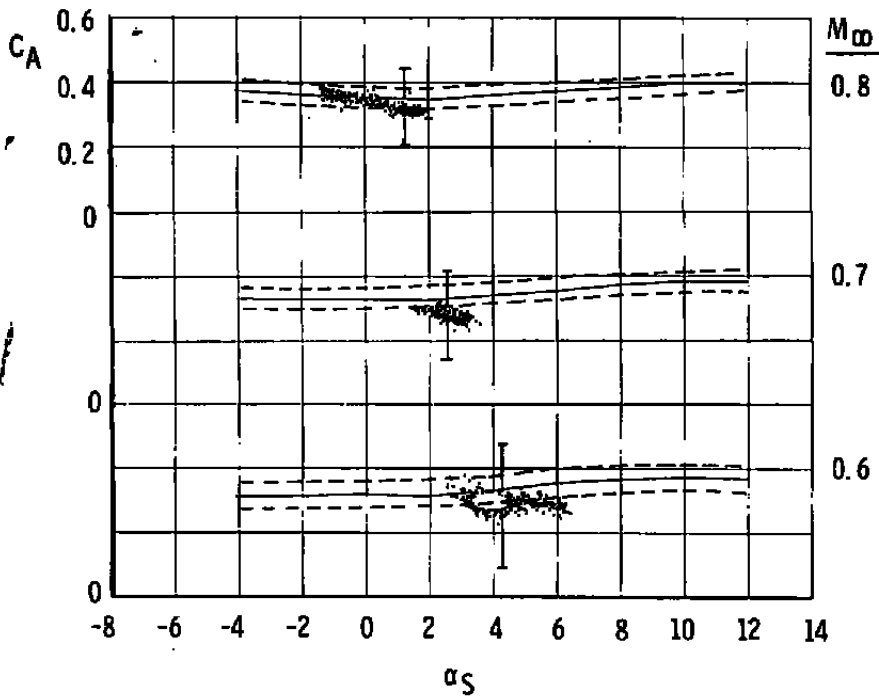
MK 83, AB 2



In-Flight Data Points (Upper and Lower Data-Precision Bars Shown for Two Separate Points).



AEDC/AT, 1/20-Scale, Including Data-Precision Band (Ref. 7)



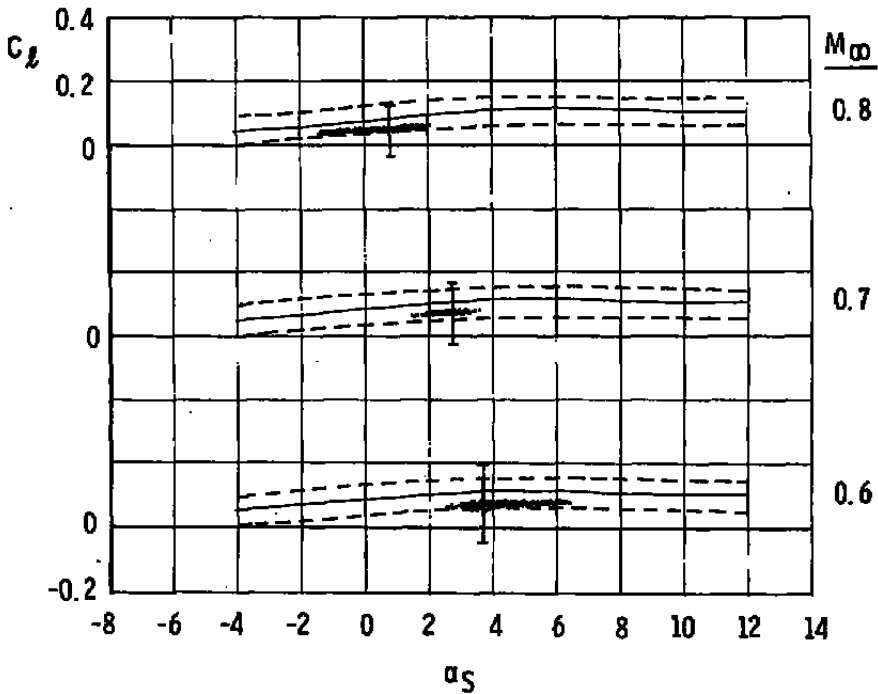
c. Axial-force coefficient  
Figure 21. Continued.

MK 83, AB 2



In-Flight Data Points (Upper and Lower Data-Precision Bars Shown for Two Separate Points).

----- AEDC/4T, 1/20-Scale, Including  
 ===== Data-Precision Band (Ref. 7)

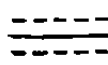


d. Rolling-moment coefficient  
 Figure 21. Continued.

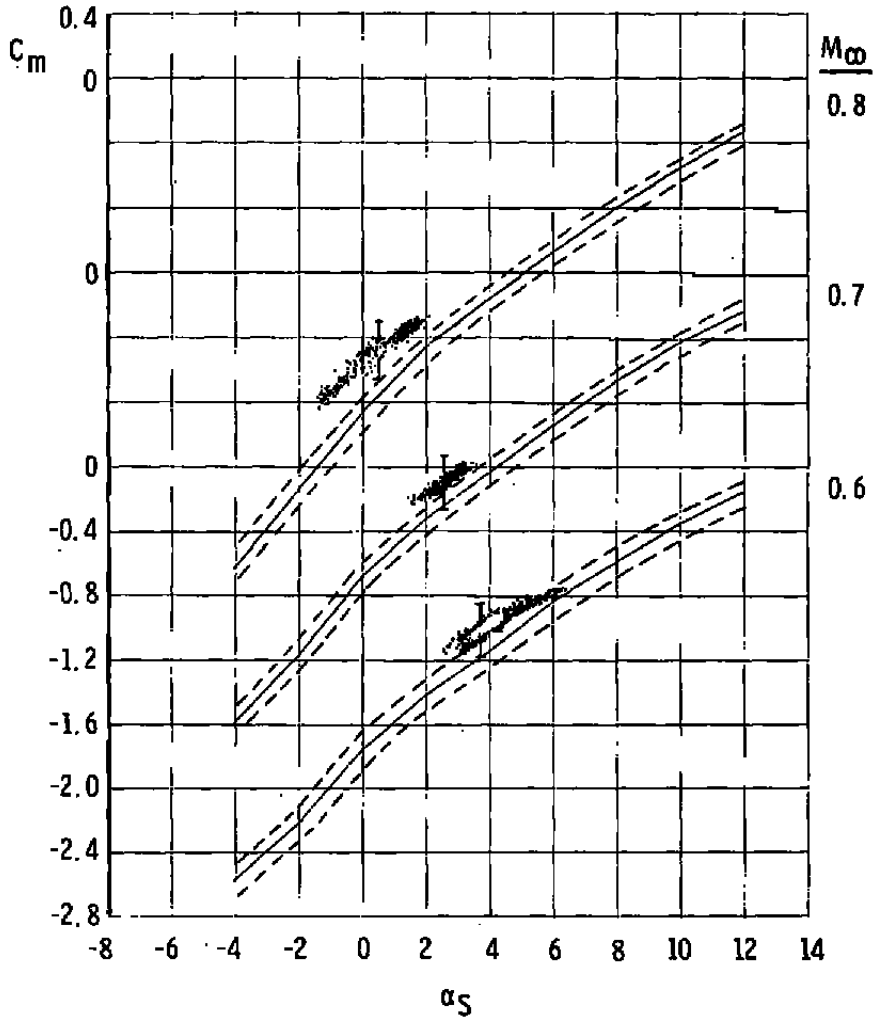
MK 83, AB 2



In-Flight Data Points (Upper and Lower Data-Precision Bars Shown for Two Separate Points).



AEDC/AT, 1/20-Scale, Including Data-Precision Band (Ref. 7)

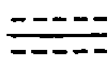


e. Pitching-moment coefficient  
Figure 21. Continued.

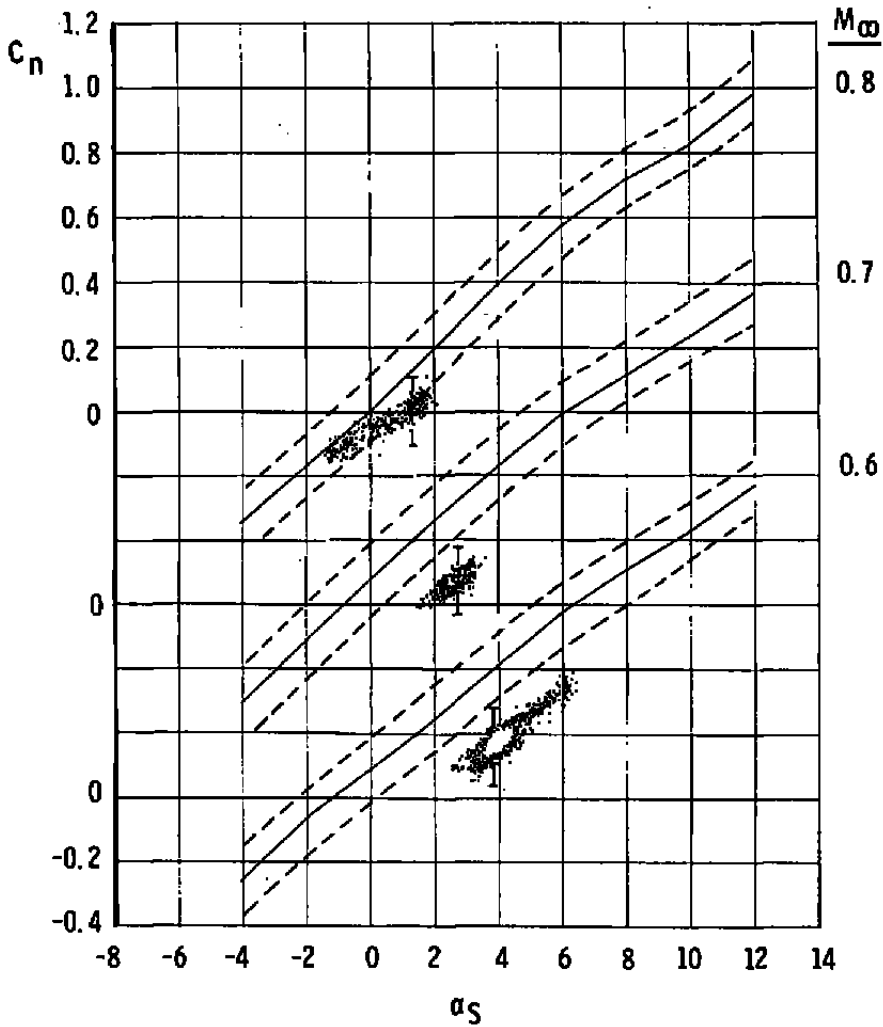
MK 83, AB 2



In-flight Data Points (Upper and Lower Data-Precision Bars Shown for Two Separate Points).



AEDC/AT, 1/20-Scale, Including Data-Precision Band (Ref. 7)



f. Yawing-moment coefficient  
Figure 21. Concluded.

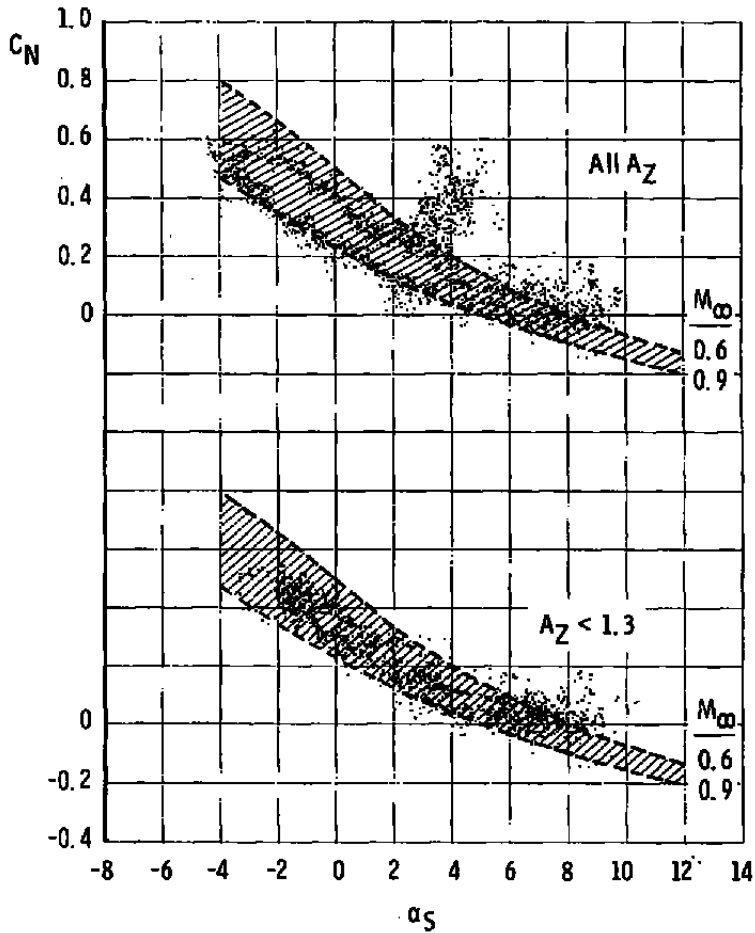
MK 83, AB 2



In-Flight Data Points for Maneuvers with Variable Mach Number



AEDC/AT, 1/20-Scale, All Mach Numbers, Including Data-Precision Band (Ref. 7)



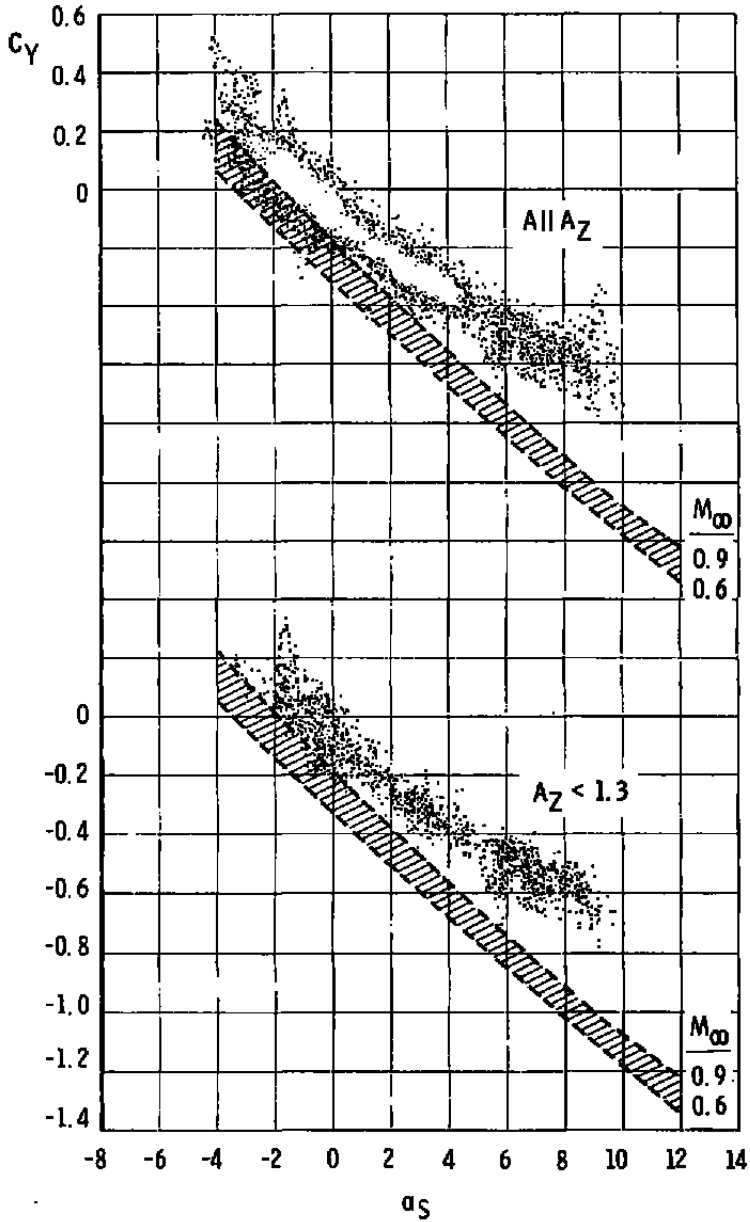
a. Normal-force coefficient

Figure 22. Comparison of wind tunnel and inflight data for maneuvering flight, AB 2.

MK 83, AB 2



-  In-Flight Data Points for Maneuvers with Variable Mach Number
-  AEDC/4T, 1/20-Scale, All Mach Numbers, Including Data-Precision Band (Ref. 7)



b. Side-force coefficient  
Figure 22. Continued.

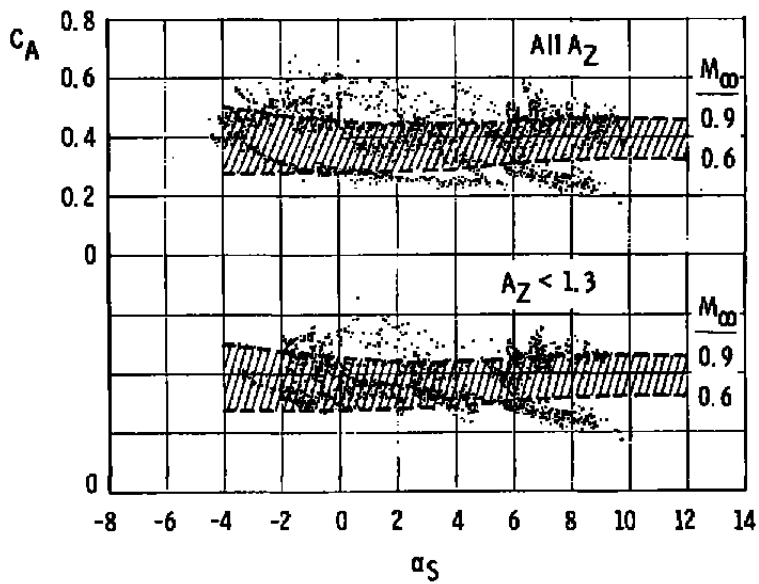
MK 83, AB 2



In-Flight Data Points for Maneuvers with Variable Mach Number

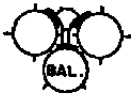


AEDC/4T, 1/20-Scale, All Mach Numbers, Including Data-Precision Band (Ref. 7)



c. Axial-force coefficient  
Figure 22. Continued.

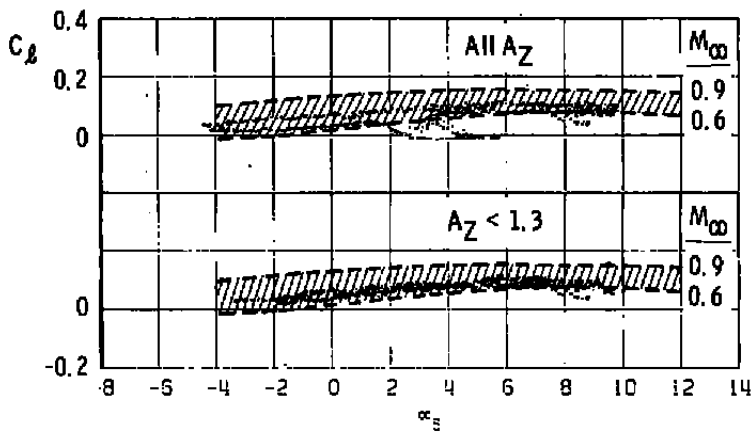
MK B3, AB 2



In-Flight Data Points for Maneuvers with Variable Mach Number

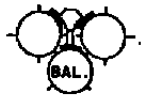


AEDC/AT, 1/20-Scale, All Mach Numbers, Including Data-Precision Band (Ref. 7)

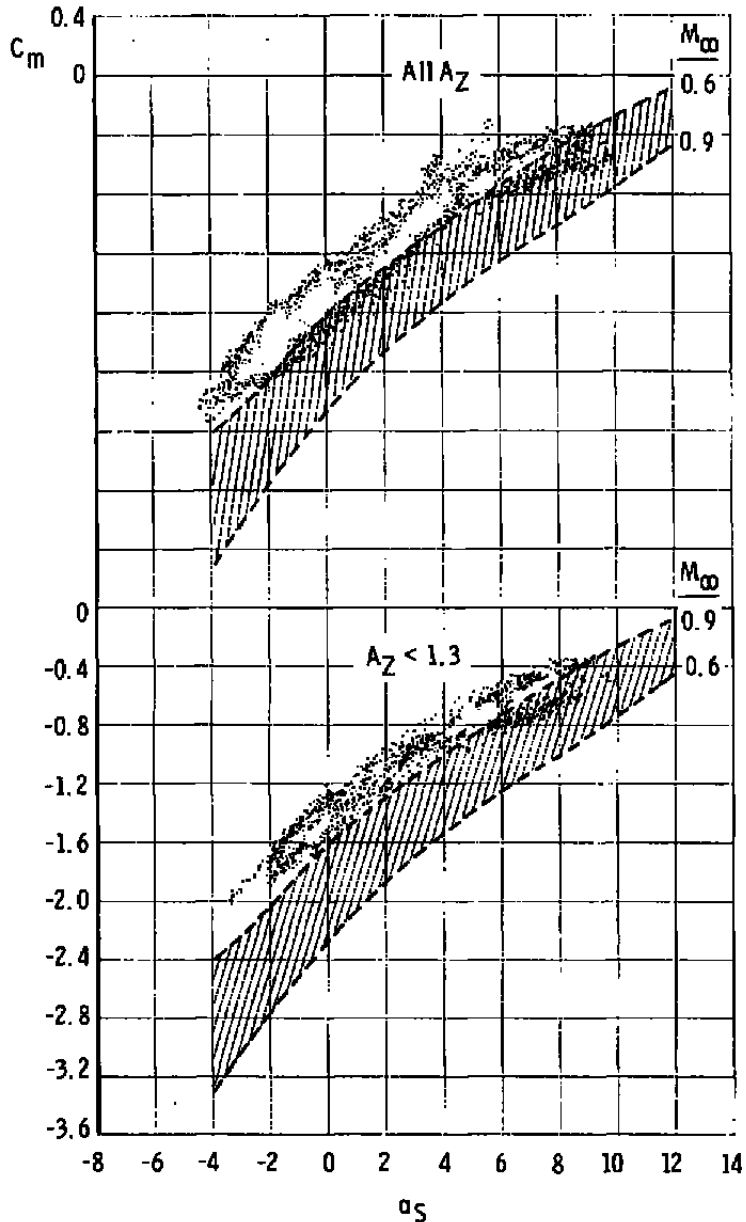


d. Rolling-moment coefficient  
Figure 22. Continued.

MK 83, AB 2



-  In-Flight Data Points for Maneuvers with Variable Mach Number
-  AEDC/4T, 1/20-Scale, All Mach Numbers, Including Data-Precision Band (Ref. 7)



e. Pitching-moment coefficient  
Figure 22. Continued.

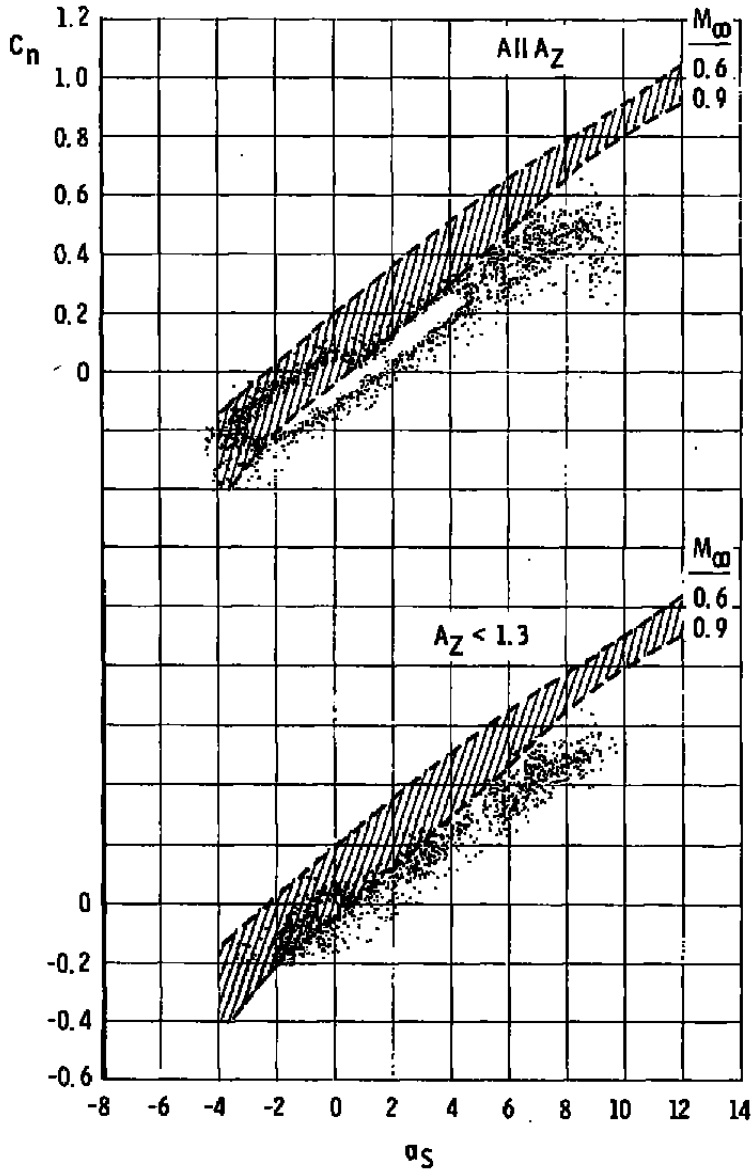
MK 83, AB 2



In-Flight Data Points for Maneuvers with Variable Mach Number

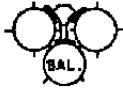


AEDC/4T, 1/20-Scale, All Mach Numbers, Including Data-Precision Band (Ref. 7)

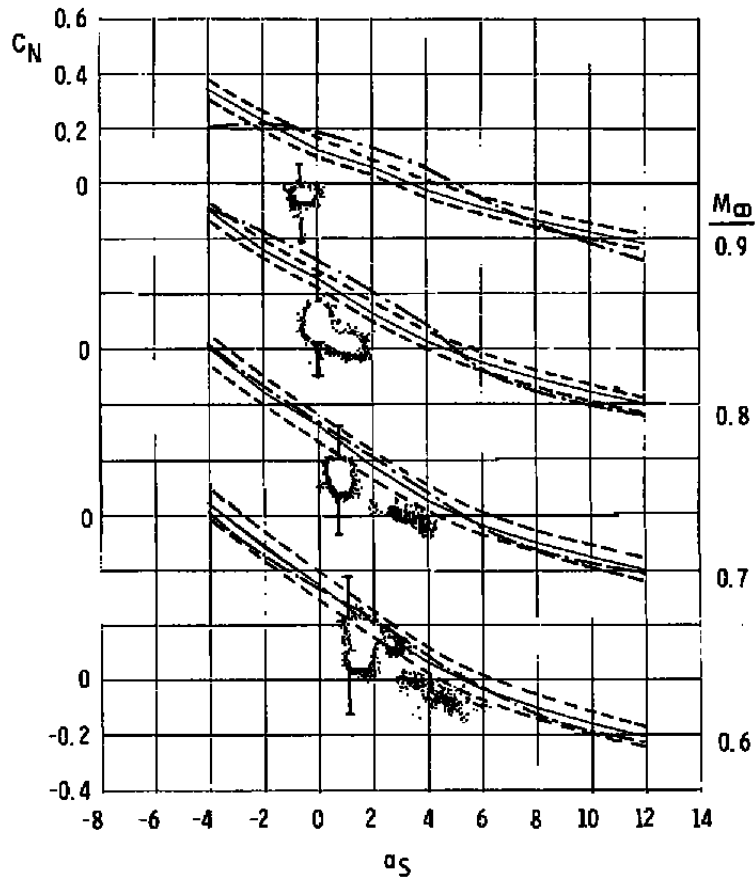


f. Yawing-moment coefficient  
Figure 22. Concluded.

MK 83, AB 1



-  In-Flight Data Points (Upper and Lower Data-Precision Bars Shown for Two Separate Points).
-  AEDC 1/20-Scale, Including Data-Precision Band (Ref. 7)
-  ARA 1/12-Scale (Ref. 9)



a. Normal-force coefficient

Figure 23. Comparison of wind tunnel and inflight data for constant Mach number, level flight plus low-g maneuvering flight, AB 1.

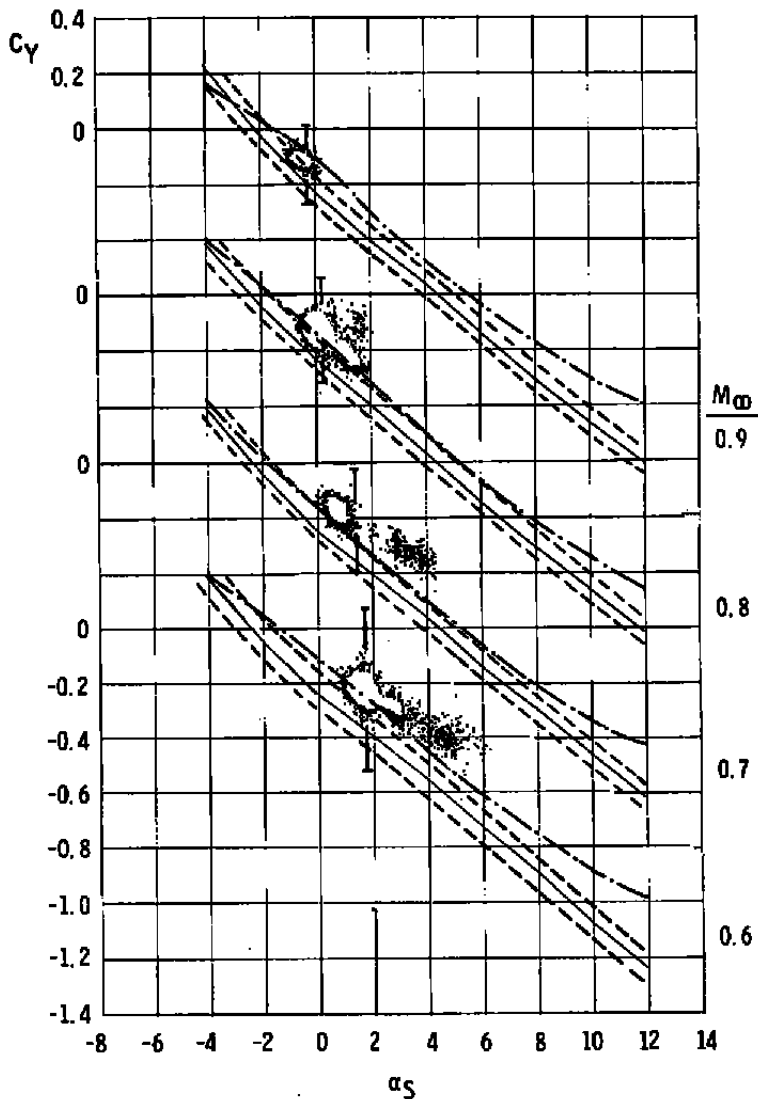
MK 83, AB 1



In-Flight Data Points (Upper and Lower Data-Precision Bars Shown for Two Separate Points).

----- AEDC/4T, 1/20-Scale, Including Data-Precision Band (Ref. 7)

----- ARA/9x8, 1/12-Scale (Ref. 9)



b. Side-force coefficient  
Figure 23. Continued.

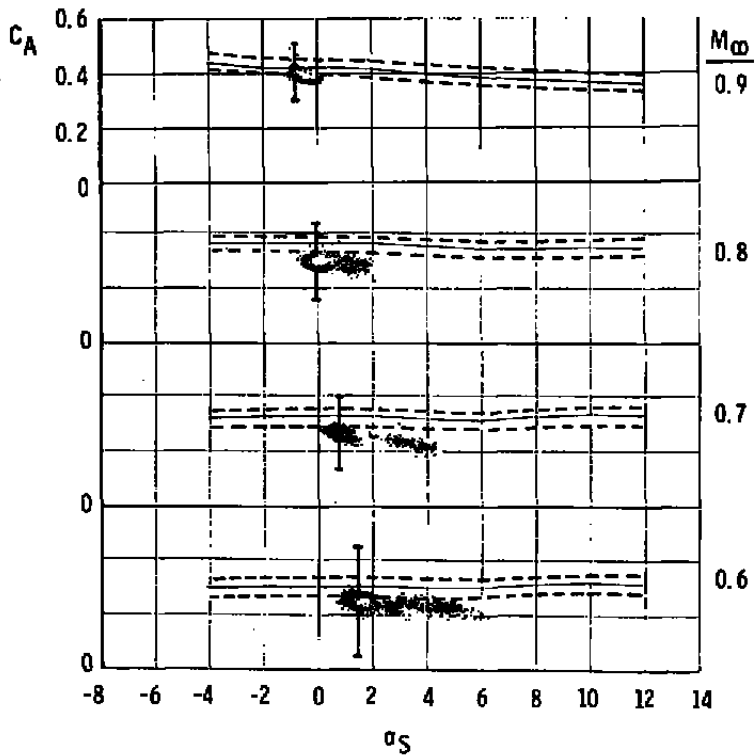
MK 83, AB 1



In-Flight Data Points (Upper and Lower Data-Precision Bars Shown for Two Separate Points).



AEDC/4T, 1/20-Scale, Including Data-Precision Band (Ref. 7)



c. Axial-force coefficient  
Figure 23. Continued.



MK 83, AB 1

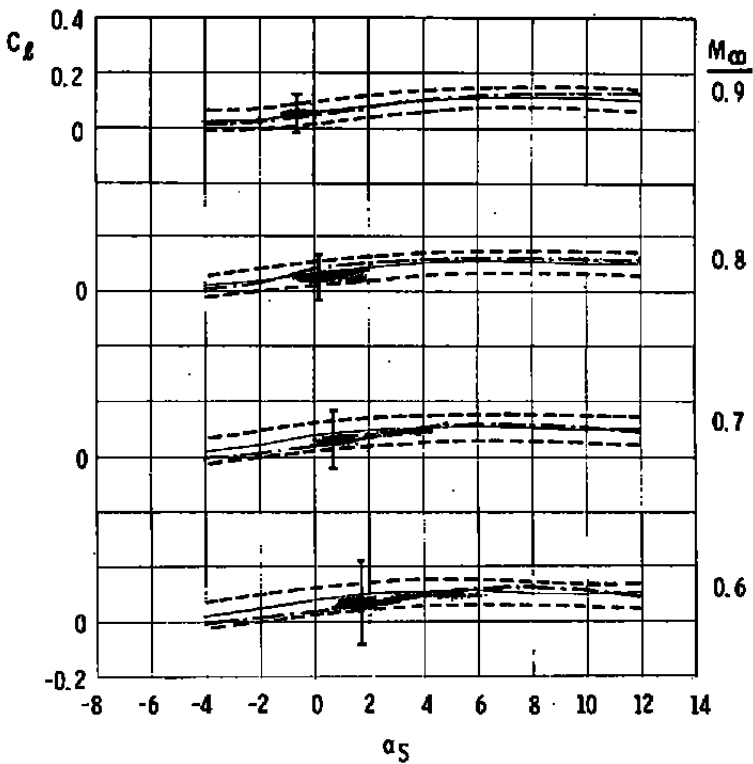


In-Flight Data Points (Upper and Lower Data-Precision Bars Shown for Two Separate Points).



AEDC 4T, 1/20-Scale, Including Data-Precision Band (Ref. 7)

ARA 79x8, 1/12-Scale (Ref. 9)



d. Rolling-moment coefficient  
Figure 23. Continued.

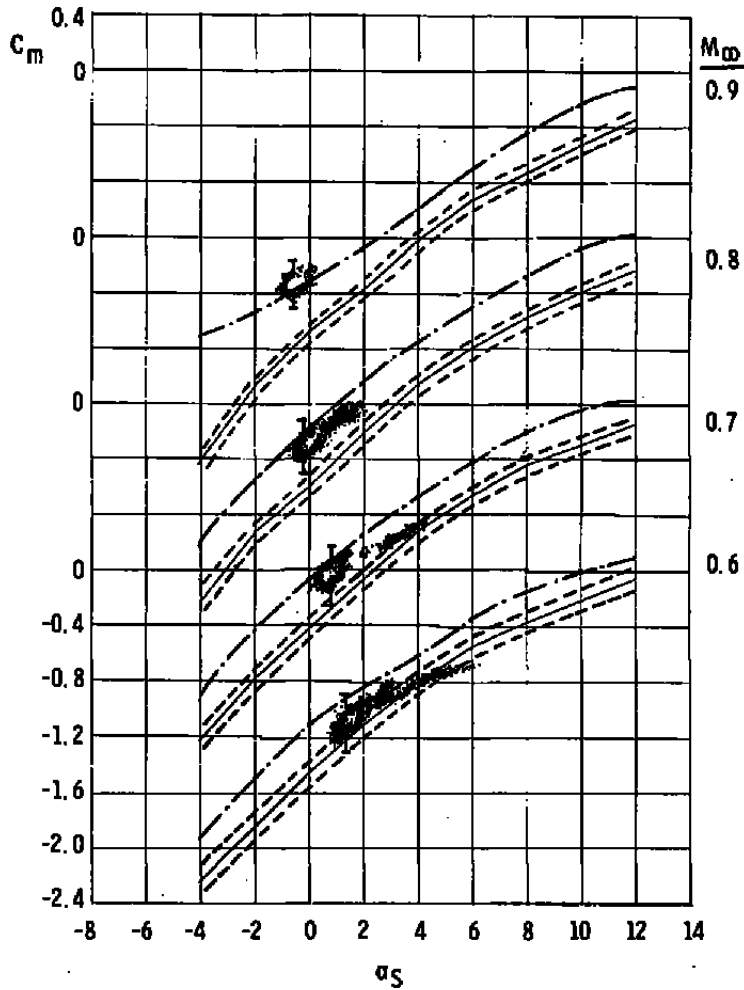
MK 83, AB 1



In-Flight Data Points (Upper and Lower Data-Precision Bars Shown for Two Separate Points).

----- AEDC/AT, 1/20-Scale, Including Data-Precision Band (Ref. 7)

----- ARA 9x8, 1/12-Scale (Ref. 9)



e. Pitching-moment coefficient  
Figure 23. Continued.

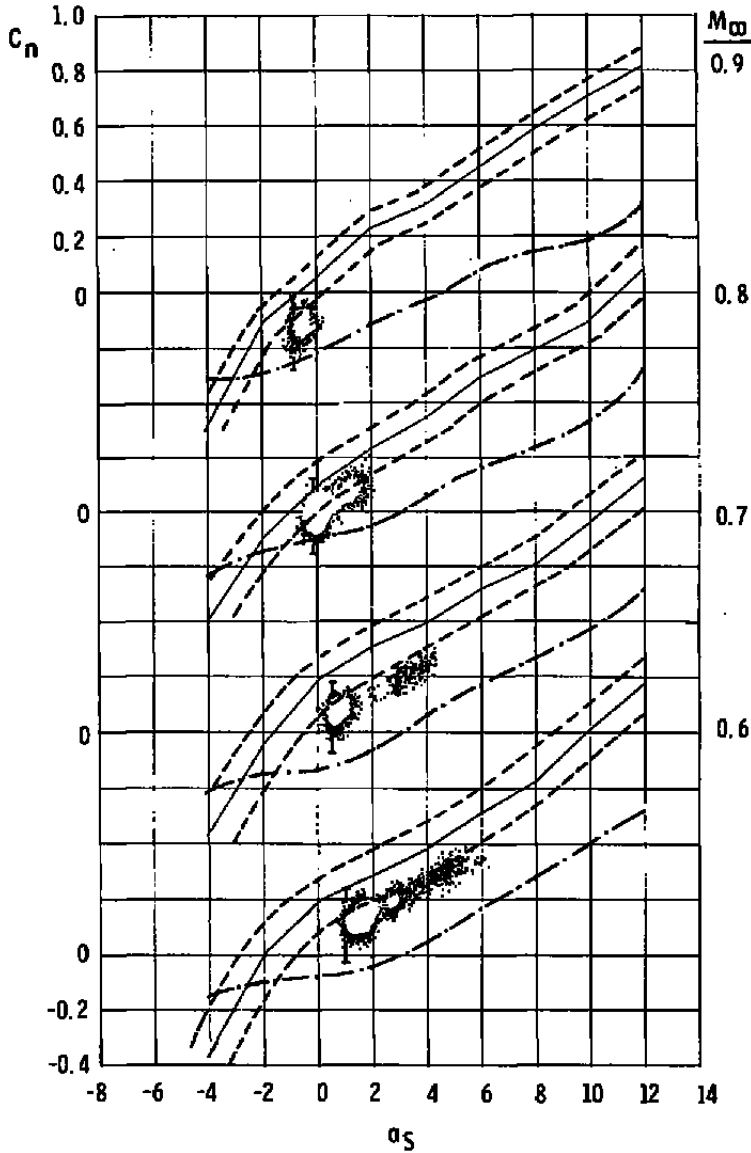
MK 83, AB 1



In-Flight Data Points (Upper and Lower Data-Precision Bars Shown for Two Separate Points).

----- AEDC/4T, 1/20-Scale, Including Data-Precision Band (Ref. 7)

----- ARA/9x8, 1/12-Scale (Ref. 9)

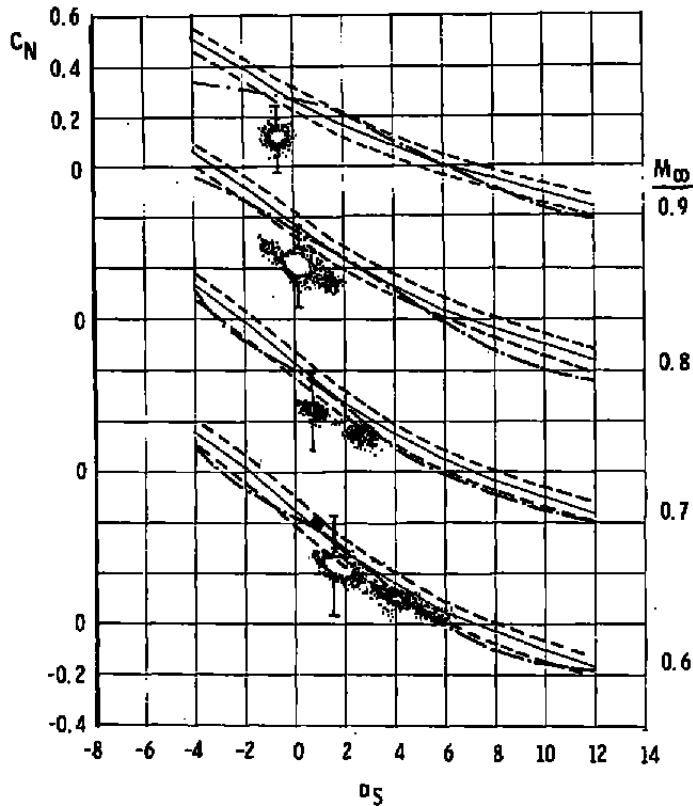


f. Yawing-moment coefficient  
Figure 23. Concluded.

MK 83, AB 2



-  In-Flight Data Points (Upper and Lower Data-Precision Bars Shown for Two Separate Points).
-  AEDC/MT, 1/20-Scale, Including Data-Precision Band (Ref. 7)
-  ARA 7x8, 1/12-Scale (Ref. 9)
-  DTNSRDC 7x10, 1/10-Scale (Ref. 8)



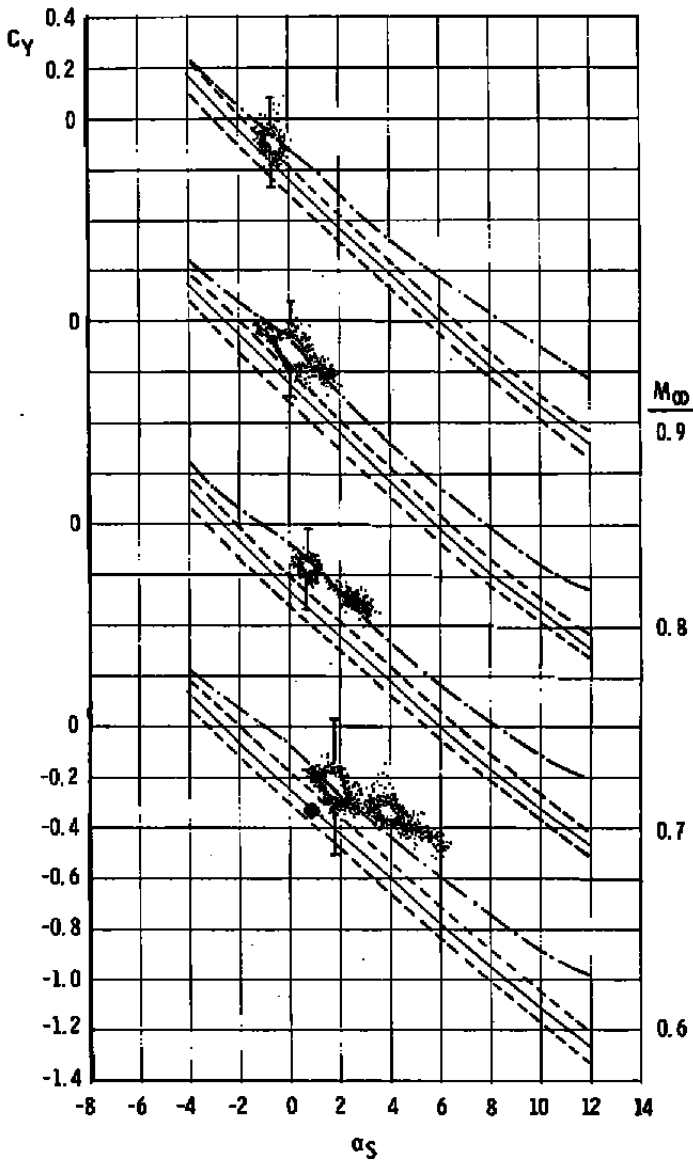
a. Normal-force coefficient

Figure 24. Comparison of wind tunnel and inflight data for constant Mach number, level flight plus low-g maneuvering flight, AB 2.

MK83, AB 2



-  In-Flight Data Points (Upper and Lower Data-Precision Bars Shown for Two Separate Points).
-  AEDC/AT, 1/20-Scale, Including Data-Precision Band (Ref. 7)
-  ARA 7x8, 1/12-Scale (Ref. 9)
-  DTNSRDC 7x10, 1/10-Scale (Ref. 8)

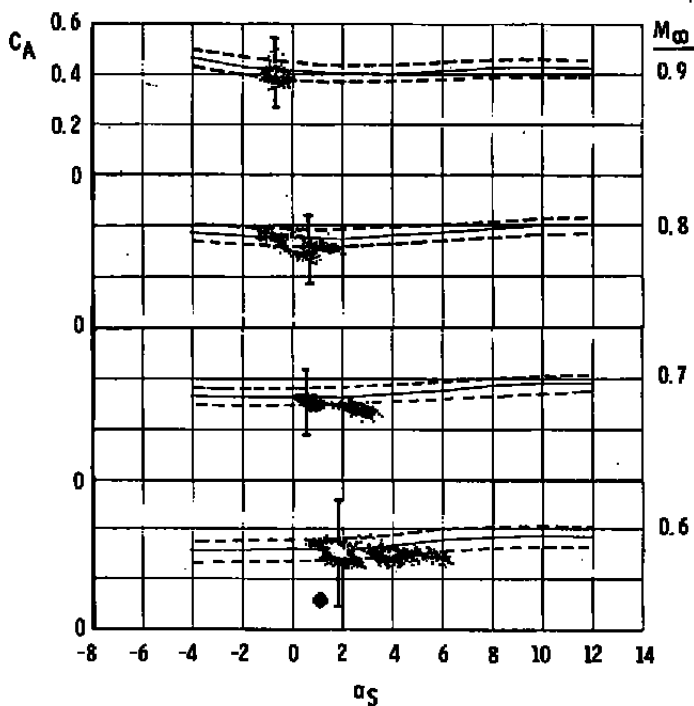


b. Side-force coefficient  
Figure 24. Continued.

MK 83, AB 2



-  1n-Flight Data Points (Upper and Lower Data-Precision Bars Shown for Two Separate Points).
-  AEDC #T, 1/20-Scale, Including Data-Precision Band (Ref. 7)
-  ARA #x8, 1/12-Scale (Ref. 9)
-  DTNSRDC #x10, 1/10-Scale (Ref. 8)



c. Axial-force coefficient  
Figure 24. Continued.



MK B3, AB 2

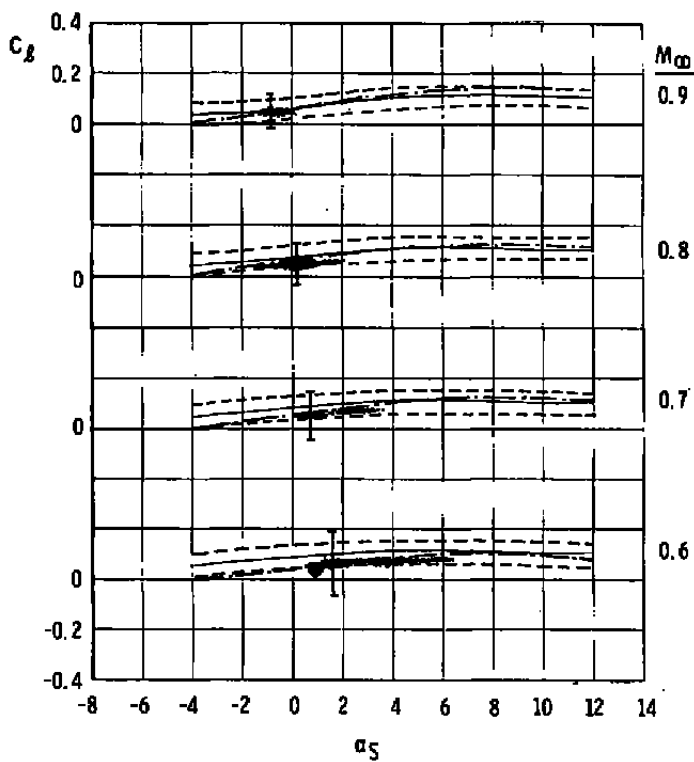


In-Flight Data Points (Upper and Lower Data-Precision Bars Shown for Two Separate Points).

----- AEDC/4T, 1/20-Scale, Including Data-Precision Band (Ref. 7)

----- ARA 9x8, 1/12-Scale (Ref. 9)

◆ DTNSRDC 7x10, 1/10-Scale (Ref. 8)



d. Rolling-moment coefficient  
Figure 24. Continued.

MK 83, AB 2

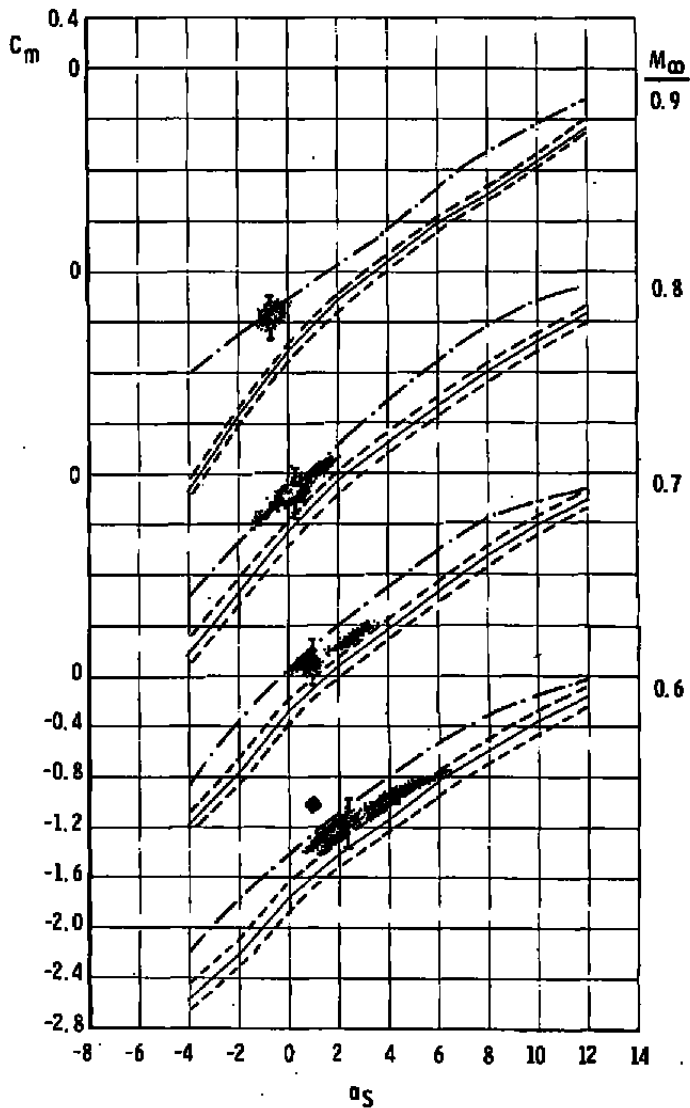


In-Flight Data Points (Upper and Lower Data-Precision Bars Shown for Two Separate Points).

--- AEDC/AT, 1/20-Scale, Including Data-Precision Band (Ref. 7)

--- ARA 19x8, 1/12-Scale (Ref. 9)

◆ DTNSRDC 7x10, 1/10-Scale (Ref. 8)



e. Pitching-moment coefficient  
Figure 24. Continued.

MK 83, AB 2

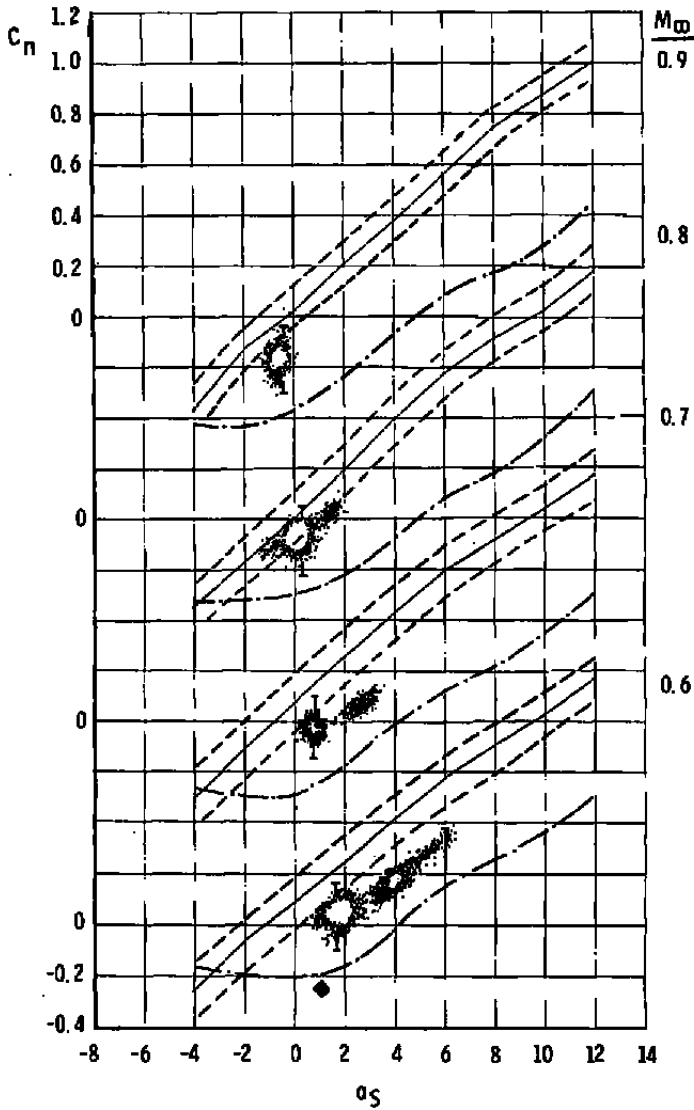


 In-Flight Data Points (Upper and Lower Data-Precision Bars Shown for Two Separate Points).

 AEDC/AT, 1/20-Scale, Including Data-Precision Band (Ref. 7)

 ARA/9x8, 1/12-Scale (Ref. 9)

 DTNSRDC/7x10, 1/10-Scale (Ref. 8)



f. Yawing-moment coefficient  
Figure 24. Concluded.

**Table 1. Data-Precision Intervals for Force and Moment Coefficients from Tunnel 4T**

$M_{\infty}$	$\Delta(C_N)$	$\Delta(C_Y)$	$\Delta(C_A)$	$\Delta(C_\ell)$	$\Delta(C_m)$	$\Delta(C_n)$
0.6	$\pm 0.04$	$\pm 0.05$	$\pm 0.04$	$\pm 0.05$	$\pm 0.08$	$\pm 0.08$
0.7	$\pm 0.04$	$\pm 0.04$	$\pm 0.03$	$\pm 0.05$	$\pm 0.07$	$\pm 0.08$
0.8	$\pm 0.03$	$\pm 0.04$	$\pm 0.03$	$\pm 0.04$	$\pm 0.07$	$\pm 0.07$
0.9	$\pm 0.03$	$\pm 0.04$	$\pm 0.03$	$\pm 0.04$	$\pm 0.06$	$\pm 0.06$

**Table 2. Data-Precision Intervals for Fundamental Flight Instrumentation Systems**

<u>Parameter</u>	<u>Symbol</u>	<u><math>\Delta(\text{Parameter})</math></u>
Aircraft Acceleration	$A_x, A_y, A_z$	$\pm 0.1 \text{ g}$
Boom Static Pressure	$p$	$\pm 28.8 \text{ psfa}$
Boom Total Temperature	$T_t$	$\pm 2.2^\circ \text{R}$
Boom Airspeed	$V_{\text{cal}}$	$\pm 0.7 \text{ ft/sec}$
Boom Angle of Attack	$\alpha$	$\pm 0.3 \text{ deg}$
Boom Sideslip Angle	$\beta$	$\pm 0.3 \text{ deg}$
Altitude	$H$	$\pm 200 \text{ ft}$

## APPENDIX A SINGLE-STORE CONFIGURATION (FLIGHT 1)

The single-store configuration (instrumented store on TER station 1, "shoulder" stations 2 and 3 empty) was not included in the series of experiments conducted in Tunnel 4T at the AEDC. At ARA, in Bedford, England, UK, a series of experiments was conducted in 1977 to repeat, in the 9- by 8-ft Transonic Wind Tunnel, the configurations and conditions of the flight program, using models of 1/12 full size. The models were fabricated using dimensions taken from the drawings of the 1/20-scale AEDC models and rescaled to 1/12 size. However, the F-4 aircraft model was of UK configuration (F-4K Phantom), but fitted with model pylons of USAF design to match the geometric features of the flight test configuration in the vicinity of the store model. Experiments were conducted with laminar-to-turbulent boundary-layer transition artificially fixed on the store model through the application of fine grit, then repeated without grit for a natural, or free, transition. Full description of the experiments is presented in Ref. 9.

In Fig. A-1, the ARA data are compared with the inflight data for constant Mach number, level flight. Precision bands, including 95 percent of the ARA data, are not known. Also, axial-force coefficient data are not available from the ARA experiments. Correlation between these wind tunnel data and flight test data is good - of the same quality as the data from the 1/20-scale models of the fully loaded TER in Tunnel 4T at the AEDC.

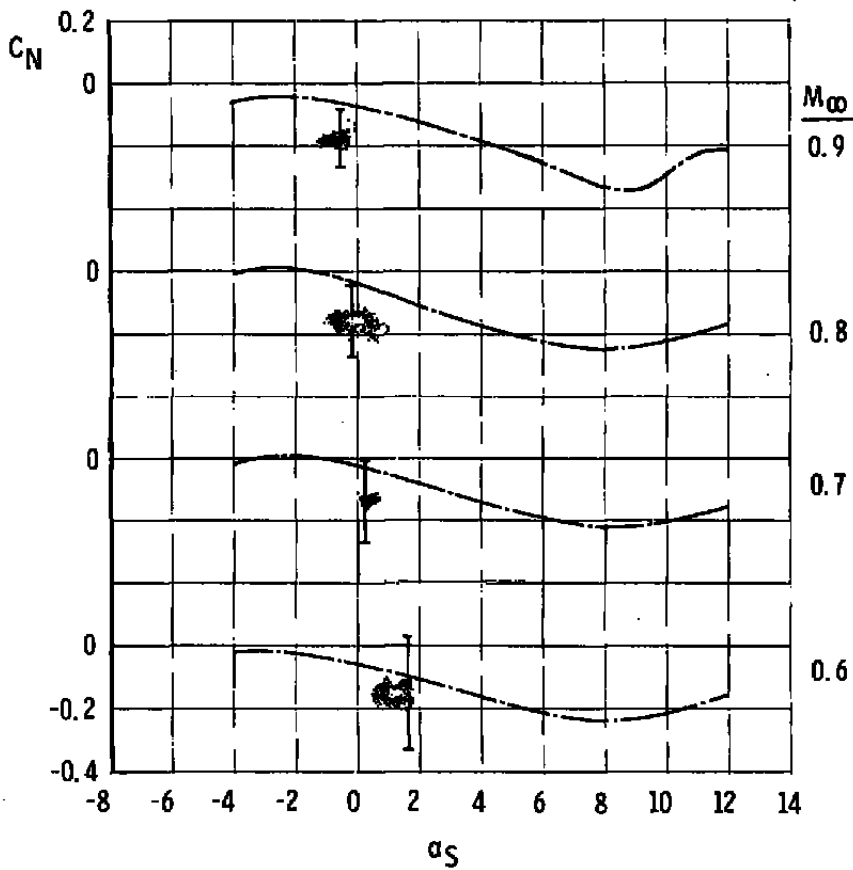
In Fig. A-2, data are presented from a gentle, almost constant Mach number dive conducted at  $M_\infty = 0.7 \pm 0.07$ . During the pullout portion from the 0.7 Mach number dive, a vertical acceleration of  $A_z = 2$  g's was experienced. The data recorded for normal force acting on the store during the dive are presented in the upper half of Fig. A-2a. Scattering of points at a store angle of attack of 3 to 4 deg is noted, just as in the case of the fully loaded TER (Section 4.2), for the high-g maneuver. Including only the inflight data recorded when  $A_z < 1.3$  g produced the groupings at the lower half of the pages of Fig. A-2. From the lower grouping of Fig. A-2a, it is clear that excluding the high-g data improved the apparent interrelationship of the data just as it did for the fully-loaded TER configuration (Section 4.2). Therefore, the scatter is not solely attributable to incorrect dynamic similitude in the wind tunnel.

MK 83, AB 1



● In-Flight Data Points, Flight 1

— ARA/9x8, 1/12-Scale (Ref. 9)



a. Normal-force coefficient

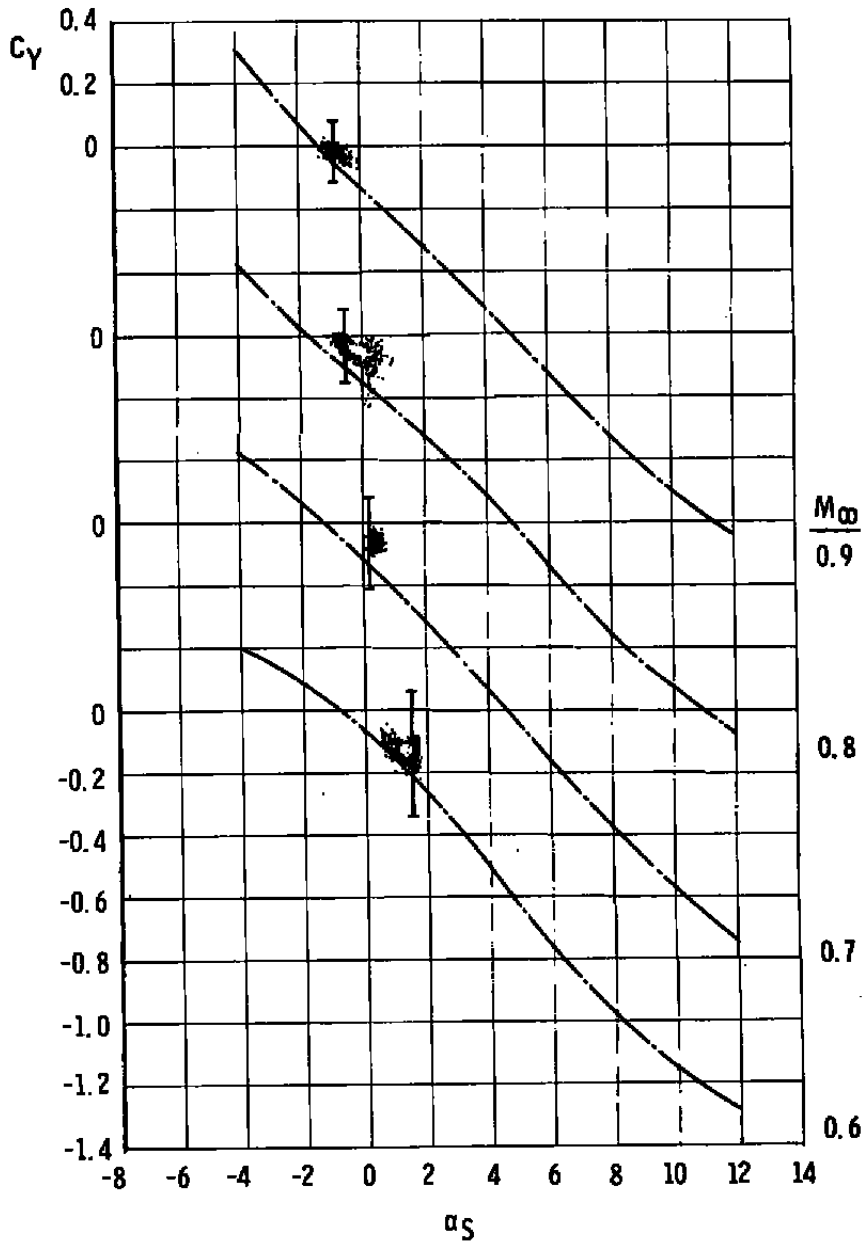
Figure A-1. Comparisons of wind tunnel and inflight data for the single-store configuration, constant Mach number, level flight.

MK 83, AB 1



● In-Flight Data Points, Flight 1

— ARA/9x8, 1/12-Scale (Ref. 9)



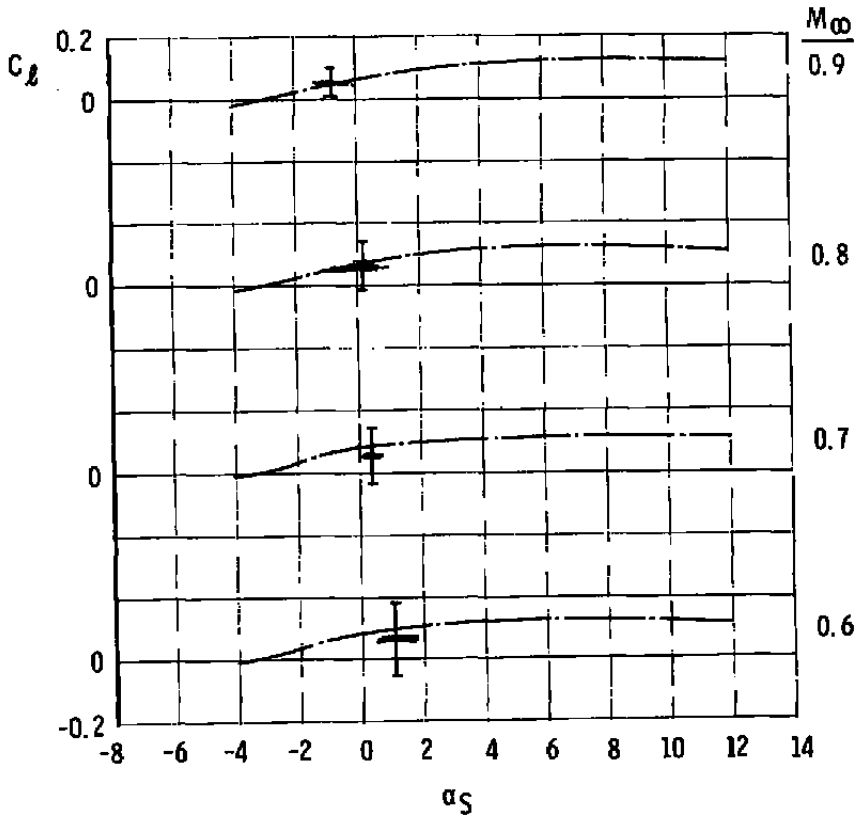
b. Side-force coefficient  
Figure A-1. Continued.

MK 83, AB 1



● In-Flight Data Points, Flight 1

— ARA 19x8, 1/12-Scale (Ref. 9)



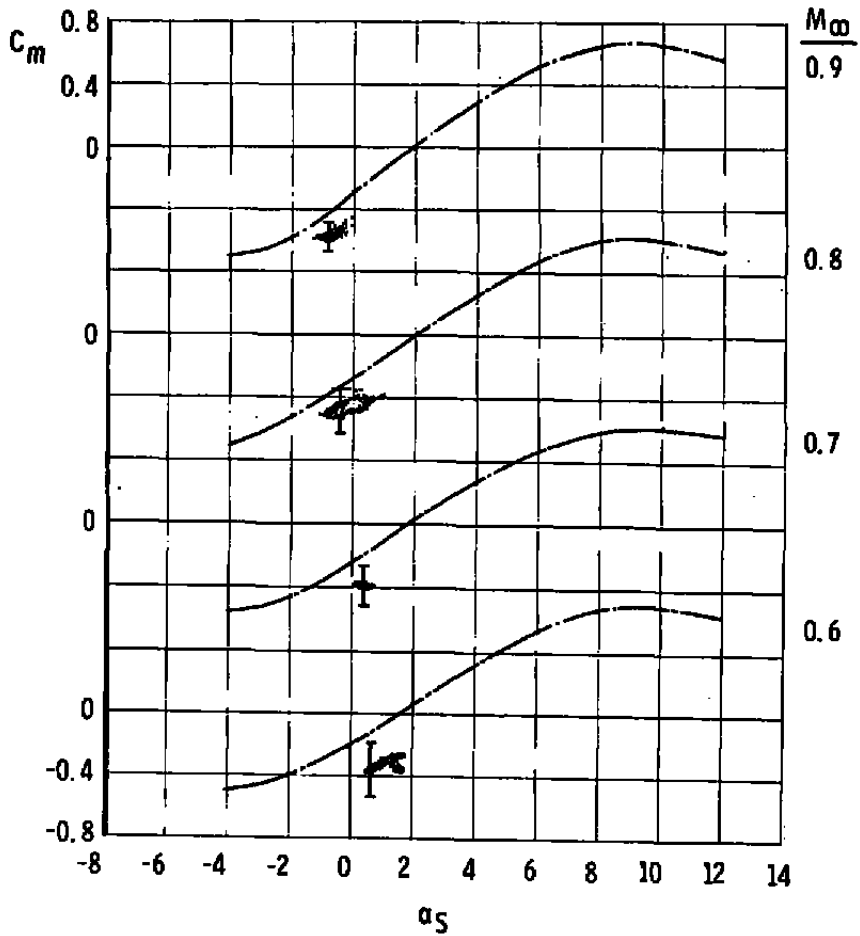
c. Rolling-moment coefficient  
Figure A-1. Continued.

MK 83, AB 1



⊗ In-Flight Data Points, Flight 1

--- ARA 19x8, 1/12-Scale (Ref. 9)



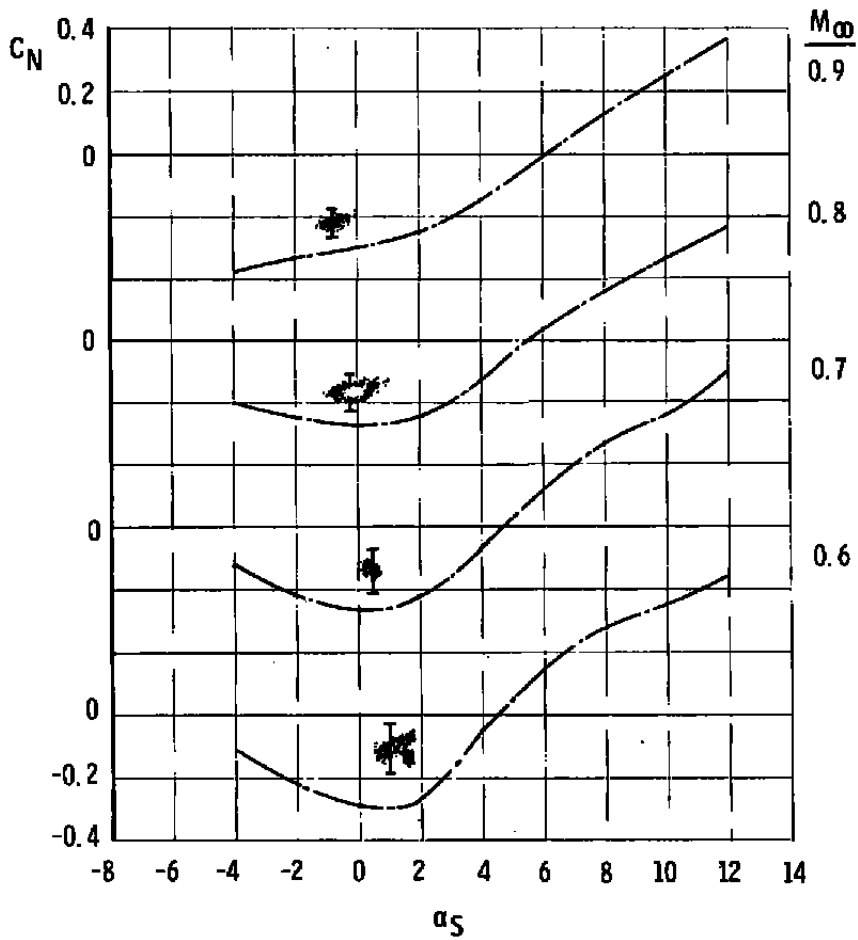
d. Pitching-moment coefficient  
Figure A-1. Continued.

MK 83, AB 1



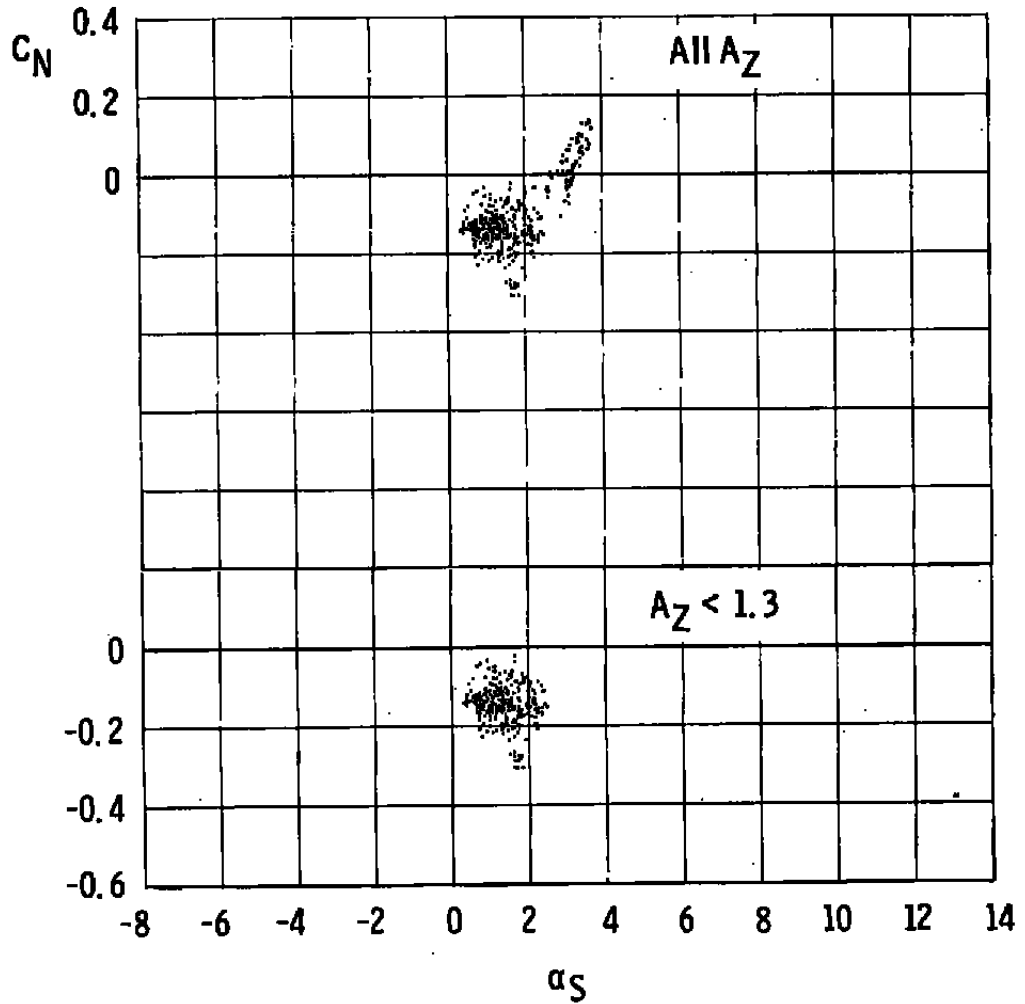
⊗ In-Flight Data Points, Flight 1

— ARA 19x8, 1/12-Scale (Ref. 9)



e. Yawing-moment coefficient  
Figure A-1. Concluded.

MK 83, AB 1


 In-Flight Data Points, Flight 1


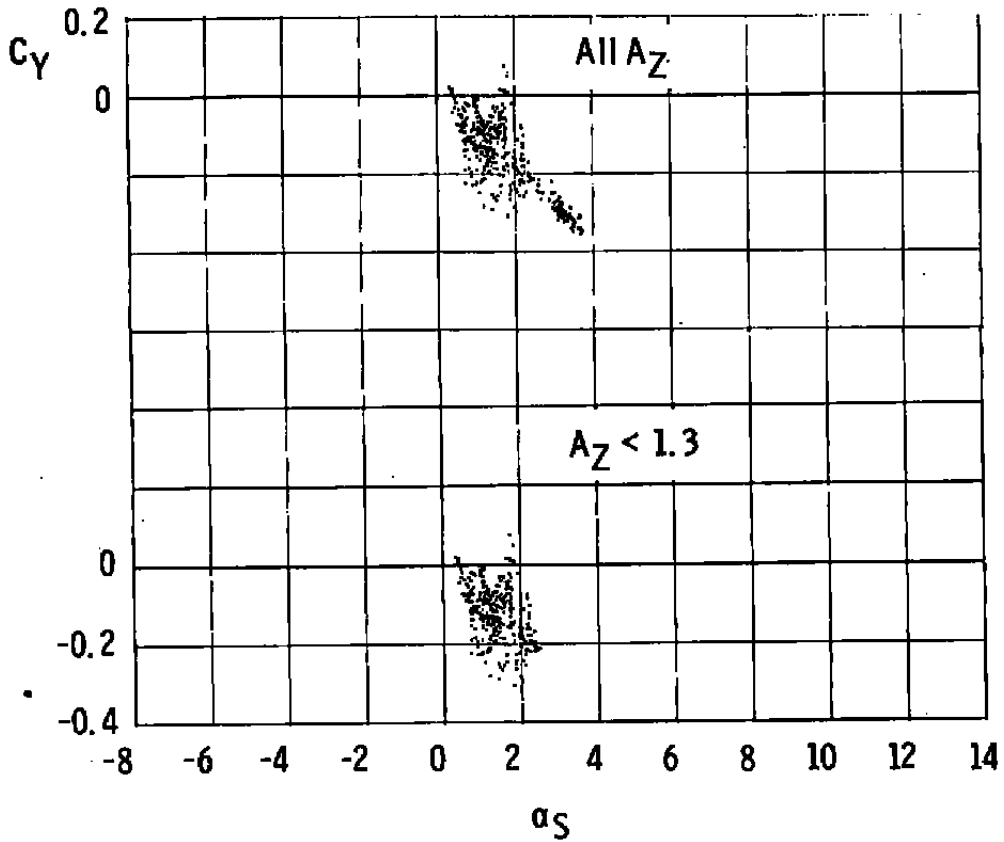
a. Normal-force coefficient

Figure A-2. Inflight data for the single-store configuration in a constant Mach number dive.

MK 83, AB 1



● In-Flight Data Points, Flight 1

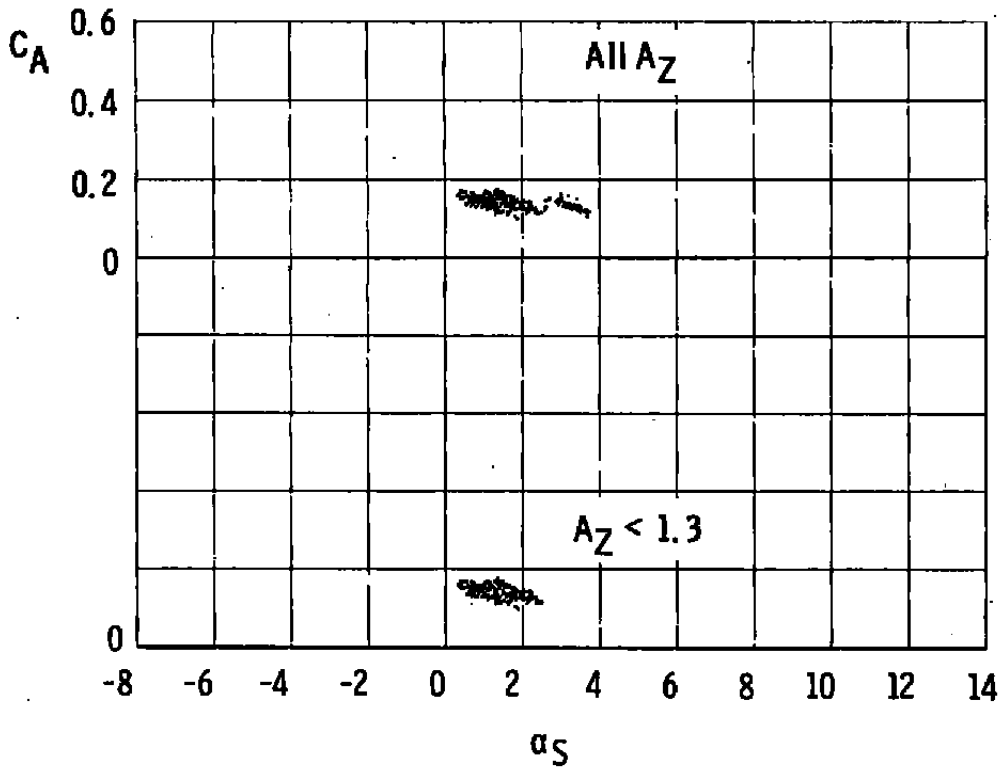


b. Side-force coefficient  
Figure A-2. Continued.

MK 83, AB 1



In-Flight Data Points, Flight 1

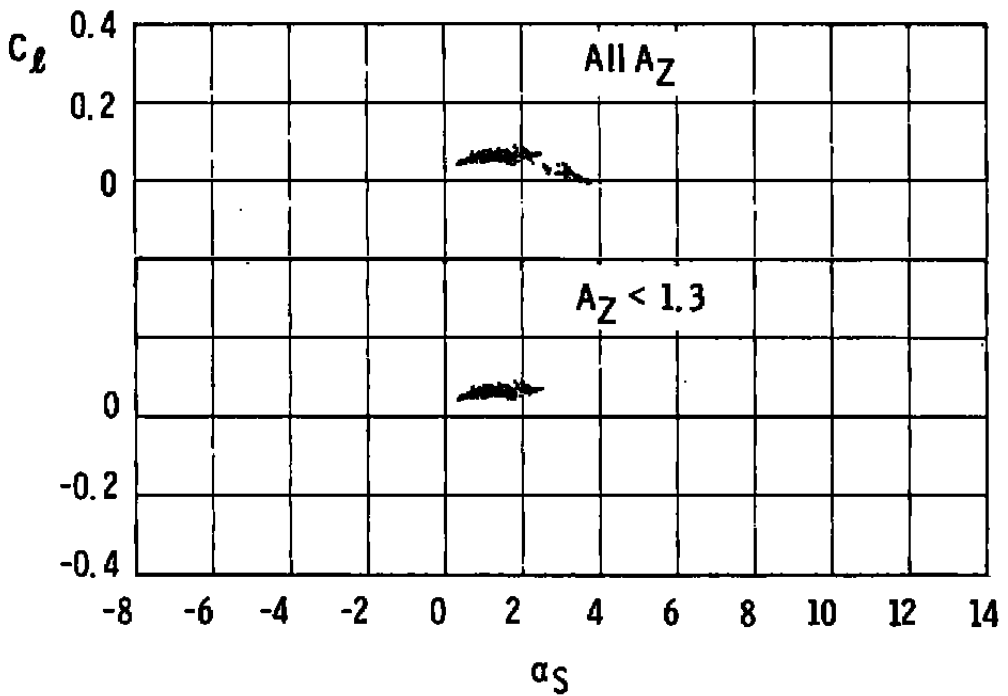


c. Axial-force coefficient  
Figure A-2. Continued.

MK 83, AB 1



In-Flight Data Points, Flight 1

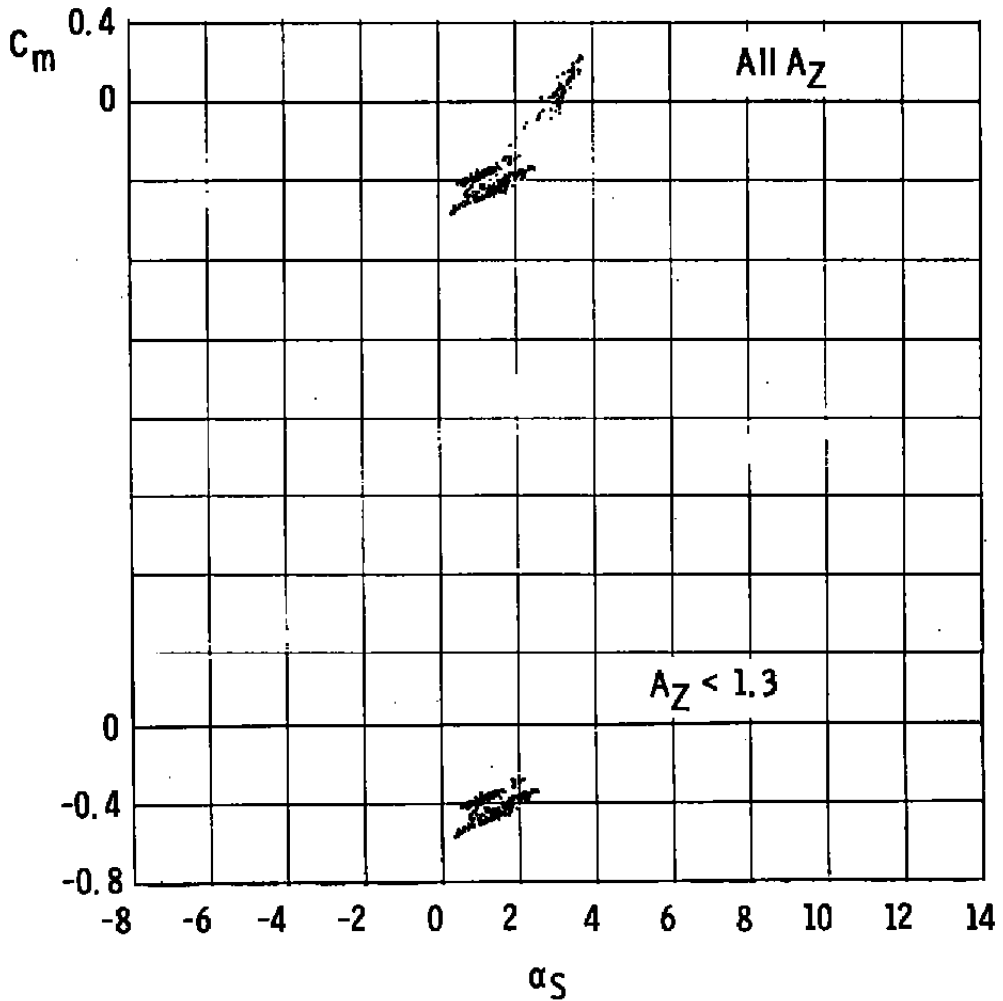


d. Rolling-moment coefficient  
Figure A-2. Continued.

MK 83, AB 1



● In-Flight Data Points, Flight 1

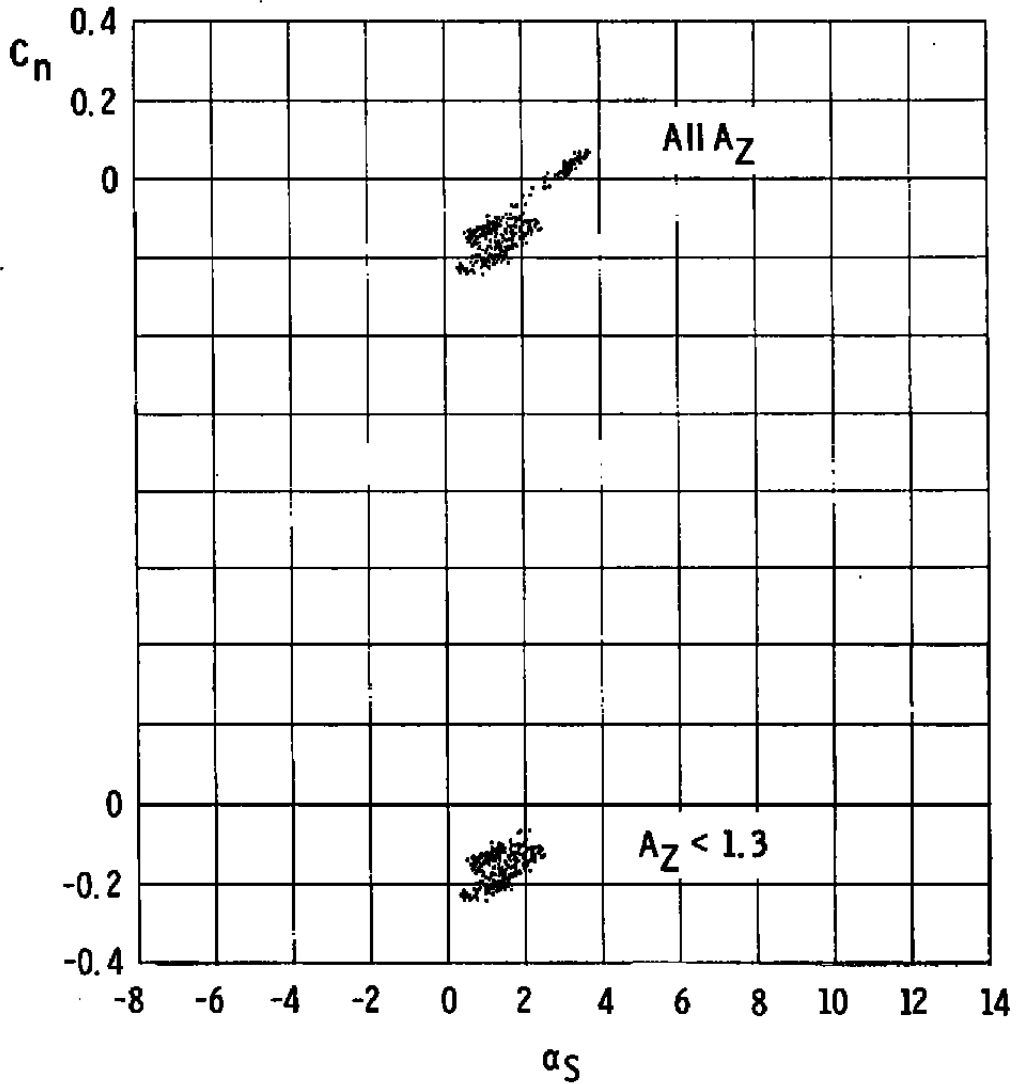


e. Pitching-moment coefficient  
Figure A-2. Continued.

MK 83, AB 1



 In-Flight Data Points, Flight 1



f. Yawing-moment coefficient  
Figure A-2. Concluded.

## NOMENCLATURE

A	Maximum cross-sectional area of the store, $(\pi D^2)/4$ , ft <sup>2</sup>
AB	Afterbody
$A_X, A_Y, A_Z$	Acceleration of the aircraft in the $X_B$ , $Y_B$ , and $Z_B$ coordinate directions, respectively, acceleration/g, cited as g's (Note: Accelerometers were nulled on the ground prior to flight. Therefore, any straight-and-level unaccelerated flight condition would be regarded as 0 g, instead of the usual 1 g.)
BL	Aircraft model buttock line, measured from the plane of symmetry of the model, in., model scale
$C_A$	Coefficient of measured axial force acting on the store; measured axial force/ $q_\infty A$
$C_\ell$	Coefficient of measured rolling moment acting about the longitudinal axis of symmetry of the store; measured rolling moment/ $q_\infty AD$
$C_m$	Coefficient of measured pitching moment acting about the cg of the store, measured pitching moment/ $q_\infty AD$
$C_N$	Coefficient of measured normal force acting on the store, measured normal force/ $q_\infty A$
$C_n$	Coefficient of measured yawing moment acting about the longitudinal axis of symmetry of the store; measured yawing moment/ $q_\infty AD$
$C_Y$	Coefficient of measured side force acting on the store, measured side force/ $q_\infty A$
cg	Center of gravity
D	Maximum diameter of the store, ft
$F_N$	Net measured normal force acting on the store, lb ("Net" indicates that corrections have been made for tare forces attributable to the weight of the store, whether at unaccelerated, "1-g" flight conditions, or during maneuvering flight.)
$F_{NST}$	Static tare for measured normal force, lb

FS	Aircraft model fuselage station, measured from the nose of the model, in., model scale
$g$	Acceleration of gravity, ft/sec <sup>2</sup>
H	Altitude, ft above mean sea level
M	Mach number
$M_{\infty}$	Free-stream Mach number
$p$	Static pressure measured at the aircraft boom, psfa
$p_{t_{\infty}}$	Free-stream total pressure, psfa
$q_{\infty}$	Free-stream dynamic pressure, psfa
Re	Reynolds number
$T_t$	Total temperature measured at the aircraft boom, °R
$V_{cal}$	Calibrated airspeed of the aircraft, derived from measurements made at the aircraft boom, ft/sec
WL	Aircraft model waterline, measured from the horizontal reference plane of the model, in., model scale
$W_N$	Static tare weight of the store, derived from the output of the normal-force strain gages of the balance, lb
$\alpha$	Angle of attack of the aircraft relative to the free-stream velocity vector, deg
$\alpha_s$	Angle of attack of the store (1 deg less than $\alpha$ ), deg
$\beta$	Angle of sideslip of the aircraft relative to the free-stream velocity vector, deg
$\Delta( )$	Data-precision interval for a measured or calculated quantity
$\delta( )$	Difference between the observed value and a hypothetical value of a parameter

**BODY-AXIS SYSTEM OF COORDINATES****Directions**

- $X_B$  Parallel to the longitudinal axis of the body, positive direction is upstream
- $Y_B$  Perpendicular to the  $X_B$  and  $Z_B$  axes, positive direction is to the right as seen by the pilot
- $Z_B$  Parallel to the plane of symmetry of the aircraft and perpendicular to the  $X_B$  and  $Y_B$  axes, positive direction is up as seen by the pilot